# THE IMPACT OF WIND GENERATORS ON A POWER SYSTEM'S TRANSIENT STABILITY


BY

**Moloantoa Khomari**




UNIVERSITY OF CAPE TOWN
IDYUNIVESITHI YASEKAPA • UNIVERSITEIT VAN KAAPSTAD

**Department of Electrical Engineering**

Supervisor: **Prof K.A. Folly**




**THESIS SUBMITTED IN FULFILMENT OF THE REQUIREMENTS FOR A MASTER OF SCIENCE DEGREE IN ELECTRICAL ENGINEERING**
**OCTOBER 2009**

# DECLARATION

I declare that the work presented in this thesis is my original work. I have used the convention for citation and referencing. Contribution from work or works of other people has been cited and referenced. I hereby affirm that this work has not been presented in this, or any other university for examination, or any other purposes.

Signed: ……

**Moloantoa Khomari**

**October 2009**

# ACKNOWLEDGEMENTS

First and foremost I would like to thank God for the inherent nature he bestowed within me of persevering and of believing that through him everything is within reach.

On behalf of my extended family, I offer my most heartfelt sincere gratitude to my M.Sc. supervisor, Prof. K.A. Folly, for his unwavering academic guidance and financial support, as well as his constructive criticism of my progress reports and papers. I am also very grateful that he gave me the opportunity to become a Teaching Assistant.

I also take this time to thank Tanya Barben for the effort and time spent in proof reading this thesis.

I would also like to express special thanks to Mr C. Wozniak for his technical assistance with regards to the optimum functionality of the power analysis software (DIgSILENT) used in the research.

Furthermore, I take this opportunity to acknowledge with gratitude the assistance and much-needed feedback given to me by the Power-Engineering Research Group in respect of the critical questions relating to all my presentations.

It is most fitting that I thank the staff at the DIgSILENT Support Center for their efforts in imparting to me the knowledge I required to solve problems related to my simulation models. The assistance they gave me enabled me to use DIgSILENT to the best of my ability.

Above all else, I express my deepest appreciation to my Parents. I have been truly blessed with their care and support which, even in the darkest moments of the journey I have undertaken, came to my aid like the light of torch. Finally, I cannot forget to thank my brothers, for their words of encouragement throughout my academic career, and my extended family and friends for their wishing me well in all my endeavors.

Moloantoa Khomari

# SYNOPSIS

The interest in wind power in many countries worldwide has significantly increased over the past years. Two types of wind generator technologies are discussed in this thesis; these are: fixed speed and variable speed wind generators. The fixed speed wind generators are characterized by the usage of squirrel cage induction generators (SCIG). Fixed speed wind generators formed the type of wind generators which were predominantly used from the early 1990s to year 2000 [1]. However, due to technological advancements in power electronics used in power systems, variable speed wind generators have since become more common in new wind farms. This is mainly due to the associated advantages of using variable speed wind generators; i.e. they are able to offer network support during grid disturbances. Another important aspect is that, they are able to supply power for a much wider range of wind speed. These variable speed wind generators comprise of two types, one being a doubly-fed induction generator (DFIG), which uses a wound rotor induction generator, and the other a converter driven synchronous generator (CDSG), which could either be excited electrically or be that of permanent magnets.

Thus, as the use of wind turbines in the production of electrical power increases, it becomes increasingly important that stability studies be conducted on power systems in effort to understand the impact they will have on power systems.

This thesis firstly describes an investigation into the transient stability of a power system connected with different types of wind generator technologies and, secondly, how the electrical characteristics of these wind generators would affect the transient stability of the power system. Its main focus is on the rotor angle and terminal voltage of the conventional synchronous generator. However, the active and reactive power of the synchronous generator and also of the wind generators is also taken into consideration in some study cases. The rationale for drawing attention to the rotor angle is that, the dynamics of the synchronous generator's rotor following a transient disturbance defines the type of stability investigated herein, i.e. angular stability.

A hypothetical power network was developed with which the different types of wind generator technologies were connected. An extensive review of literature regarding the power network models and the concept of transient stability was conducted. The literature review consequently contains technical papers and reports on the dynamic behavior of power systems connected with wind energy conversion systems (WECS). The models of interest were the synchronous generator, two winding transformers, medium length transmission lines, a fixed speed wind generator, a doubly-fed induction generator and the converter driven synchronous generator, which has an analogous electrical behavior to the direct drive synchronous generator.

A three-phase short-circuit was chosen to be the type of transient disturbance applied to one of the power network's transmission lines, since it is the most severe type of fault. The investigations show that windfarms placed at areas which are further away from the power network, and thus requiring long transmission lines to connect to the power network affect the power system's transient stability negatively. Furthermore, to optimally compensate a squirrel cage induction generator based windfarm for the best transient response using set capacitor banks, one would need to rigorously investigate different capacitor values since the rated reactive power drawn by the windfarm cannot be used as a reference. The IEEET1 AVR and IEEEG2 speed governor were used in some case studies. The AVR proved to be much more effective compared with the governor with respect to enhancing the power system's transient stability. The positive effect of a higher inertia of the squirrel cage induction generators on the power system's transient stability led to a recommendation that it would be advisable for wind generators to be designed with a relatively high inertia.

The power system experienced a better transient response when doubly-fed induction generators (DFIGs) were integrated into the power network using the same topology as that used to connect the squirrel cage induction generators, particularly with respect to the rate at which the terminal voltage of the conventional synchronous recovered after a grid disturbance. This was in comparison with having fixed speed wind generators. The reactive power set points of the grid side voltage source converter (VSC) of the doubly-fed induction generators were also assessed. With the VSC reactive power set to its minimum value, the

conventional synchronous generator was forced to supply more reactive power. When no system controllers were activated i.e. AVR and speed governor, and the DFIGs VSC set to its minimum reactive power setting, the terminal voltage of the synchronous generator did not recover to an acceptable level after the fault. In this case, the terminal voltage settled to about 0.63 p.u. of the prefault voltage level. When the DFIGs VSC was set to its maximum reactive power, the terminal voltage of the synchronous generator settled to about 0.97 p.u. of its prefault voltage following the fault. The proportional gain of the VSC current controller was explored under different settings. It was increased from 0.01 to 0.1 and then to 1.0. It can be said that setting the proportional gain of the VSC current controller with the aforementioned values resulted with the terminal voltage having a similar transient response. However, when the gain was set to 0.1 and 1.0, the magnitude of the first swing and that of the subsequent oscillations was relatively bigger than when the gain was set to 0.01. It was seen that the grid disturbance had a more severe consequence on the transient stability of the power system when the speed of the wind turbines was above their synchronous speed. The grid disturbance caused the wind turbines to operate at higher angular velocities, and thus, this resulted in a further increase in rotational speed following the fault. This led to an increased reactive power demand on the power system.

The topology used to connect the converter driven synchronous generators (CDSGs) onto the power network was the same as that used to connect the doubly-fed induction generators. Emphasis was placed on the line side converter of the CDSGs since it had a significant impact on the reactive power exchange between the windfarm and the power network. Increasing the number of CDSGs on the power network resulted in a negative impact on the transient stability of the power network since the swing of the rotor angle also increased after the grid disturbance. However, it seems the level of penetration of the CDSGs does not affect the rate at which the terminal voltage of the synchronous generator recovers after a grid disturbance. The simulation results suggest that, the line side converter of the CDSG plays a more critical role than the generator side converter in relation to the grid interaction of the CDSG. The different reactive power set points of the generator side converter (GSC) set within operating limits of the voltage source converter did not have any impact on the reactive power generated or absorbed by the conventional synchronous generator in steady state operating conditions.

Conversely, similar settings of reactive power set points were explored with the line side converter (LSC) within the same steady state operating conditions, and the reactive power generated or absorbed by the conventional synchronous generator was significantly affected by the changed settings of the line side converter's reactive power set point. Operating the LSC at unity power factor in steady state proved to be more favourable in relation to the conventional synchronous generator. This is based on the synchronous generator supplying the least amount of reactive power while at the same time not being under excited. This effectively meant that, the excitation system was operated well within its limits. Equipping the conventional synchronous generator with the IEEET1 AVR only, improved the transient stability of the power grid compared to when only the IEEEG2 speed governor was used and when there were no system controllers connected. The effect of the AVR was that the magnitude of the rotor oscillations, subsequent to the first swing after the fault, were reduced. Furthermore, the AVR helped return the terminal voltage of the conventional synchronous generator to its prefault level after the grid fault. A comparison between the effect of CDSGs and DFIGs on the power system's transient stability was conducted with system controllers inactive. It was then noted that, the terminal voltage recovered much quicker following a fault when CDSGs were connected, as compared to when DFIGs were connected. This brought to fore, the superiority of the CDSG design in relation to the terminal voltage of the synchronous generator.

It can thus be concluded from these investigations that variable speed wind generators have a more favourable impact on the transient stability of the power network.

# TABLE OF CONTENTS

# LIST OF TABLES

# LIST OF FIGURES

# NOMENCLATURE

| | |
|---|---|
| rpm | - revolutions per minute |
| ac | - alternating current |
| dc | - direct current |
| TSP | - transient stability programme |
| WF | - wind farm |
| $e_d, e_q, e_0$ | - stator voltages in the *dqo* reference frame |
| $\psi_d, \psi_q, \psi_0$ | - stator flux linkage in the *dqo* reference frame |
| $\omega_r$ | - rotor angular velocity |
| $R_a$ | - armature resistance |
| $i_d, i_q, i_0$ | - stator currents in the *dqo* plane |
| $e_{fd}$ | - rotor field voltage along the d-axis |
| $R_{fd}, R_{1d}, R_{1,2q}$ | - rotor circuit resistances |
| $i_{fd}, i_{1d}, i_{1,2q}$ | - field and amortisseur circuit currents |
| $T_e$ | - electrical torque |
| $R_{Cu,HV}$ | - high voltage winding resistance |
| $R_{Cu,LV}$ | - low voltage winding resistance |
| $X_{\sigma,HV}$ | - high voltage winding leakage reactance |
| $X_{\sigma,LV}$ | - low voltage winding leakage reactance |
| $X_M$ | - magnetization reactance |
| $R_{Fe}$ | - iron loss admittance |
| $\mu_c$ | - core magnetic permeability |
| $\phi_c$ | - core magnetic flux |
| $R_c$ | - core reluctance |
| $V_{eq}$ | - equivalent wind speed |
| $\theta_{pitch}$ | - pitch angle of the rotor blades |
| $\theta_{wtr}$ | - turbine rotor position |
| $T_{ae}$ | - aerodynamic torque |
| $\omega_{wtr}$ | - turbine rotor speed |
| $\alpha_{ss}, S_c$ | - soft starter angle, capacitor bank switch signals |
| $\omega_{gen}$ | - generator speed |
| $P_{ms}, Q_{ms}$ | - active and reactive power at the main switch |

$U_{wtt}, I_{wtt}$ - generator voltage and current interfacing with the power system

$R$ - rotor radius

$\Omega_{wtr}$ - turbine angular velocity

$v_{eq}$ - equivalent free wind speed

$T_{lss}$ - torque on low speed shaft

$T_{hss}$ - torque on high speed shaft torque

$K_s$ - flexible shaft stiffness

$C_s$ - flexible shaft damping coefficient

$\lambda$ - tip speed ratio

VSC - voltage source converter

$f_s$ - grid frequency

$n_s$ - ac machine's synchronous speed

$n_r$ - induction machine's rotor speed

$s$ - induction machine slip

$R_{th}$ - thevenin equivalent stator terminal resistance

$X_{th}$ - thevenin equivalent stator reactance

$V_{th}$ - thevenin equivalent stator voltage

$X'_2$ - rotor equivalent reactance

$R'_2$ - rotor equivalent resistance

$T_{\max}$ - maximum torque

$S_{T_{\max}}$ - slip at maximum torque

$\omega_{sync}$ - angular synchronous speed

$U_{s,r}$ - stator , rotor voltage

$R_{s,r}$ - stator , rotor voltage

$i_{s,r}$ - current through stator winding and rotor windings

$\psi_{s,r}$ - flux linkage in stator and rotor

Gen - conventional synchronous generator

$E$ - excitation voltage

$P_e$ - electrical power

$P_m$ - mechanical power

$H$ - generator inertia

$K_D$ - damping factor

$\delta_{cc}$ - critical clearing angle

CCT - Critical Clearing Time

FCT - Fault Clearing Time

$E'$ - transient electromotive force

cc - current controller

# INTRODUCTION

# 1

This thesis discusses the investigations carried out on the different types of wind generators and how these would affect the transient stability of a hypothetical power network as presented in this report. Focus was on the transient responses of the conventional synchronous generator's rotor angle and terminal voltage when connected to different types of wind generators. The three different wind generator technologies explored were the squirrel cage induction generator (SCIG), doubly-fed induction generator (DFIG) and the converter driven synchronous generator (CDSG).

## 1.1 Background to Research

In the last decade, environmental issues and concerns about global warming and the depletion of fossil fuels have increasingly come to the fore. Energy conservation policies in several countries have, therefore, been developed to be in support of the usage of renewable energy or so called "*green energy*" sources in an effort of reducing greenhouse gas emissions from the burning of fossil fuels for energy. These renewable energy sources could be wind, hydro, solar and biomass [2].

Among the renewable energy technologies being vigorously developed, wind turbine technology has undergone dramatic developments and is currently the world's fastest growing energy source [3]. By the end of 2008, there was a global total of 120 GW of installed wind power [4]. The continuing development of wind power, therefore, will require wind farms to offer a performance similar to that provided by the large synchronous generators [5]. Moreover, the high penetration of wind power in the electrical power system will begin to have an influence on the overall behaviour of the power system. Thus, limits may be placed on the permissible wind farm capacity that can be connected to the adjoining utility network.

Such limits could be founded on issues concerning flicker, dynamic stability (particularly for larger wind farms) and harmonic pollution. Generally, however, voltage rise tends to be the limiting factor. This condition typically arises when a peak in wind power generation occurs at the same time when there is a minimum demand on the power grid. The wind power reduction option which is used at times is that of a voltage control unit which limits the wind farm output [6].

The increased penetration over the last decade of wind energy into power systems has led to power system operators revising new grid interconnection codes in countries like Denmark and Germany. These newer connection conditions usually require wind generators to ride-through network faults and to participate in reactive power control, or atleast reconnect shortly after disturbances [7].

There is a demand on the controllability of the wind turbines on the basis that the overall performance of the power grid will increasingly be affected by the characteristics of the wind turbines. Because of this, one of the major concerns related to the high penetration level of the wind turbines is their impact on the stability of the power system [3].

## 1.2 Problem Statement

The number of wind generators that are being connected to power systems is going to continue increasing due to the essential need for clean energy and the depletion of fossil fuel which is used in powering some thermal power stations. However, wind generator concepts have different design characteristics. These characteristics will differently affect the power systems to which they will be connected.

## 1.3 Objectives of the Research

The objectives of this research are to:

- Investigate how the penetration level of squirrel cage induction generator, doubly-fed induction generator and converter driven synchronous generator models would affect the transient stability of the power system.

- Explore the influence that the controllers of the conventional synchronous generator i.e. automatic voltage regulator and speed governor, would have on the transient stability of the power system.

- Assess how the reactive power compensation technology of the different wind generator concepts affects the power system's transient stability.

- Discuss the dynamic behavior of the current controller of the variable speed wind generators (e.g. doubly-fed induction generator and converter driven synchronous generator) in transient conditions.

- Investigate the degree to which the variable speed wind generators current controller influences the transient stability of the power system.



## 1.4 Research Methodology

The approach which the author undertook the research was as follows:

- An extensive literature review was conducted on the electrical models to be used in the research. Past M.Sc. and Ph.D dissertations related to wind turbines and power system dynamics were used to find out what kind of power analysis software could be used in researching the impact of wind turbines on the transient stability of power systems.

- A hypothetical single machine infinite bus power network was developed using power analysis software (*DIgSILENT V13.2*) for the transient time domain simulations performed. Particular reference was made from [15] on the typical parameters for transmission lines rated at 230 kV. The simple power network model on which much of the quantitative simulations were done, was chosen so that it would be easier to distinctively place focus on how the electrical characteristics of the different wind generator concepts would affect the power system's transient stability.

## 1.5 Thesis Outline

The contents and arrangements of the seven chapters in the dissertation are described below:

**Chapter 1** introduces the main focus of the thesis. It further gives background information on the growth of wind power on power systems as well as associated concerns from the power network operators' point of view. It then presents the problem statement which formed the platform on which the research investigation was constructively carried out on. The objectives of the research are outlined accordingly and, the research methodology is described thereof. Contributions of the thesis are then listed and lastly the list of publications is presented.

**Chapter 2** contains a review of literature pertaining to wind power development, an analysis of different stability models and the principles behind the different reactive power control strategies used in variable speed wind generators. The theoretical aspects of the models (synchronous generators, wind generators, transformers and transmission lines) implemented in the simulation case studies are reviewed. The principal objective of this chapter is to enhance and reinforce theoretical understanding of used models and to bring about a clearer understanding of the simulation results. The concept of transient stability is also presented.

**Chapter 3** pays attention to the generic model of a wind turbine system. It elaborates on the wind model, aerodynamic model, transmission model and the generator model of the wind turbine. Models used for stability studies with respect to the different wind generator concepts are explained in mathematical terms. The chapter also looks into the power electronic systems used in wind energy conversion systems.

**Chapter 4** goes further to explore the transient stability of the power network with the connection of a squirrel cage induction generator based wind farm (WF). It highlights the aspect of having the WF located far away from the power grid and also how increasing the reactive power compensation affects transient stability. The principles of how the inertia of the squirrel cage induction generator (SCIG) affects the transient stability of the power system are explained. The power system controllers (AVR and speed governor) are introduced, and their influence on transient stability is also investigated.

**Chapter 5** introduces the DFIG model and its effect on the transient stability of the power system as the penetration level of the DFIG increases. First, the system controllers were not included, and later the AVR is included and its effect on the transient stability of the power system is observed. Focus is shifted to the effect of different reactive power set-points of the doubly-fed induction generator voltage source converter on the power system's transient stability. The Effect of different slip values of the doubly-fed induction were investigated in relation to the power network's transient stability. Different values of the VSC current controller's proportional gain were explored and the impact on the transient stability was analyzed thereof. There is also a comparison of the electrodynamic response of the power system when connected to a squirrel cage induction generator and when connected to a doubly-fed induction generator following a transient disturbance.

**Chapter 6** introduces the converter driven synchronous generator (CDSG) and its effect on the transient stability of the power system as the penetration level of the CDSG increases, whereby system controllers were not included. It explores the effect of different reactive power set points of the converter driven synchronous generator's voltage source (VSC) on the power network's transient stability. The influence of the system controllers on the transient stability of the power network is investigated with the CDSGs connected. The effect of the CDSG on the transient stability of the power system is compared with that of the DFIG, whereby no system controllers were included.

**Chapter 7** presents conclusions and recommendations for future work.

## 1.6 Contributions of the Thesis

- The simulation results brought about awareness that, the best level of reactive power compensation for a SCIG WF, in relation to the transient stability of the power system is not necessarily that level which is equal to the reactive power drawn by the wind farm. In this work, 0.67 p.u. of the rated reactive power drawn by the wind farm was found to be the level of reactive power compensation which resulted with the most preferred transient response of the power system.

- The IEEEG2 speed governor with the used parameters does not have any impact on the transient stability of the power system. The theoretical expectation was that, inclusion of the IEEEG2 speed governor would minimise the resultant acceleration power of the synchronous machine following the fault on the power grid. However, the IEEEG2 speed governor with the used parameters did not function to reduce the net imbalance between the mechanical power and the electrical power of the synchronous generator, and thus improve on the power system's transient stability.

- It was observed that changing the value of the proportional gain of the doubly-fed induction generator's current controller does not have a significant impact on the transient stability of the power system. This observation is based on the used gain settings of the current controller.

- A choice of the converter driven synchronous generator over the doubly-fed induction generator could be due to its superior support to the conventional synchronous generator's terminal voltage following a fault. The conventional synchronous generator's terminal voltage recovers much quicker when the CDSG is connected to the power system compared with when the DFIG was connected. Furthermore, increasing the number of CDSGs connected to the power grid, does not have much of an effect on the recovery time of the terminal voltage of the conventional synchronous generator.

## 1.7 List of Publications

Some of the results attained from the simulations conducted with the wind generator models in DIgSILENT were presented at two different conferences (IASTED 2008 and SAUPEC 2009). In both conferences the papers were presented to technical review committees comprising of experts before being accepted for publication. Having them published and presented in two different conferences indicated that the results were rational and also contributed to the global research with regards to the influence of wind generators on power system dynamics. The paper titled: *Effect of the Current Controller of a Converter Driven Synchronous Generator on the Transient Stability of a Power System* was accepted for publication in the proceedings of the AFRICON 2009 conference on the 12/07/2009.

- **IASTED** *Gaborone* (Botswana) 2008: *Impact of Wind Generators and Synchronous Generator Controllers on a Power System Transient Stability*

- **SAUPEC** *Stellenbosch* (R.S.A) 2009: *Effect of Fixed Speed Wind Generator Capacitor Bank on Transient Stability of a Power System*

- **AFRICON** *Nairobi* (Kenya) 2009: *Effect of the Current Controller of a Converter Driven Synchronous Generator on the Transient Stability of a Power System*

# LITERATURE REVIEW

# 2

## 2.1 Introduction

A wind energy conversion system is the most rapidly growing technology for renewable power generation in the world. This means that, designers are continuously improving on the development of the generators, power electronics, and the implementation of modern control strategies. With time, wind turbine designs have changed from being conventional to having optimal performance functionality. As wind power penetration keeps increasing, a need arises for wind turbines to be developed in such a way that they will be able to support the grid. The integration of large wind farms onto power systems has brought about concerns regarding power quality. These issues on power quality can be divided into two categories, *local issues* and *global issues* [1]. Local issues relate to voltage quality in distribution systems, whereas, global issues relate to the power system's control and stability. It is due to the impact of wind turbines on power systems that transmission system operators (TSO) issued special grid codes for wind turbine connection. Denmark and Germany are amongst several other countries revising such grid codes. The grid codes set specifications for the required standard of wind generator performance in order for the wind generators to be connected to the respective transmission system. Attention is placed mainly on the wind turbines fault ride through capability, as this is directed towards avoiding significant loss of the wind turbines production in the event of grid faults. An additional requirement to the Danish grid code is the power control capability of the wind turbines [1].

Market interest in fixed speed wind turbines has decreased over the years, whereas the market penetration of doubly-fed induction generator has increased from 0 % up to more than 60 % of the yearly installed power between 1995 – 2005, thus becoming the most dominant wind generators used for new wind farms by the end of 2005. By 2005, the countries considered to

form huge markets for wind power were Germany, Spain, USA, India and Denmark. However, Denmark leads in the manufacturing of wind turbines. The doubly-fed induction generator was first introduced in 1996 by a wind turbine manufacturering company called Tacke in Germany [1]. The full scale variable speed wind generator has experienced a slow increase in market penetration over the years. One of the reasons for the high penetration level of the doubly-fed induction generator (DFIG) over the squirrel cage induction generator (SCIG) for high capacity wind farms is that, DFIGs are able to control electrical torque (active power) and reactive power exchanged with the power network. In essence, DFIGs provide variable speed operation which translates to a higher energy yield given the same wind speed profile. Moreover, they offer superior performance in system stability during grid disturbances [9].

Nowadays, DFIG wind turbines constitute the mainstream configuration for large wind turbines. Thus their ability to support the grid during faults is of high priority [1]. DFIG based wind turbines are able to supply reactive current using rotor and line side converters. However, local severe grid faults may lead to the separation of the rotor side converter from the rotor circuit when the crowbar resistance is connected to the rotor circuit [8].

With regard to wind generator modelling, the fifth-order model of the induction generator is able to represent stator and rotor transients accurately. However, in stability studies, transient phenomena of the electrical network are not considered. Thus, by neglecting stator transients, the induction generator model leads to a third order model. In [10], reduced order models of the DFIG were validated against higher order DFIG models after being subjected to a relatively strong grid disturbance (i.e. three-phase short circuit at the point of connection of the wind generators to the transmission network) and a weak disturbance (i.e. three-phase short circuit at the terminals of the conventional synchronous generator, which is further away from the wind farm).The results thereof, with particular reference to the speed of the synchronous generator and the voltage profile of the wind farm at the point of common coupling, show that the simplified DFIG model including crow bar protection, together with a simplified grid side converter provide sufficient accuracy for carrying out stability studies in large power systems. However, [11] also validates a third order SCIG against a fifth order SCIG. Results in [11] highlight notable discrepancy between the two models whereby the

generator's different order models were exposed to a three phase short circuit in the power transmission network to which they were connected to. The third order model, which is representative of generator response without the fundamental-frequency transients, showed that the current magnitude is lower as compared with that of the fifth order model following the grid disturbance. With the third order machine, the speed of the generator increases immediately when the power network is subjected to a fault. In contrast, however, the fifth order model showed that the generator speed decreases shortly after the fault occurred on the power grid. Since the reactive power consumption of the SCIG depends on the generator rotor slip, a larger acceleration of the rotor results in large reactive power absorption. Hence the third order model predicts a more pessimistic voltage profile at the point of common coupling of the SCIG based wind farm after the transient fault, than is the case of a fifth order generator model. Reference [12] goes further to point out that, when there are voltage dips on the grid, the rotor speed of the SCIG may increase to a point where the SCIG loses its stability. In the progression of the transient event, the rotor speed may be reduced to some degree, by the possible active power exchange with the grid during the voltage dip. This effectively reduces the risk of disconnection of the SCIG upon triggering of the overspeed protection. With respect to the DFIG, it is shown that if the rotor side converter blocks during a voltage dip on the power grid, the DFIG behaves as a SCIG, and the voltage dip recovers relatively quickly to its initial value following the clearing of the fault [12]. The need for reactive power from the induction generator due to its magnetization is compensated to a certain extent by the reactive power produced by the rotor converter if connected [12]. Looking at the synchronous wind generator coupled with a full scale converter, the response following a voltage dip on the grid is that, the voltage dip recovers to its initial value after the fault is cleared. As it is, the converters of the synchronous wind generator can control the frequency on the stator of the wind generator as well as the active power supplied to the grid. This serves to aid the wind generator through voltage dips without loss of stability.

The squirrel cage induction generator consumes reactive power when in operation, hence, in practice, the induction machine is compensated using shunt capacitors which provide constant reactive power. However, for a controllable reactive power source, a static compensator (STATCOM) can be deployed. The STATCOM uses insulated gate bipolar transistors (IGBT)

and shifted pulse width modulation for generation of the gating signals. Another aspect to using the STATCOM is that, it also serves to limit voltage fluctuations resulting from variable output power [13].

The line side converter (LSC) of the DFIG can contribute to reactive power control, and in addition the LSC can provide reactive power support if operated as STATCOM [9]. The different modes of DFIG reactive power control are [9]:

***Fixed power factor operation***: Power factor is normally maintained at unity, even though other pf values (e.g. 0.95 lagging to 0.95 leading) can be set within operating limits. In this mode, rotor excitation is attained such that all magnetizing current is supplied through the rotor while the stator's reactive power is neutral.

***Voltage control by rotor excitation***: In this mode, the reactive power from the stator is changed in order to maintain the set voltage at the point of common coupling in accordance to the reference values. The reactive power is attained through the use of a PI controller with set reactive power limits.

***Voltage control through a LSC***: The line side converter (LSC) operates in an ac voltage – oriented reference frame whereby, d and q axis current components control the active and reactive power respectively. The d-axis current ensures that the rotor power is absorbed or supplied into the power network so that the dc-link voltage is maintained at a constant 1 p.u. The q-axis current, is varied so as to control terminal voltage by adjusting the reactive power output of the LSC.

***Voltage control using both the RSC and the LSC***: The concept of using both rotor side converter (RSC) and line side converter (LSC) for voltage control, is based on the operational principle of minimizing losses in both converters. In this mode of reactive power control there are two possible strategies, it is the *uncoordinated voltage control* and the *coordinated voltage control.* The *uncoordinated voltage control* is where, both the reactive power of the LSC and RSC are regulated to offer voltage control. The risk is that, circulating currents may occur between the stator and the LSC. Each of the two controllers would be trying to regulate the voltage without being aware of the state of operation that the other one would be in. With the *coordinated voltage control,* the RSC can be set as the default controller and the LSC can be used as a supplementary source for specific situations. Alternatively, the LSC can be the default controller, and then the rotor excitation can be increased when the LSC gets to its

current limit. Another solution is to have the reactive power split according to a given ratio. Where, for instance, two-thirds of $Q_{ref}$ can be supplied by the stator as this is also in relation to the rating of the machine being two to three times greater than the rating of the LSC [9]. With respect to the synchronous wind generator having its stator terminals coupled to a full scale converter, the grid side inverter's controller's objective is to regulate the output power of the wind turbine (WT) when connected to the power grid. The controller comprises of an inner current loop which is based on a hysteresis controller. Its prime objective is to fine-tune the output currents to their reference values [14].

Due to the unpredictable nature of wind energy, high penetration levels into power network systems raises problems. These could be related to unreliability in planning for wind farm output power, increased frequency oscillations and reduced suitability of system governors for maintaining stability against major load fluctuations [50]. In large wind farms connected to the transmission network, the main technical constraint on high penetration of wind power on power systems is characterized by the transient stability of the power network [51].

## 2.2 Synchronous Machine

### 2.2.1 Description of a Three Phase Synchronous Machine

Synchronous generators (alternators) are used as the main sources of electric power within power systems. This machine belongs to the family of electric rotating machines, in which the induction generator or motor and the direct current (dc) generator or motor are a part of.

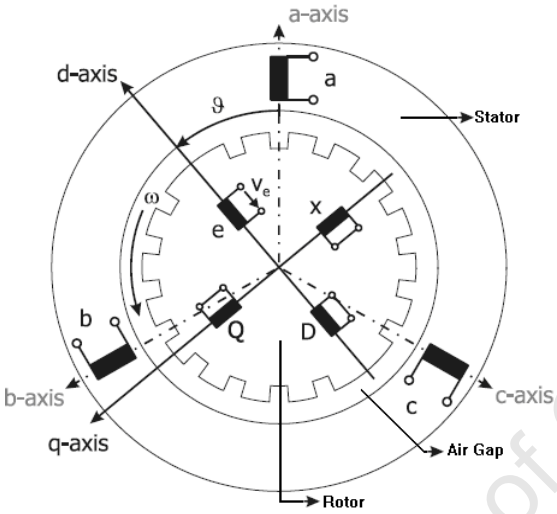


**Fig.2.1:** Round rotor synchronous machine[16]

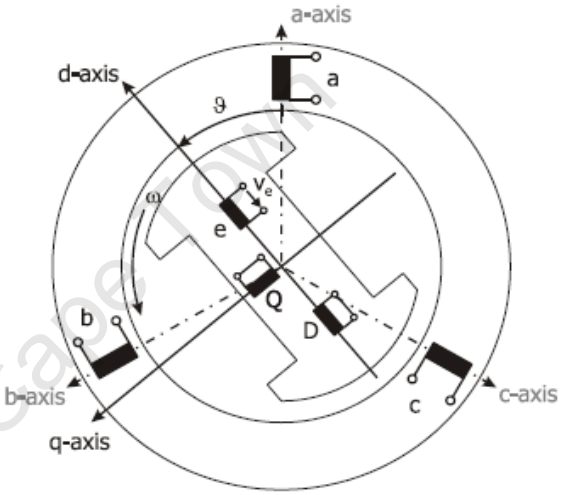


**Fig 2.2:** Salient rotor synchronous machine[16]

Figures 2.1 and 2.2 show the schematic of the cross section of a three-phase round rotor and salient rotor synchronous machine. The machine is made of two critical elements: the field and the armature windings labeled **Ve** and (**a,b,c**) respectively. The field winding carries direct current and produces a magnetic field which induces alternating voltages in the armature windings as the rotor rotates within the air gap of the stator. The windings indicated with **D, X** and **Q** in both the d and q axes are the damper windings or amotisseurs, and they damp out speed oscillations. The three – phase windings of the armature are distributed and 120° apart so that uniform rotation of the magnetic field produces voltages displaced by 120° in the armature windings [15]. The symbol $\vartheta$ represents the rotor angle, which is the angle between the d-axis and the stator field [16].

When balanced three – phase currents flow through the armature, a magnetic field rotating at synchronous speed will be produced in the air gap. The field created by the direct current in the field winding revolves with the rotor. Steady torque is developed when the stator and rotor

fields rotate at the same speed, hence the rotor's angular speed should be at the synchronous speed. The synchronous speed is defined as:

$$n_s = \frac{120 * f_s}{p_f} \tag{2.2-1}$$

where $n_s$ is speed in rpm, $f_s$ is frequency in Hz, and $p_f$ is the number of field poles.

Synchronous generators with a round rotor are used when the shaft is to rotate with or close to synchronous speed of 1500 rpm to 3000 rpm. These types are normally used in thermal or nuclear power plants. Slow rotating synchronous generators with salient rotors, rotate with speeds of 60 rpm to 750 rpm. They are commonly used in hydro or diesel power plants [16].

## 2.2.2 Mathematical Description

To describe the generator equations, it is common practice not to use instantaneous values leading to a three dimensional problem in the abc coordinate system, but to transform all values into a rotating reference frame as shown in the following equations. This transformation is called *dqo,* or *Park's* Transformation [16].

***Per unit stator voltage equations***

$$e_d = \frac{d\psi_d}{dt} - \psi_q \omega_r - R_a i_d \tag{2.2-2}$$

$$e_q = \frac{d\psi_d}{dt} + \psi_d \omega_r - R_a i_q \tag{2.2-3}$$

$$e_0 = \frac{d\psi_0}{dt} - R_a i_0 \tag{2.2-4}$$

where :

$e_d, e_q, e_0$ - *d*, *q*, *0* - axis components of terminal voltage
$\psi_d, \psi_q, \psi_0$ - *d*, *q*, *0* - axis components of stator flux
$i_d$ , $i_q$ , $i_0$ - *d*, *q*, *0* - axis components of stator current
$R_a$ - stator resistance

***Per unit rotor voltage equations***

$$e_{fd} = \frac{d\psi_{fd}}{dt} + R_{fd} i_{fd} \tag{2.2-5}$$

$$0 = \frac{d\psi_{1d}}{dt} + R_{1d} i_{1d} \tag{2.2-6}$$

$$0 = \frac{d\psi_{1q}}{dt} + R_{1q} i_{1q} \tag{2.2-7}$$

$$0 = \frac{d\psi_{2q}}{dt} + R_{2q} i_{2q} \tag{2.2-8}$$

where:

$e_{fd}$ - rotor field voltage along the *d* - axis
$\psi_{fd}, \psi_{1d}$ - flux in field winding and damper winding in *d* - axis
$\psi_{1q,} \psi_{2q}$ - flux in damper windings in the *q* - axis
$R_{fd}$ - resistance in rotor field winding in *d* - axis
$R_{1d}, R_{1,2q}$ - resistance in damper windings in *d*, *q* - axis
$i_{fd}$ - current in field winding in *d* - axis
$i_{1d}, i_{1,2q}$ - current in damper windings along *d*, *q* – axis

***Per unit air gap torque***

$$T_e = \psi_d i_q - \psi_q i_d \tag{2.2-9}$$

.

***Per unit rotor equations of motion***

$$\frac{d}{dt}\omega_r = \frac{1}{M}\left(T_m - T_e - T_D\right) \tag{2.2-10}$$

$$\frac{d}{dt}\delta = \left(\omega_r - 1\right) \tag{2.2-11}$$

$$T_D = K_D\left(\omega_r - 1\right) \tag{2.2-12}$$

where:

$T_m, T_e, T_D$ - mechanical torque, electrical torque and damping torque
$M$ - generator moment of inertia
$\delta$ - generator rotor angle
$K_D$ - damping factor

## 2.3 Power Transformer

Generation of power in large generating stations is usually in the range of 11 kV to 30 kV. Effective and efficient transmission over long distances requires much higher voltages. These high voltages can be in the ranges of 138, 230, 275, 345, 400,765 kV or higher. The different levels of transmitting high voltage vary globally. In South Africa, the power transmitted over these high voltage lines is fed to Eskoms's major substations where the voltage is reduced and the electricity is distributed to smaller substations all over the country at sub-transmission levels (i.e 132 kV, 88 kV or 66 kV). At the smaller substations, voltage is reduced further to 22 kV and 11 kV known as reticulation voltage level. Distribution of power is at much lower voltage levels of 2400 V or 4160 V, which is stepped down to 440 V for typical industrial use or 240/120 V for commercial residential use. The change in voltage levels is realized by the usage of a transformer [17, 18].

A transformer is fundamentally made of two or more windings coupled by a mutual magnetic field .Ferromagnetic cores are used to provide intense magnetic coupling and high flux densities. Such transformers are known as iron core transformers [19].

## 2.3.1 Modelling of a Two Winding Transformer

Figure 2.3 is a detailed model of a three - phase, two winding transformer which is schematically showing connection of one phase.

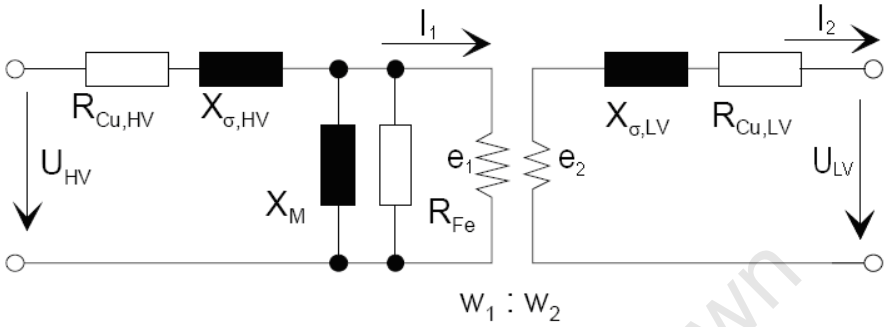


**Fig 2.3** Model of a two winding transformer [20]

Where $R_{Cu,HV}$, $R_{Cu,LV}$ represent the winding resistances of the high voltage (HV) and low voltage (LV) side , $X_{\sigma,HV}$, $X_{\sigma,LV}$ refer to the HV and LV leakage reactances respectively . $X_M$ is the magnetization reactance and $R_{Fe}$ is the iron loss admittance [20]. An ideal transformer model is more often assumed in an effort to characteristically explain the chief operation of a transformer. With the ideal transformer model, the following assumptions are put in place:

- The windings have zero resistance, thus $I^2R$ losses in the windings are zero
- The core permeability $\mu_c$ is infinite, relating to zero core reluctance $R_c$. Hence the exciting current required to establish flux in the core is negligible.
- There are no core losses
- There is no leakage flux , the entire flux $\phi_c$ is confined to the core and links both windings [21].

The product of the core reluctance and core magnetic flux is expressed as follows

$$R_c \cdot \phi_c = W_1 I_1 - W_2 I_2 \qquad (2.3\text{-}1)$$

where $W_{1,2}$ is the primary and secondary winding, and $I_{1,2}$ is current in primary winding and secondary winding respectively.

With $R_c = 0$ then

$$\frac{W_1}{W_2} = \frac{I_2}{I_1} \tag{2.3-2}$$

When the high voltage winding (primary winding) is connected to a time varying voltage $U_{HV} = v_1$ a time varying flux $\phi_c$ is established in the core. A voltage $e_1$ will be induced in the winding and will equal the applied voltage if resistance of the winding is neglected;

$$v_1 = e_1 = W_1 \frac{d\phi_c}{dt} \tag{2.3-3}$$

The core flux links the secondary windings and induces a voltage $e_2$ which is equal to the terminal voltage $U_{LV} = v_2$ such that

$$v_2 = e_2 = W_2 \frac{d\phi_c}{dt} \tag{2.3-4}$$

From equation (2.3-3) and (2.3-4) the following expression is deduced

$$\frac{v_1}{v_2} = \frac{W_1}{W_2} \tag{2.3-5}$$

## 2.4 Transmission Lines

Electrical power is transferred from generating stations to consumers through over head transmission lines or underground cables. All transmission lines in power systems have the following electrical properties; series resistance ($R$), series inductive reactance ($X_L$), shunt conductance ($G$) and shunt susceptance ($B$). It therefore follows that the line series impedance ($Z$) is defined as:

$$Z = R + jX_L \tag{2.4-1}$$

and the line shunt admittance is defined as:

$$Y = G + jB \tag{2.4-2}$$

The $R$ accounts for line losses ($I^2R$), $X_L$ causes voltage drop, $B$ delivers reactive power by giving rise to line charging current and $G$ factors the $V^2G$ line losses due to leakage currents between the conductors or between conductors and the ground .The leakage currents are insignificant compared with the current flowing in the transmission line and may thus be disregarded. For 50 Hz power systems short lines have a length ($l$) < 100 km. Medium length lines have 100 km < $l$ < 300 km and long lines have $l$ > 300 km. For short lines, the capacitance in the line model is overlooked without factoring error that is noteworthy to the line model. Figure 2.4 shows a model circuit used for medium length transmission lines.

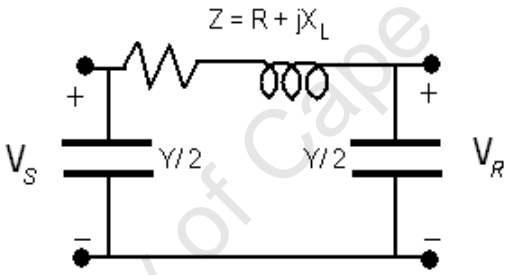


**Fig 2.4:** Nominal $\pi$ circuit model of a medium length transmission line

Where $V_{S,R}$ is the sending and receiving end voltage respectively. For this model, line charging current is considerable and the shunt capacitance is included. Half of the total capacitance may be lumped at each end of the transmission line. The circuit model of Figure 2.4 is referred to as the nominal $\pi$ circuit. For lines of 300 km (for a 50 Hz system) and longer, line constants $R$, $L$ and $C$ are not lumped , but uniformly distributed along the line. Thus, it is fitting to represent the terminal characteristics of a long transmission line by using an equivalent $\pi$ circuit model [22].

### 2.4.1 Surge Impedance Loading

In power systems, high voltage lines are assumed to be lossless i.e. $R = G = 0$, when focus is on lightning and switching surges [15]. In this context, the characteristic impedance (surge impedance) $Z_c$ of the line is defined as;

$$Z_c = \sqrt{\frac{Z}{Y}} = \sqrt{\frac{L}{C}} \ \ \Omega \tag{2.4-3}$$

which is purely resistive. It is a function of the line inductance and capacitance and is independent of the length of the line. The surge impedance loading (SIL) of a transmission line is defined as the active power delivered by the line to a purely resistive load which is equal in magnitude to its surge impedance [48]. Hence,

$$\text{SIL} = \frac{\left|k V_{R(L-L)}\right|^2}{Z_c} \ \text{MW} \tag{2.4-4}$$

Where:

SIL - surge impedance loading
$\left|k V_{R(L-L)}\right|$ - rated line-line voltage of the line in kilovolts
$Z_c$ - surge impedance in ohms

It can be noted that;

- At SIL, the magnitude of voltage and current at any given point along a lossless line is constant, and thus the voltage profile is flat.
- Real power along a lossless line at SIL is constant from the sending end to the receiving end.
- Reactive power is zero at SIL, i.e. the reactive power losses in the inductance of the line are offset by the reactive power supplied by the shunt capacitance of the line.

SIL is a useful measure of the capacity of the transmission line since it indicates a loading where the line's reactive power requirements are small. On long transmission lines, light loads which are significantly less than the SIL result in a rise of voltage at the receiving end. Heavy loads which are much greater than the SIL will produce a large dip of the voltage at the receiving end of the line [22].

## 2.5 Power System Stability

Power system stability may be defined as that feature of a power system which makes it possible for the power system to maintain a state of equilibrium when operating under normal conditions and to be able to attain an acceptable state of operation after being exposed to a disturbance. In order to understand stability problems, it becomes a necessity to classify stability into various categories, in this case, focus will be on rotor angle stability [15].

Rotor angle stability is defined as the capability of interconnected synchronous machines of a power system to remain operational in synchronism. This stability problem is premised on the study of the electromechanical oscillations inherent to power systems. A prime factor in this problem is the manner in which the output power of the synchronous machines varies as their rotors oscillate. It is common practice to subdivide the rotor angle stability into two categories, namely, transient stability and small – signal stability, with the former being of particular interest and relevance to the work presented in subsequent chapters [15, 23].

### 2.5.1 Transient Stability

Transient stability is associated with the ability of the power system to maintain synchronism after being exposed to a severe disturbance such as a short-circuit on a transmission line, sudden load change, and the loss of a tie between two subsystems. The response of the system after being subjected to a large disturbance is characterized by large excursions of the generator rotor angle (first swing stability) and is influenced by the nonlinear power – angle relationship. Stability primarily depends on magnitude and location of the disturbance and, to a lesser extent, upon the initial state or operating condition of the system. Time domain simulations have traditionally been used to mostly assess the first swing stability and also to gain insight into the dynamics of subsequent rotor oscillations following the first swing [23, 24].

The focal point thus culminates in whether the power system will return to a steady state and maintain synchronism following a severe fault of a transient period.

In some large power systems, transient instability may not always occur as first swing instability, it could be due to the interaction of several modes of oscillation causing large excursions of rotor angle beyond the first swing [15].

#### 2.5.1.1 Factors Influencing Transient Stability [15]

- Post-fault transmission system reactance;
- Generator output during fault. This depends on the fault location and type;
- Fault clearing time;
- Generator reactance: lower reactance increases peak power and reduces initial rotor angle;
- Generator inertia: the higher the inertia, the slower the rate of change in angle. This reduces the kinetic energy gained during the fault;
- Generator internal voltage magnitude: this depends on the field excitation;
- The degree to which the generator is loaded; and
- The infinite bus voltage.

#### 2.5.1.2 Synchronous Machine Equation of Motion

Non – linear system equations are used to analyze the problem of transient stability. Hence, the rotor motion is determined by Newton's second law as follows [23]:

$$\frac{2H}{\omega_{sync}}\frac{d^2\delta}{dt^2} = P_m - P_e - \frac{K_D}{\omega_{sync}}\frac{d\delta}{dt} = P_a \qquad (2.5\text{-}1)$$

where $H$ is the rotor inertia , $\delta$ is rotor angular position with respect to a synchronously rotating reference , $P_m$ is the mechanical power, $P_e$ is electrical power, $K_D$ is the damping factor, $P_a$ is the acceleration power and $\omega_{sync}$ is synchronous angular speed.

Equation (2.5-1) is called the swing equation, which is the fundamental equation that determines rotor dynamics in transient stability studies. Generally damping is not considered to be a critical factor in transient stability and may be neglected from the swing equation [23].

### 2.5.1.3 Synchronous Machine Model in Stability Studies

For stability analysis of large power systems, it is necessary to neglect the transformer voltage terms (stator flux transients) $\frac{d\psi_d}{dt}$ and $\frac{d\psi_q}{dt}$ from the stator voltage. This is rationalized by the quick decay of transients associated with the network. The effect of speed variations on the stator voltage is also neglected, this is because changes in $\omega_r$ are small and thus have an insignificant effect on the stator voltage. Therefore $\omega_r$ is assumed to have a per unit value of 1.0 [15]. These simplifications result in the following stator voltage equations as simplified from equations 2.2-2 and 2.2-3.

$$e_d = -\psi_q - R_a i_d \tag{2.5-2}$$

$$e_q = \psi_d - R_a i_q \tag{2.5-3}$$

Figure 2.5 shows the simplified transient model of the synchronous generator.

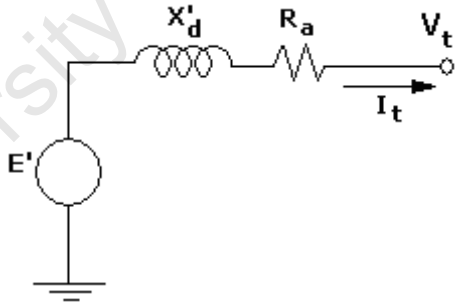


**Fig 2.5:** Positive sequence equivalent circuit of a synchronous machine [15]

The value of the positive sequence reactance $X_d$ depends on the time frame of interest: sub transient $X''_d$, transient $X'_d$ and steady state $X_d$ [15], where $E'$ is the generator excitation voltage and $V_t$ is the generator's terminal voltage.

During a transient disturbance, the excitation voltage $E'$ is assumed to be constant and is defined as:

$$E' = V_t + R_a I_t + jX'_d I_t \tag{2.5-4}$$

In most stability studies the machine losses and network resistances are neglected [15], hence equation (2.5-4) is normally expressed without the armature resistance $R_a$, which would also be neglected in Figure 2.5.

### 2.5.1.4 Synchronous Machine Model Including Saliency

Since the type of synchronous generator model used in the simulations is of a salient – pole, it becomes a necessity to include the effect of saliency. This is on the basis that, salient – pole rotor results in a non-uniform magnetic reluctance in the air gap. The reluctance along the direct axis is considerably less than that along the quadrature axis. The reactance therefore has a high value $X_d$ along the direct axis and a low value $X_q$ along the quadrature axis. These reactances produce voltage drop in the armature and are taken into account by resolving the armature current $I_t$ into two components $I_d$ in time quadrature with the excitation voltage and $I_q$ which is in phase with the excitation voltage $E$. During a transient period, the effect of transient saliency is included and the direct axis transient reactance $X'_d$ is used. The quadrature axis transient reactance $X'_q$ remains the same as $X_q$ because the field is on the direct axis [23].

The fundamental (phasor) voltage equation for a salient pole generator is [25]:

$$E_q = V_t + jX_dI_d + jX_qI_q \tag{2.5-5}$$

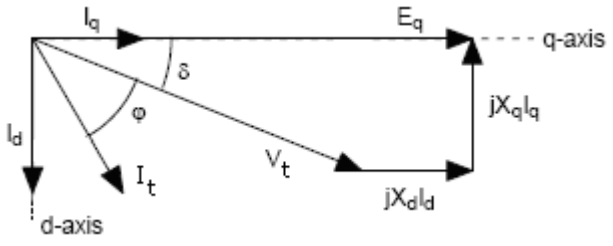


**Fig 2.6:** Phasor diagram of a salient - pole synchronous generator [25]

The power angle equation for steady – state condition is given as [23]:

$$|E_q| = |E| = |V_t|\cos\delta + X_d I_d = |V_t|\cos\delta + X_d |I_t|\sin(\delta+\varphi) \tag{2.5-6}$$

From Figure 2.6 it is observed that:

$$|V_t|\sin\delta = X_q I_q = X_q |I_t|\cos(\delta+\varphi) = X_q |I_t|(\cos\delta\cos\varphi - \sin\delta\sin\varphi) \tag{2.5-7}$$

which equates $\delta$ to:

$$\delta = \tan^{-1}\frac{X_q |I_t|\cos\varphi}{|V_t| + X_q |I_t|\sin\varphi} \tag{2.5-8}$$

It then follows that:

$$I_d = |I_t|\sin(\delta+\varphi) \tag{2.5-9}$$

$$I_q = |I_t|\cos(\delta+\varphi) \tag{2.5-10}$$

To calculate the transient excitation voltage $E'$ of the generator $X_d$ is replaced with $X'_d$ in the following equation:

$$|E'_q| = |V_t|\cos\delta + X'_d I_d = |V_t|\cos\delta + X'_d |I_t|\sin(\delta+\varphi) \tag{2.5-11}$$

From equation (2.5-6), we find that:

$$|I_t|\sin(\delta+\varphi) = \frac{|E_q| - |V|\cos\delta}{X_d} \tag{2.5-12}$$

This then, by substitution of (2.5-12) into (2.5-11) leads to:

$$|E'_q| = \frac{X'_d |E_q| + (X_d - X'_d)|V_t|\cos\delta}{X_d} \tag{2.5-13}$$

The steady-state active and reactive powers output of the generator are then defined as [25]:

$$P_e = \frac{E_q V_t}{X_d}\sin\delta + \frac{V_t^2}{2}\left(\frac{1}{X_q} - \frac{1}{X_d}\right)\sin 2\delta = P_{field} + P_{reluc\,\tan ce} \qquad (2.5\text{-}14)$$

$$Q_e = \frac{E_q V_t}{X_d}\cos\delta - V_t^2\left(\frac{\cos^2\delta}{X_d} + \frac{\sin^2\delta}{X_q}\right) \qquad (2.5\text{-}15)$$

The transient power – angle equation is obtained by substituting $X_d$ with $X'_d$ and $E_q$ with $E_q^{'}$ in (2.5-14).

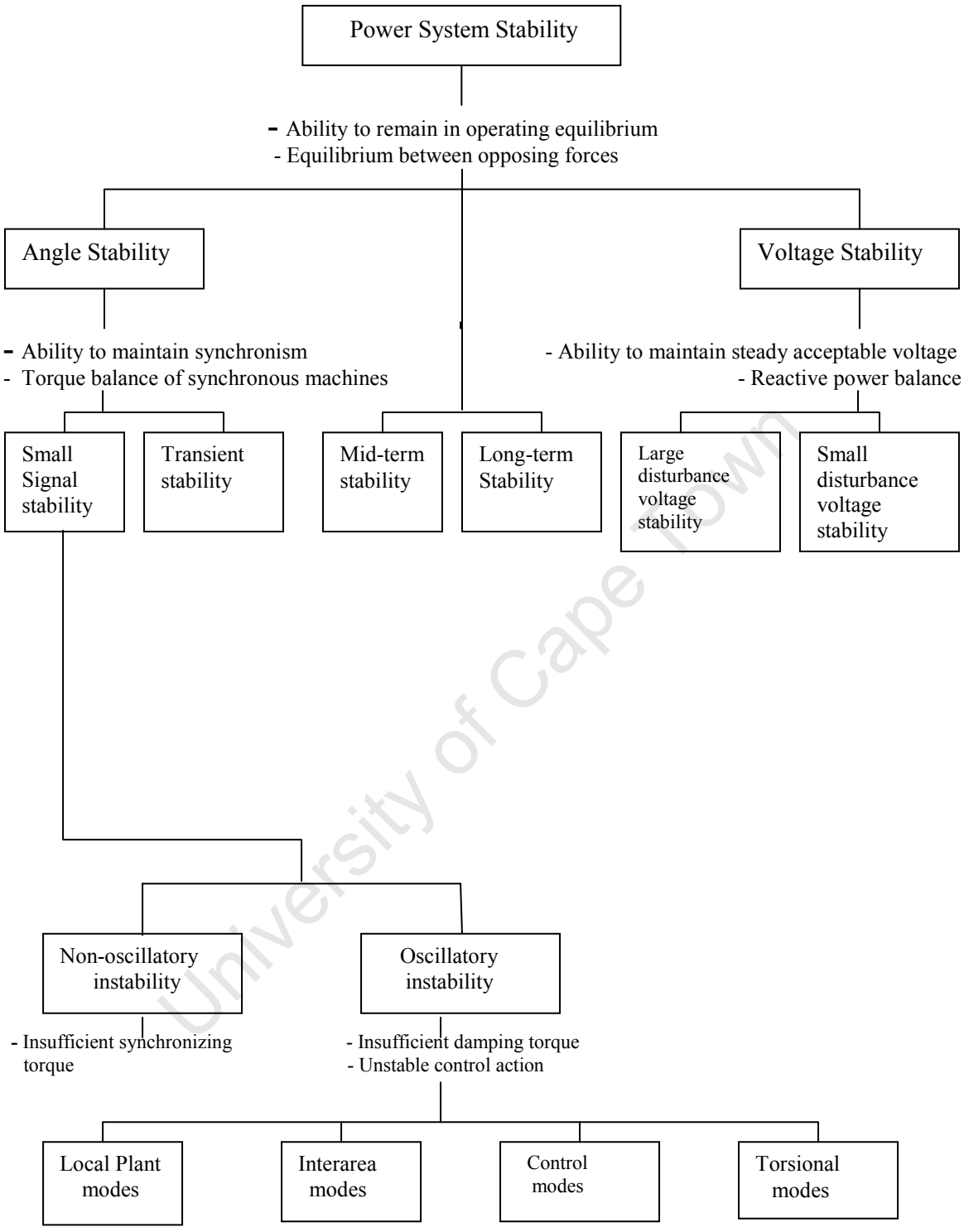




**Fig 2.7:** Classification of power system stability [15]

## 2.5.2 Power System Stability Assessment

Amongst several adopted theoretical methods used in evaluating a power systems transient stability, the Equal Area Criterion (EAC) is the most famously used. It is a graphical method that compares the amount of accelerating energy during the fault, with the amount of decelerating energy after the fault is cleared [26].This method is explained further in Appendix 5. However, the inefficiency of this method is its inapplicability in multi-machines system. It is in such situations that time domain simulations become most practical, and predominantly used tools.

### 2.5.2.1 Time Domain Simulations

Transient stability is normally evaluated with use of special transient stability programs (TSPs), such as PSS/E™ (Power System Simulator for Engineers), Simpow™ , Netomac™, CYMSTAB and DIgSILENT PowerFactory. These computer programs generally have a phasor representation of all electrical components. In some of these TSPs, only the positive sequence is represented, whereas other TSPs include a representation of the negative and zero sequences. Simulations are thereof performed in the time domain, and immediate simulation outputs are the root mean square (RMS) values of voltages, currents and other quantities derived therein [27].

Typical ranges of time periods used in different categories of time domain simulations are as follows [24]:

- Short – term simulations are approximately not longer than 10 seconds, but some cases could be as long as up to half a minute. These simulations investigate the transient stability of a power system.

- Mid – term simulations are run for up to five minutes , however they can also be extended to ten minutes. These types of simulations investigate dynamic stability (oscillatory stability) of the power system.

- Long – term simulations are longer than twenty minutes.

MATLAB is software which can be used for steady state stability calculations and slow dynamic stability studies. It is greatly accepted by engineers and researchers due to its detailed applications and versatility. Another software which has been in use for some time since the beginning of computer applications is PSS/E. This software yields good results when short–term and mid-term electromechanical oscillations are to be investigated [24].

#### 2.5.2.2 Transient Stability Program used in this Study

DIgSILENT PowerFactory was chosen for carrying out the time domain simulations presented in the subsequent chapters. The basis for choosing DIgSILENT is that, it provides a comprehensive library of models for electrical components in the power system e.g. generators, motors, power plant controllers, dynamic loads, transmission lines, transformers, shunts and static loads. The software also provides electrical components of the wind turbine, built with standard component models from the DIgSILENT library. The wind speed model, aerodynamic model, mechanical model and the control parts of the wind turbine can only be built and implemented in the dynamic simulation language DSL of DIgSILENT. DSL makes it possible for the user to employ specific models that are not standard in the DIgSILENT library. In respect of this aspect, the user will have created his own definition blocks, either as modifications to the existing models or as entirely new models. The developed models are gathered in a personal library which can be used for further modeling of other system configurations. DIgSILENT combines a transient EMT (electromagnetic transient) simulation tool for power systems with the RMS simulations of long term dynamics. RMS simulations are based on electromechanical transient models which are more simplified models as compared with the electromagnetic models used in EMT simulations. RMS simulations are more suitable for long simulation periods without transients, as is the case in most studies of power quality and power system stability. However, simulations of instantaneous EMT values with detailed models are essential for steadfast simulations of the behaviour of the system and its components during grid faults [28].

The RMS simulations deployed in DIgSILENT use third order models for the generators. Here the states of interest are the rotor speed, rotor angle and the flux linkage with respect to the field winding on the direct axis.

# WIND GENERATOR CONCEPTS AND MODELLING FOR STABILITY STUDIES

# 3

## 3.1 Introduction

A block diagram of how a wind energy conversion system's chief sub-models are arranged is presented below. It is in this chapter that, the wind model, which is primarily used in studies pertaining to power quality, is explained. The aerodynamic model and the mechanical model are further elaborated on. The modelling description of an induction machine is presented as well as the modelling used in stability studies as applied in TSPs in relation to the three types of wind generator concepts (i.e. fixed speed, doubly-fed and converter driven synchronous wind generators). Moreover, the power electronic systems used in wind energy conversion systems are also documented.



## 3.2 Wind Turbine Modelling

Figure 3.1 shows a simplified block model of a wind turbine. The wind turbine model is essentially made of the wind model, an aerodynamic model, a transmission system, generator model and a control model.

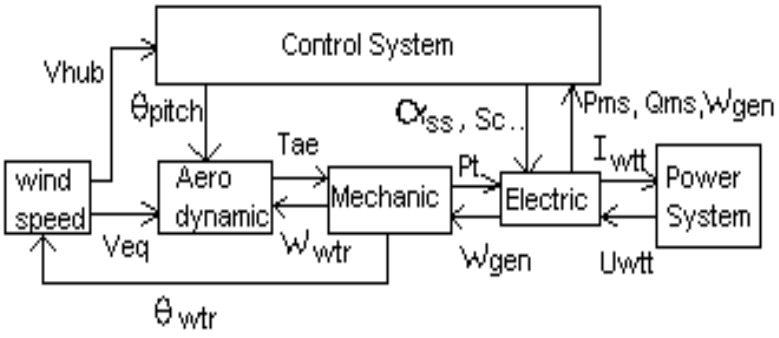


**Fig 3.1:** Block diagram of a systematic connection of wind turbine sub-models [30]

Where:

$V_{hub}$ is hub Wind Speed, $V_{eq}$ is equivalent wind speed, $\theta_{pitch}$ is pitch angle of the rotor blades, $\theta_{wtr}$ is turbine rotor position, $T_{ae}$ is aerodynamic torque, $\omega_{wtr}$ turbine rotor speed, $\alpha_{ss}, S_c$ is Soft starter angle and capacitor bank switch signal, $\omega_{gen}$ is generator speed, $P_{ms}, Q_{ms}$ is active and reactive power at the main switch and $U_{wtt}, I_{wtt}$ is generator voltage and current interfacing with the power system .

### 3.2.1 Wind Model

A wind speed model is ideal for simultaneous simulation of a large number of wind turbines, making it possible to estimate efficiently the impact of a large wind farm on the power quality [29]. It is often assumed in literature concerning the simulation of wind power in electrical systems that the wind speed is made up by the sum of the following four components [27]:

- Average value;
- A ramp component, representing a steady increase in wind speed;
- A gust component , representing a gust ;
- A component representing turbulence.

This leads to the following equation:

$$v_w(t) = v_{wa} + v_{wr}(t) + v_{wg}(t) + v_{wt}(t) \tag{3.2-1}$$

in which $v_w(t)$ is the wind speed at time $t$ , $v_{wa}$ is the average value of the wind speed, $v_{wr}(t)$ is the ramp component, $v_{wg}(t)$ is the gust component and $v_{wt}(t)$ is the turbulence component.

However, in simulation cases concerned with transient faults on the power network, the wind speed can be assumed constant on the basis that, grid disturbances are much faster than wind speed variations [29].

### 3.2.2 Aerodynamic Model

The aerodynamic model is based on the aerodynamic efficiency coefficient $c_p(\lambda, \theta_{pitch})$, which is a function of the tip speed ratio ($\lambda$) and the pitch angle ($\theta_{pitch}$) . This simplification is acceptable for as long as only the effect of the aerodynamic torque is taken into consideration [30].

The tip speed ratio is defined as:

$$\lambda = \frac{R \cdot \omega_{wtr}}{V_{eq}} \tag{3.2-2}$$

where $R$ is turbine rotor radius.

For a given turbine rotor, $c_p(\lambda, \theta_{pitch})$ depends on the pitch angle and the tip speed ratio. The aerodynamic efficiency is then used to determine the aerodynamic power $P_{ae}$ developed on the main shaft of a wind turbine with a given rotor blade radius at a given wind speed and air density [30]. This power is defined as follows:

$$P_{ae} = 1/2\, \rho \cdot \pi \cdot R^2 \cdot V_{eq}{}^3 \cdot C_p\left(\lambda, \theta_{pitch}\right) \tag{3.2-3}$$

This mathematical expression is derived from the following mathematical argument:

- The kinetic energy of a mass of air $m$ having the speed $v_{eq}$ is given by [31]:

$$E_k = \frac{m}{2} \cdot V_{eq}{}^2 \tag{3.2-4}$$

- the power associated with this moving air mass is the derivative of the kinetic energy with respect to time:

$$P_o = \frac{\partial E_k}{\partial t} = \frac{1}{2} \cdot \frac{\partial m}{\partial t} \cdot V_{eq}{}^2 = \frac{1}{2} \cdot q \cdot V_{eq}{}^2 \tag{3.2-5}$$

- where $q$ represents the mass flow given by the expression

$$q = \rho \cdot V_{eq} \cdot A \tag{3.2-6}$$

Where $A$ = cross section of the air mass flow.

Only a fraction of the total kinetic power can be extracted by a wind turbine and converted into rotational power at the shaft. This fraction is dependant on the aerodynamic efficiency coefficient $c_p$ [31]. This can be realized as:

$$c_p = \frac{P_{wind}}{P_o} \tag{3.2-7}$$

where $P_{wind}$ = Wind Power

$P_o$ = Power associated with moving air

- the resultant is the aerodynamic power:

$$P_{ae} = 1/2 \cdot \rho \cdot \pi \cdot R^2 \cdot V_{eq}{}^3 \cdot C_p\left(\lambda, \theta_{pitch}\right) \tag{3.2-8}$$

Once the aerodynamic power has been calculated the aerodynamic torque $T_{ae}$ can be calculated as follows:

$$T_{ae} = \frac{P_{ae}}{\omega_{wtr}} = \frac{\pi}{2 \cdot \lambda} \cdot \rho \cdot R^3 \cdot V_{eq}{}^2 \cdot C_p\left(\lambda, \theta_{pitch}\right) \tag{3.2-9}$$

### 3.2.3 Mechanical Model of a Wind Turbine

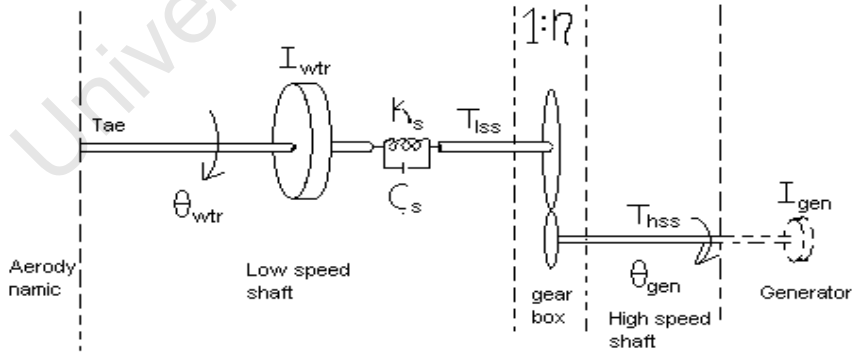


**Fig 3.2:** Transmission system of a wind turbine [28]

In the mechanical model, the aerodynamic torque is converted into the torque on the low speed shaft $T_{lss}$, which is geared up through the gearbox to the torque on the high speed shaft $T_{hss}$. The drive train is a 2 mass model connected by a flexible low speed shaft, which is modelled by stiffness $K_s$ and damping coefficient $C_s$. The masses are the large turbine rotor inertia $I_{wtr}$ representing the hub and the blades and a small inertia $I_{gen}$ to represent the induction generator. The model includes a gear exchange with the ratio of $(1:\eta)$. The high speed shaft torque can be defined as [30]:

$$T_{hss} = \frac{T_{lss}}{\eta} \tag{3.2-10}$$

Where $\eta$ is the gear ration

### 3.2.4 Modelling Description of an Induction Machine

The induction machine, which is also referred to as an asynchronous machine, is the most widely used machine in industry. Like the synchronous machine, the induction machine is also made of a stator and a rotor mounted on bearings and separated from the stator by an air gap. Alternating current is supplied to the stator winding directly, while the rotor winding currents are induced by electromagnetic induction from the stator .The rotor windings are either internally short-circuited or connected through slip rings to an external circuit. The induction machine can operate both as a generator, for instance, in some wind generator concepts and as a motor. When balanced three – phase currents of frequency $f_s$ Hz are supplied to the stator windings, a field rotating at synchronous speed $n_s$, is produced in the stator windings as given in equation 2.2-1. If the rotor circuit is closed, induced voltages in the rotor windings produce rotor currents that interact with the air gap field to produce torque, resulting in the rotational movement of the rotor in the direction of the rotating field. The rotor will eventually reach a steady – state speed $n_r$ that is less than synchronous speed $n_s$. If $n_r = n_s$, then, there will be no induced voltage and current in the rotor circuit and hence no torque. The difference between the synchronous speed $n_s$ and the rotor speed $n_r$ in per unit of the synchronous speed of the rotating magnetic field is called the slip $s$ and is defined as

$$s = \frac{n_s - n_r}{n_s} \tag{3.2-11}$$

At no load, the machine operates with negligible slip. However, when a mechanical load is applied, the slip increases as the rotor speed decreases to such an extent that the induced voltage and current produces the torque required by the load. The machine thus operates as a motor. The rotor of the induction machine in wind turbine applications is driven by the wind turbine's shaft at a speed greater than that of the stator field via a gearbox, and the outcome is negative slip. The polarities of the induced voltages are reversed so that the resulting torque is opposite in direction to that of rotation. The machine now operates as an induction generator. Figure 3.3 shows the thevenin equivalent circuit of an induction machine.

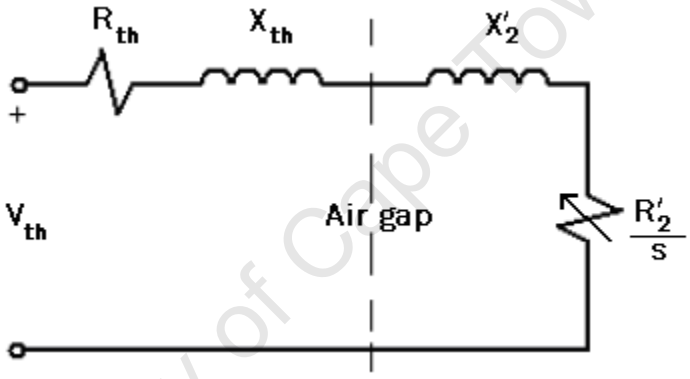


**Fig 3.3:** Thevenin equivalent circuit of an induction machine [24]

where $V_{th}$ is the equivalent thevenin stator voltage, $R_{th}$ is the equivalent thevenin stator resistance, $X_{th}$ is the equivalent stator reactance, $X'_2$ is the rotor equivalent reactance and $R'_2$ is the rotor equivalent resistance.

Figure 3.4 shows the torque vs slip characteristics of an induction machine for its different modes of operation.

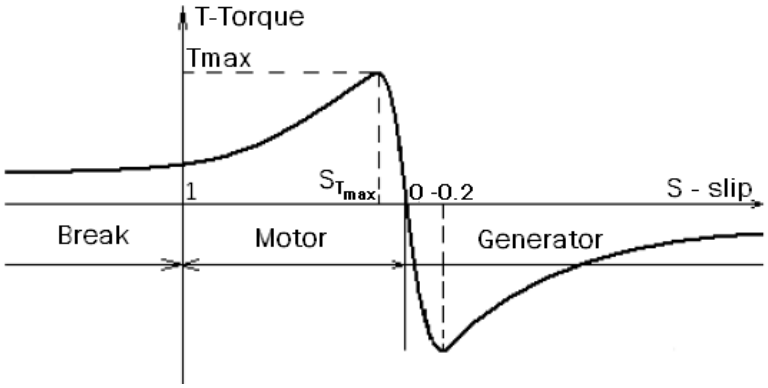


**Figure 3.4:** Torque vs slip graph of an induction machine [24]

Where maximum torque $T_{\max}$ of the machine is governed by the following expression [24]:

$$T_{\max} = \frac{1}{2\omega_{sync}} \frac{V_{th}^2}{R_{th} + [R_{th}^2 + (X_{th} + X'_2)^2]^{1/2}} \tag{3.2-12}$$

and the slip at maximum torque $S_{T_{\max}}$ is given by [24]:

$$S_{T_{\max}} = \frac{R'_2}{[R_{th}^2 + (X_{th} + X'_2)^2]^{1/2}} \tag{3.2-13}$$

### 3.2.4.1 Induction Generator Inertia

Inertia constant $H$ is defined as the kinetic energy in watt-seconds at rated speed divided by the VA base [15]. Inertia can also be understood as the tendency of an object to resist change in motion [32]. It is expressed as follows:

$$H = \frac{stored\ energy\ at\ rated\ speed\ in\ MW \cdot s}{MVA\ rating} \tag{3.2-14}$$

### 3.2.5 Wind Turbine Generator Concept Models

A wind turbine can be equipped with any type of three - phase generator, which can either fall under the fixed speed topology or the variable speed topology. The demand for a grid-compatible electric current can be met by connecting frequency converters to generators supplying alternating current of variable frequency or direct current. Some generic wind generators which can be used in wind turbines are presented below:

#### 3.2.5.1 Fixed Speed Wind Turbine

The squirrel cage induction generator (SCIG), which at times is referred to as the fixed speed wind generator, uses a squirrel cage topology for its induction generator. It operates in such a way that regardless of the wind speed, the wind turbine's rotor speed is fixed and determined by the frequency of the supply grid, gear ratio and generator design [27]. Figure 3.5 shows the principle arrangement of a squirrel cage induction generator. The generator's stator terminals are connected to a soft starter, which connects to the grid via a step up transformer which serves to boost the generator's voltage to that of the network's nominal voltage. The generator's rotor is connected to a high speed shaft which connects to the wind turbine's low speed shaft via a gearbox. In order to prevent the induction generator from being damaged at high wind speeds, the turbine blades are often designed to operate at lower efficiency during high wind speed (*stall control*), or the angle of the blades can be actively adjusted according to the wind speed (*pitch angle control*) [33] . The induction generator is connected with a capacitor bank for reactive power compensation.



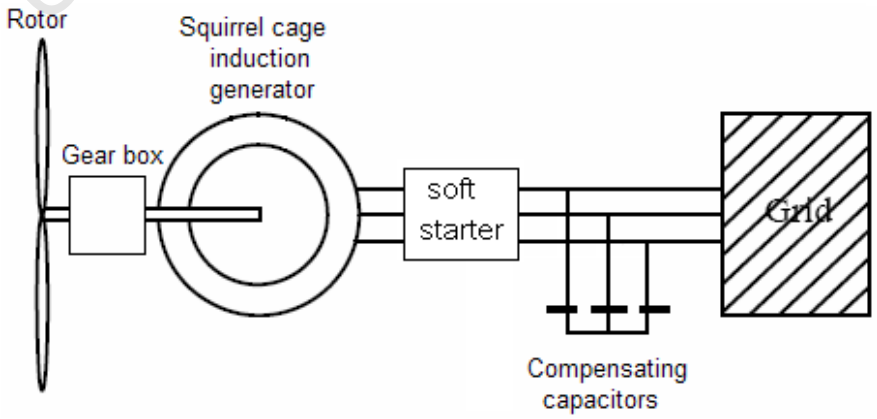


**Fig 3.5:** Schematic of a squirrel cage induction generator [27]

The mathematical model of the induction generator is governed by stator and rotor voltage equations, equation of electrical torque, slip, active power and reactive power consumed. The d – q (direct - quadrative) reference frame is used in expressing the voltage equations of the squirrel cage induction generator. The generator convention is used. This means that a current leaving the machine is positive and current entering the machine is negative. The voltage equations are defined as follows:

$$u_{ds} = -R_s i_{ds} - \omega_s \psi_{qs} + \frac{d\psi_{ds}}{dt} \tag{3.2-15}$$

$$u_{qs} = -R_s i_{qs} + \omega_s \psi_{ds} + \frac{d\psi_{qs}}{dt} \tag{3.2-16}$$

$$u_{dr} = -R_r i_{dr} - s\omega_s \psi_{qr} + \frac{d\psi_{dr}}{dt} \tag{3.2-17}$$

$$u_{qr} = -R_r i_{qr} + s\omega_s \psi_{dr} + \frac{d\psi_{qr}}{dt} \tag{3.2-18}$$

where $u$ is the voltage, $i$ is the current, $R$ is the resistance, $s$ is the slip, and $\psi$ is the flux. All quantities are in per unit. The subscripts $s$ and $r$ stand for stator and rotor respectively, $d$ and $q$ for direct and quadrature component respectively.

The flux linkage in the d - q voltage equations can be calculated as follows:

$$\psi_{ds} = -(L_{s\sigma} + L_m) i_{ds} - L_m i_{dr} \tag{3.2-19}$$

$$\psi_{qs} = -(L_{s\sigma} + L_m) i_{qs} - L_m i_{qr} \tag{3.2-20}$$

$$\psi_{dr} = -(L_{r\sigma} + L_m) i_{dr} - L_m i_{ds} \tag{3.2-21}$$

$$\psi_{qr} = -(L_{r\sigma} + L_m) i_{qr} - L_m i_{qs} \tag{3.2-22}$$

where $L$ is the inductance. Indices $m$, $r$ and $\sigma$ stand for mutual, rotor and leakage, respectively.

In stability studies, stator $\frac{d\psi}{dt}$ terms (transformer voltage term) are neglected, and as such, the stator quantities only have fundamental frequency components. Moreover, the stator voltage terms are represented as algebraic equations. Since the stator $\frac{d\psi}{dt}$ terms represent stator transients, their omission eliminates the dc offset in the stator phase currents and the associated effects on the dynamic performance of the machine [15].

The flux equations are then substituted into the stator and rotor voltage equations while neglecting the stator transients, in accordance to the aforementioned reason.

$$u_{ds} = -R_s i_{ds} + \omega_s \left[ (L_{s\sigma} + L_m) i_{ds} - L_m i_{dr} \right] \tag{3.2-23}$$

$$u_{ds} = -R_s i_{ds} - \omega_s \left[ (L_{s\sigma} + L_m) i_{qs} - L_m i_{qr} \right] \tag{3.2-24}$$

$$u_{dr} = 0 = -R_r i_{dr} + s\omega_s \left[ (L_{r\sigma} + L_m) i_{qr} + L_m i_{qs} \right] + \frac{d\psi_{dr}}{dt} \tag{3.2-25}$$

$$u_{qr} = 0 = -R_r i_{qr} - s\omega_s \left[ (L_{r\sigma} + L_m) i_{dr} + L_m i_{ds} \right] + \frac{d\psi_{qr}}{dt} \tag{3.2-26}$$

The rotor voltage of the fixed speed wind generator is equal to zero because the rotor windings are shorted, and thus there is not potential difference across the windings.

The electrical torque $T_e$ of the induction generator is defined as follows:

$$T_e = \psi_{qr} i_{dr} - \psi_{dr} i_{qr} \tag{3.2-27}$$

The equation of motion of the generator is:

$$J \frac{d\omega_r}{dt} = T_r - T_e \tag{3.2-28}$$

where $J$ is moment of inertia, $T_e$ is electrical torque and $T_r$ is the torque applied to the generator's rotor.

The active power $P$ generated and the reactive power $Q$ consumed are :

$$P_s = u_{ds} i_{ds} + u_{qs} i_{qs} \tag{3.2-29}$$

$$Q_s = u_{qs} i_{ds} - u_{ds} i_{qs} \tag{3.2-30}$$

#### 3.2.5.2 Variable – Speed Wind Turbine with Partial Scale Frequency Converter

The component arrangement of the doubly-fed induction generator is shown in Figure 3.6. The doubly-fed induction generator (DFIG) is rotor-voltage controlled, with the generator's rotor connected to the wind turbine via a gearbox as shown in Figure 3.6. The stator terminals are connected directly to the grid by means of a step up transformer to convene with the network voltage. This scheme employs a wound rotor induction generator connected to an ac-dc-ac IGBT (insulated gate bipolar transistor) voltage source converter by utilizing slip rings. IGBTs are switchable transistors which are contemporarily the most common transistors. As switchable transistors, they can control both active and reactive power. The typical switching frequency range of an IGBT lies between 2 to 20 kHz. The converter is normally rated to handle between 25% - 30% of the generator's nominal power to achieve full control of the generator [34]**.** The converter controls the magnitude and phase angle of rotor voltage and thus is able to control the output reactive and active output power of the DFIG [35]. The machine and converters are protected by voltage limits and an over current 'crowbar' [36]. As a variable speed wind generator, it is designed to achieve maximum aerodynamic efficiency over a wide range of wind speeds. This is done by continuously adapting the rotational speed of the wind turbine to that of the wind speed. This mechanism maintains a constant tip speed ratio which corresponds to the maximum power coefficient [27].

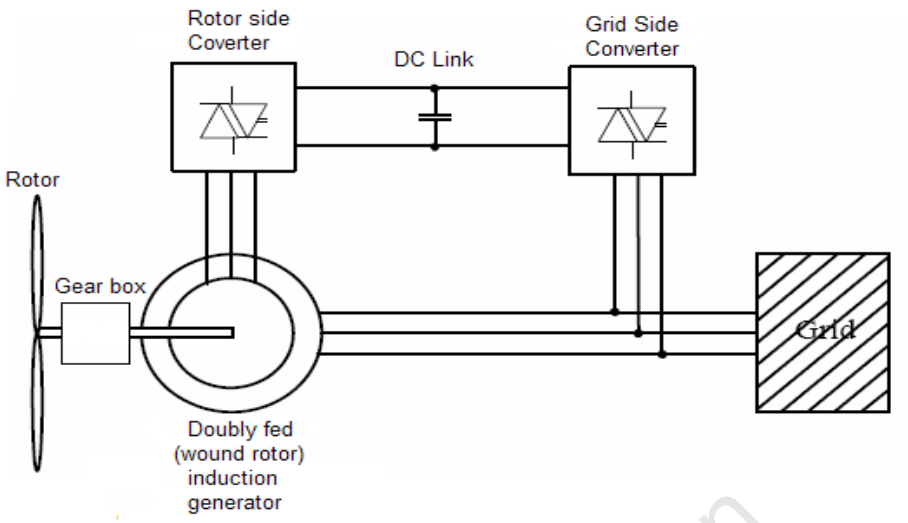


**Fig 3.6:** Schematic of a doubly - fed induction generator [27]

Equations that describe a doubly-fed induction generator are the same as those of the squirrel cage induction generator. The main difference is that the rotor winding is not short-circuited, hence the rotor voltages are not equal to zero. Furthermore, the rotor transients are neglected. The following current-voltage equations are in per unit [27].

$$u_{ds} = -R_s i_{ds} + \omega_s \left[ (L_{s\sigma} + L_m) i_{ds} - L_m i_{dr} \right] \tag{3.2-31}$$

$$u_{ds} = -R_s i_{ds} - \omega_s \left[ (L_{s\sigma} + L_m) i_{qs} - L_m i_{qr} \right] \tag{3.2-32}$$

$$u_{dr} = -R_r i_{dr} + s\omega_s \left[ (L_{r\sigma} + L_m) i_{qr} + L_m i_{qs} \right] \tag{3.2-33}$$

$$u_{qr} = -R_r i_{qr} - s\omega_s \left[ (L_{r\sigma} + L_m) i_{dr} + L_m i_{ds} \right] \tag{3.2-34}$$

The equations giving the electrical torque and the motion of the doubly-fed induction generator are identical to those of a squirrel cage induction generator. The equations for active power and reactive power are different since the rotor winding of the generator is accessible. The resultant equations incorporating the rotor quantities are as follows:

$$P = P_s + P_r = u_{ds} i_{ds} + u_{qs} i_{qs} + u_{dr} i_{dr} + u_{qr} i_{qr} \tag{3.2-35}$$

$$Q = Q_s + Q_r = u_{qs} i_{ds} - u_{ds} i_{qs} + u_{qr} i_{dr} - u_{dr} i_{qr} \tag{3.2-36}$$

### 3.2.5.3 Variable – Speed Wind Turbine with Full Scale Frequency Converter

Figure 3.7 shows a pictorial view of how the components of the direct drive synchronous wind generator (DDSG) are connected. This generator model also falls in the category of variable speed wind generators. The wind turbine's shaft is directly connected to the rotor of the synchronous generator. This scheme does not employ a gearbox. The generator has about 60 poles as it is designed for low speeds. The stator terminals are connected to a full scale frequency converter which is rated to handle the synchronous generator's rated power. The stator of the generator can either be of an electrically excited synchronous generator or be that of a permanent magnet topology. The frequency converter performs the role of reactive power compensation for the respective connected grid [27]. The output of the full scale frequency converter is attached to a step up transformer which steps up WG voltage to that of the grid.

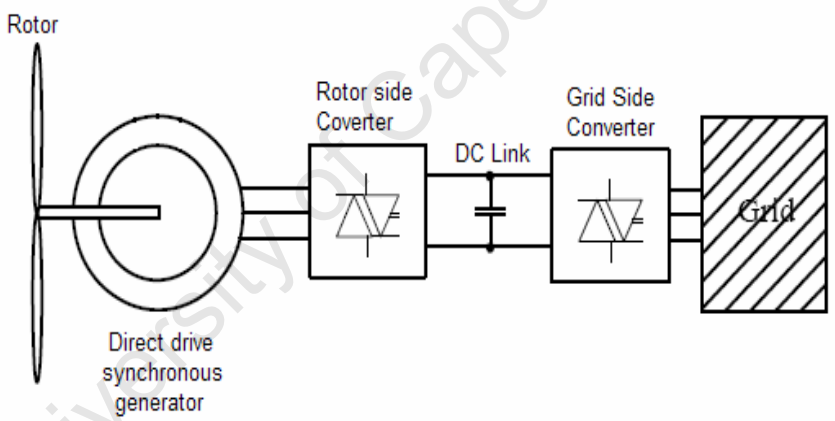


**Fig 3.7:** Diagram of a direct drive synchronous generator [37]

The converter driven synchronous generator as depicted in Figure 3.8 has an electrical performance which is analogous to the direct-drive synchronous generator [37]. The converter driven synchronous generator (CDSG) has a gearbox which couples the wind turbine's low speed shaft to the synchronous generator's high speed rotor shaft. The presence of the gearbox allows for a smaller number of poles and thus a generator which is smaller in size as compared with that used in direct-drive wind-generators. The generator is connected to a back-to-back voltage source converter rated to handle the generator's rated power .The grid side connection is realized by a self-commutated pulse-width modulated (PWM)

converter that imposes a pulse–width modulated voltage on the ac-terminal. The level of harmonics at the point of connection is extremely low [37].

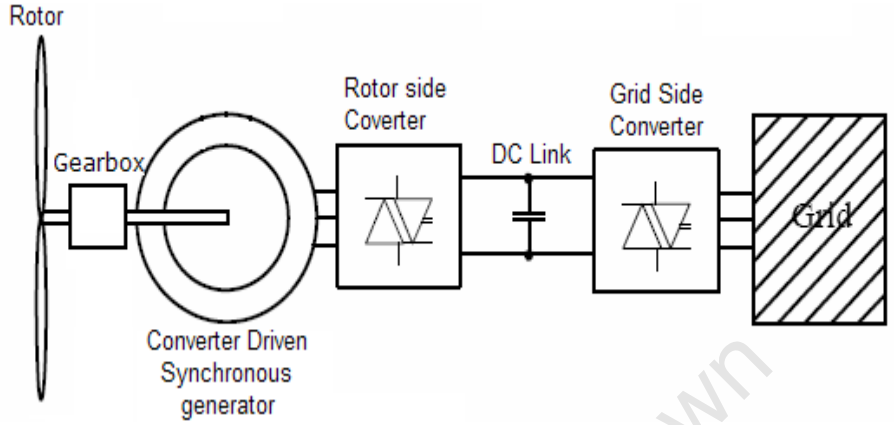


**Fig 3.8:** Schematic of a converter driven synchronous generator [37]

The voltage equations of a wound rotor synchronous generator in the d-q reference frame are:

$$u_{ds} = -R_s i_{ds} - \omega_m \psi_{qs} + \frac{d\psi_{ds}}{dt} \tag{3.2-37}$$

$$u_{qs} = -R_s i_{qs} + \omega_m \psi_{ds} + \frac{d\psi_{qs}}{dt} \tag{3.2-38}$$

$$u_{fd} = R_{fd} i_{fd} + \frac{d\psi_{fd}}{dt} \tag{3.2-39}$$

The subscript fd indicates field quantities. Quantities are in per unit values.

The flux equations are given as:

$$\psi_{ds} = -(L_{dm} + L_{\sigma s}) i_{ds} + L_{dm} i_{fd} \tag{3.2-40}$$

$$\psi_{qs} = -(L_{qm} + L_{\sigma s}) i_{qs} \tag{3.2-41}$$

$$\psi_{fd} = L_{fd} i_{fd} \tag{3.2-42}$$

By omitting the $\frac{d\psi}{dt}$ terms in the stator voltage equations, the voltage flux relationships are expressed as follows:

$$u_{ds} = -R_s i_{ds} + \omega_m (L_{s\sigma} + L_{qm}) i_{qs} \tag{3.2-43}$$

$$u_{qs} = -R_s i_{qs} - \omega_m (L_{s\sigma} + L_{dm}) i_{ds} \tag{3.2-44}$$

$$u_{fd} = R_{fd} i_{fd} + \frac{d\psi_{fd}}{dt} \tag{3.2-45}$$

The $\frac{d\psi}{dt}$ transformer voltage terms are neglected on the basis that, associated time constants are small, and thus taking them into account would necessitate for the development of a detailed representation of the power electronic converter. This would then include a phenomenon which is not of particular interest.

The electromechanical torque $T_e$ is given by the following equation:

$$T_e = \psi_{ds} i_{ds} - \psi_{qs} i_{ds} \tag{3.2-46}$$

## 3.2.6 Power Electronics in Wind Turbines

The power electronics devices used in wind power applications include soft-starters, capacitor banks, rectifiers, inverters and frequency converters.

### 3.2.6.1 Soft Starter

The soft-starter consists of two thyristors in each phase of the connection line. They are connected anti-parallel for each phase. Its functionality is to reduce the transient current during connection or disconnection of the generator to the grid, thereby limiting disturbances to the grid. When the generator speed exceeds the synchronous speed, the soft-starter is connected. The generator is then smoothly connected to the grid over a predefined number of grid periods through the use of the firing angle control of the thyristors. The relationship between the firing angle ($\alpha$) and the resulting amplification of the soft starter is non-linear and also depends on the power factor of the connected load. For a resistive load, $\alpha$ may vary between 0 (full on) and 90 (full off) degrees. For an inductive load, $\alpha$ will vary between 90 (full on) and 180 (full off) degrees. Without a soft-starter, the inrush current can be up to 7-8 times the rated current which can cause severe voltage disturbances on the grid.

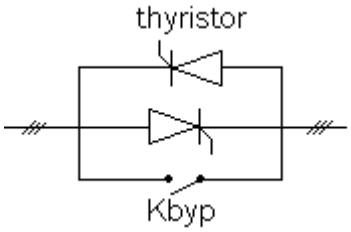


**Fig 3.9:** Soft-starter used for grid connection of induction generators [38]

When the generator is completely connected to the grid, a contactor (Kbyp) bypasses the soft-starter in order to reduce the losses during normal operation [27, 38].

### 3.2.6.2 Capacitor Bank

For power factor compensation of the reactive power of the fixed speed generator, alternating current capacitor banks are used. The switching of capacitors is done as a function of the average value of measured reactive power during a certain period [38]. The amount of reactive power supplied by the capacitor banks is defined as

$$Q_c = \frac{V^2}{X_c} \tag{3.2-47}$$

where $Q_c$ is the reactive power from the capacitor bank , $X_c$ is the capacitive reactance of the capacitor and $V$ is the voltage on the bus bar onto which the capacitor bank is connected to.

Thus

$$V = \sqrt{\frac{Q_c}{2 \cdot \pi \cdot f \cdot C}} \tag{3.2-48}$$

shows the relationship of how the voltage on the bus local to the generator and the capacitor bank, increases as the amount of reactive power injected by the capacitor bank increases where $f$ is the grid frequency and $C$ is the capacitance of the capacitor.

### 3.2.6.3 PWM Voltage Source Converter

The variable – speed wind turbine concept uses a power electronic system (voltage source converter-VSC) that is capable of adjusting the generator frequency and voltage to the grid. The VSC makes it possible for a wind farm to be used as a source of reactive power with the added feature of having the wind farm's active and reactive power being controllable. The reactive power exchanged with the grid depends not only on the control of the generator but also on the control of the grid side of the converter. The following active and reactive power equations apply to the converter [27]:

$$P_c = u_{dc} i_{dc} + u_{qc} i_{qc} \tag{3.2-49}$$

$$Q_c = u_{qc} i_{dc} - u_{dc} i_{qc} \tag{3.2-50}$$

in which the subscript c stands for converter .The most commonly used converter topology in the DFIG and DDSG wind turbines is the back-to-back converter. The back-to-back converter is a bidirectional power converter made of two conventional pulse-width modulated (PWM) VSC. Figure 3.10 shows the aforementioned converter topology. The dc link voltage is boosted to a level higher than the amplitude of the grid line-to-line voltage in order to achieve full control of the grid current. The boost inductance reduces the demands on the input harmonic filter and offers some protection for the converter against abnormal conditions on the grid. The capacitor between the inverter and rectifier makes it possible to decouple the control of the two inverters, allowing for compensation of asymmetry on both the generator and the grid side. The power flow at the grid-side converter is controlled to keep the dc link voltage constant. The control of the generator – side converter is set to suit the magnetisation demand and the desired rotor speed [27].

The network – side converter operates at a network frequency and controls the voltage level in the dc link circuit. It can also deliver reactive power to supply the grid if needed. The rotor – side frequency converter operates at different frequencies, as determined by the rotor speed. Frequency converters that are capable of fault ride – through include an over – current protection system called a crowbar. This protection scheme safe guards the rotor circuit and the rotor – side converter of the DFIG against high currents during grid disturbances [39].

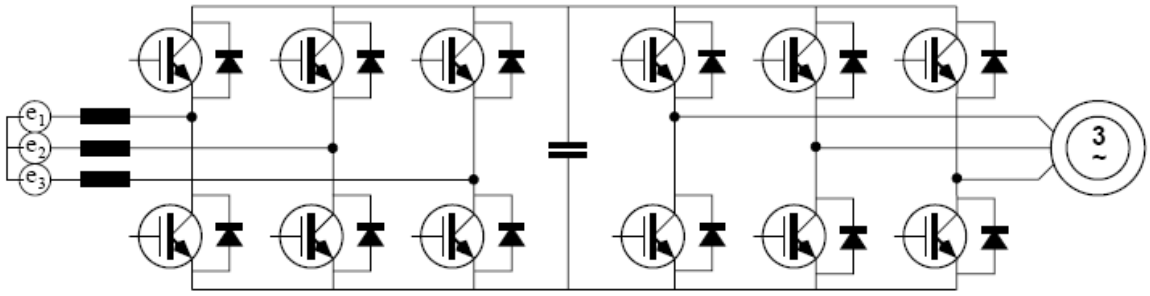


**Fig 3.10:** Representation of a back-to-back PWM voltage source converter [27]

As mentioned earlier, the functionality of the PWM voltage source converter is realized by the application of insulated gate bipolar transistors (IGBTs). The circuit symbol for an IGBT is shown in Figure 3.11 and its *i*-*v* characteristics are shown in Figure 3.12. The IGBT has a high impedance gate, which requires only a small amount of energy to switch the device. It also has a small on-state voltage, even in devices with large blocking voltage ratings (e.g. $V_{on}$ is 2-3 V in 1000 V device) [40].

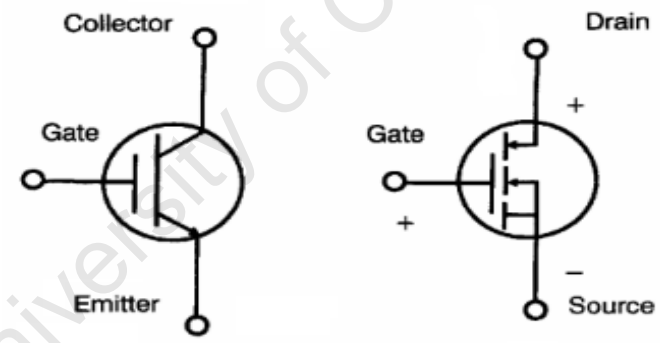


**Fig 3.11:** IGBT circuit symbols [41]

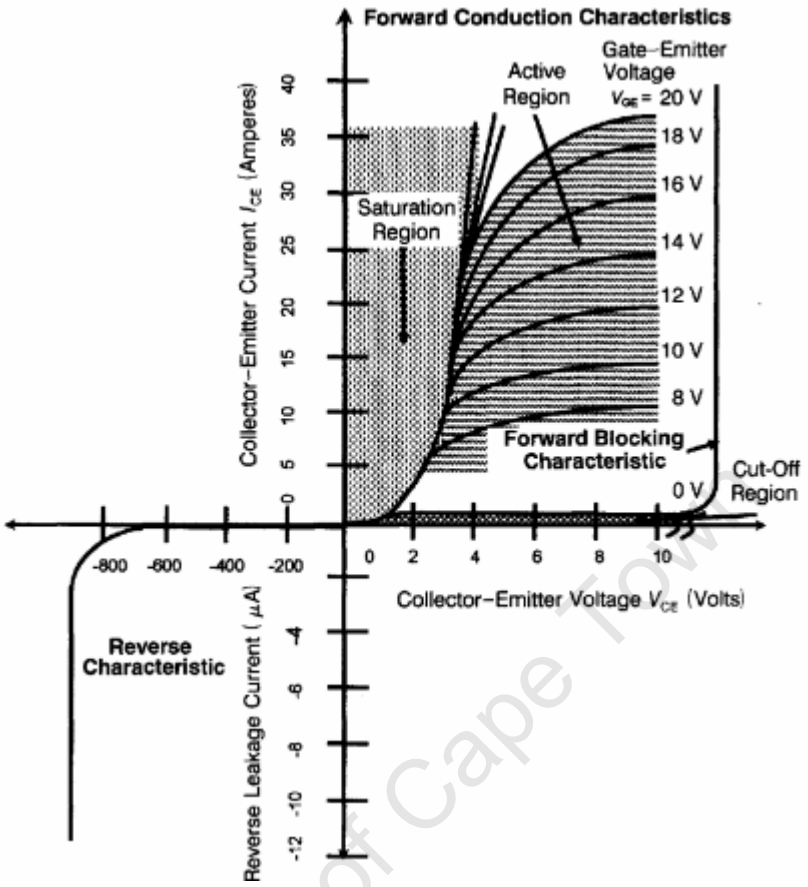


**Fig 3.12:** IGBT *i-v* characteristics [41]

These IGBTs are used in line-frequency phase controlled converters such as the PWM VSC, whereby the conversion from ac to dc to ac is controlled. Figure 3.12 shows that, when there is a positive voltage applied on the collector terminal with no gate-source voltage, the IGBT will be in its forward voltage blocking mode. The IGBT will only conduct when a gate-source voltage is applied for a short duration. Once the IGBT conducts, it is in latchup, and the gate no longer has any control of the collector current. The gate cannot be used to turn the IGBT off. Turn-off can be accomplished by using an external circuit, thus reducing the collector current below the holding current for a minimum specified period of time.

### 3.2.6.3.1 Theoretical Background on Switch-Mode Inverters [40]

Switch-mode inverters are used in ac motor drives and uninterruptible ac power supplies where the objective is to produce a sinusoidal ac output with controllable magnitude and frequency. This switch-mode inverter is a converter through which the power flow is reversible. The input to the switch-mode inverter is assumed to be a dc-voltage source, hence these inverters are referred to as voltage source inverters (VSI) or converters (VSC), depending on the direction of power flow. In this context, focus is on power flowing from the dc voltage source to the ac side of the inverter, and thus the switch-mode inverter will be referred to as the voltage source inverter (VSI).

The VSIs can be divided into the following three general categories, *Pulse-Width-Modulated (PWM) inverters, Square Wave inverters* and *Single-Phase inverter with Voltage Cancellation*. However, focus will be on the PWM inverters, since that is the type used in variable speed wind generators.

*Pulse-Width-Modulated Inverters*: In these inverters, the input dc voltage $V_d$ is fundamentally constant in magnitude as referred in Figure 3.13. The magnitude and frequency of the output voltage of the inverter is controlled by pulse-width-modulating the inverter switches. The prime objective of the pulse-width-modulating scheme is to shape the output ac voltages to be like a sine wave.



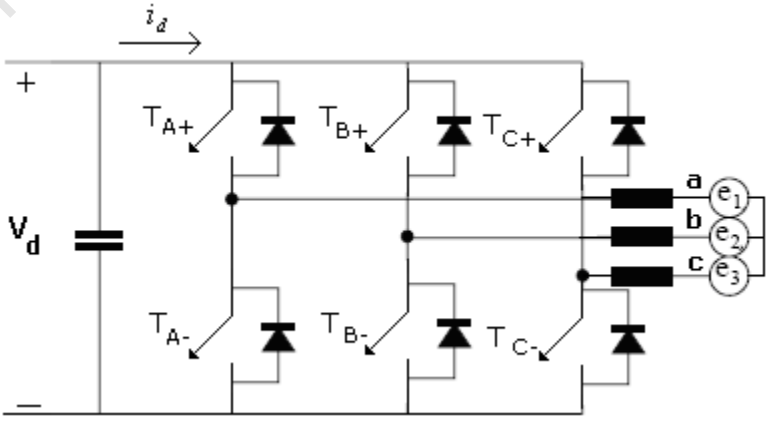


**Fig 3.13:** Schematic of a PWM inverter topology

To obtain balanced three-phase output voltages in a three-phase PWM inverter, triangular voltage waveforms are compared with three sinusoidal control voltages that are 120° out of phase, as seen in Figure 3.14 (a) .

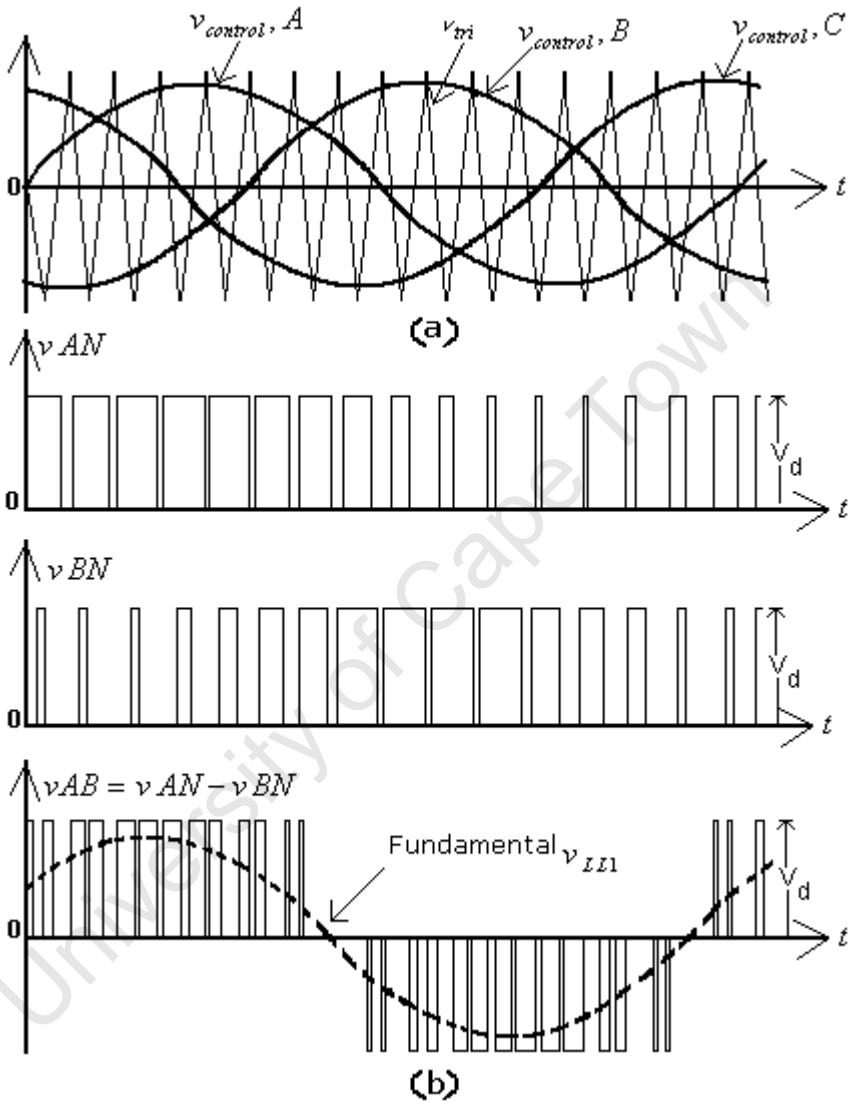


**Fig 3.14:** Control and output signals of a three-phase PWM inverter [40]

The control signals $v_{control}\ A,B,C$ are each fed into a comparator circuit designated for each phase of the three phases, and compared with $v_{tri}$ which has a constant amplitude of the triangular waveform. The output signal of each of the three comparators defines the switching signals of the inverter switches as shown in Figure 3.14. Figure 3.15 shows a typical circuit arrangement through which the switching signals are produced.

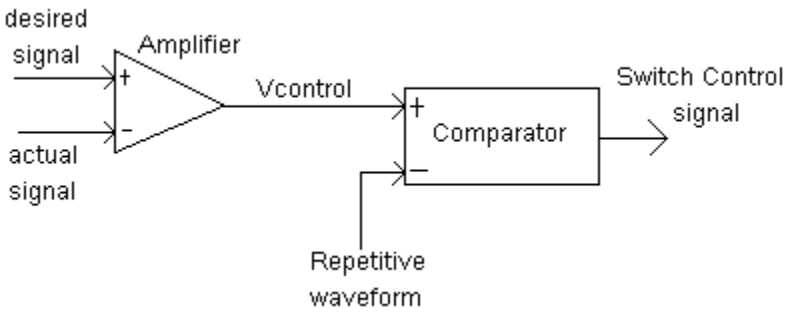


**Fig 3.15:** Comparator circuit for the switching signals in the PWM inverter [40]

The control signals $v_{control}\ A,B,C$ (slowly varying), are compared with a repetitive switching – frequency triangular waveform in order to generate the switching signals of $v\,AN$ and $v\,BN$ as shown in Figure 3.14. $v\,CN$ was not included, but is generated in as much the same way as $v\,AN$ and $v\,BN$. By controlling the switch duty ratios in this way it is possible to control the average ac output voltage. In order to produce a sinusoidal output voltage waveform at a desired frequency, a sinusoidal control signal at the desired frequency is compared with a triangular waveform as shown in Figure 3.14 for each phase of the three - phase inverter. The frequency of the triangular waveform governs the inverter switching frequency and is generally kept constant with its amplitude $\hat{V}_{tri}$. The $v_{control}\ A,B,C$ signals are used to modulate switch duty ratios since they have frequency $f_1$ , which is the fundamental frequency of the inverter voltage output.

The amplitude modulation is defined as

$$m = \frac{\hat{V}_{control}}{\hat{V}_{tri}} \tag{3.2-51}$$

Where $\hat{V}_{control}$ is the peak amplitude of the control signal, and $\hat{V}_{tri}$ is the constant triangular waveform. In a sinusoidal PWM, the amplitude of the fundamental-frequency component of the output voltage varies linearly with $0 < m \leq 1.0$. This range is referred to as the linear range of the inverter.

The IGBTs used in the PWM inverters have been represented by the switches designated as $T_{A+,}T_{A-,}T_{B+,}T_{B-,}T_{C+}$ and $T_{C-}$ as shown in Figure 3.13. Control of these switches is based on the comparison of $v_{control}\ A,B,C$ and $v_{tri}$ independent of the direction of $i_d$. By looking at switches $T_{A+}$ ,$T_{A-,}$ it is observed that when $v_{control\ ,A} > v_{tri}$, $T_{A+}$ is on and $T_{A-}$ is off. When $v_{control\ ,\ A} < v_{tri}$, $T_{A+}$ is off and $T_{A-}$ is on, since the two switches are never off simultaneously [40].

### 3.2.6.5 Converter Model used in DIgSILENT

The model represents a self-commutated, voltage sourced ac / dc converter. The circuit is built from IGBTs and is based on the fundamental frequency model. Sinusoidal modulation is chosen over rectangular modulation due to considerably lower amounts of harmonics. Thus, sinusoidal modulation is the standard modulation method in power applications. If no modulation is applied, the modulation indices are equal to one, and the converter cannot be controlled. The pulse width modulation index $m$ is the control variable of the PWM converter. The ac voltage can be represented as:

$$|V_{ac}| = \frac{\sqrt{3}}{2 \cdot \sqrt{2}}\ m\ V_{dc} \tag{3.2-52}$$

for $0 \le m < 1$ . For values larger than 1, the converter starts saturating and the level of low order harmonics start increasing. The converter model is completed by the power conservation equation:

$$V_{dc}\ I_{dc} + \sqrt{3}\ \mathrm{Re}\left(\underline{V}_{ac}\ \underline{I}^{*}_{ac}\right) = 0 \tag{3.2-53}$$

which assumes a loss-less converter with a dc voltage controlled ac voltage source conserving active power between ac and dc side [45].

# IMPACT OF FIXED SPEED WIND GENERATORS ON THE TRANSIENT STABILITY OF A POWER NETWORK

# 4

## 4.1 Introduction

The case studies presented here focus on the impact of fixed speed wind generators on a power system's transient stability. The assumption made when the simulations were performed is that, by the time the three-phase fault is applied on one of the transmission lines, the squirrel cage induction generators (SCIGs) would have long been operating under steady state conditions. With this supposition, there was no rationale in including the soft-starter to the induction generator models. One unit of the SCIG had a power rating of 10 MVA, operating at a lagging power factor of 0.8 and having a nominal voltage of 11 kV. This nominal voltage is then stepped up to 230 kV via transformer 2 (TR 2). The three-phase fault was applied to line 1 of the double transmission lines of Figure 4.1, and was cleared by taking the line out of service after 0.2 sec following the occurrence of fault. Loads 1 and 2 were both rated to draw 80 MW and 40 MVAr. The conventional synchronous generator had a rating of 100 MVA at a lagging power factor of 0.8. The terminal voltage of the conventional synchronous generator was set to 13.8 kV, and stepped up to 230 kV via transformer 1 (TR 1) for transmission.

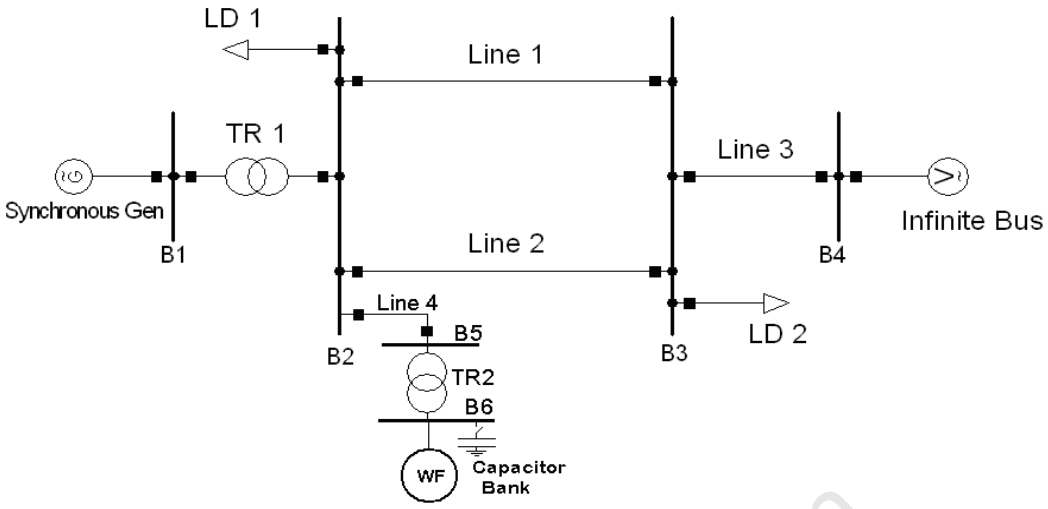


**Fig 4.1:** Power network connected with a SCIG wind farm

## 4.2 Impact of Wind Farm Distance on System Transient Stability

The connection of one squirrel cage induction generator, with no capacitor bank to the power network at 1 km away from the synchronous generator, did not cause the system to be transiently unstable with a fault clearing time (FCT) of 0.2 sec when the faulted line was put out of service. At this point, the synchronous generator was not equipped with any controllers (i.e. automatic voltage regulator and speed governor).When the length of the transmission line connecting the wind farm to the power network was increased (to 100 km, 300 km , 500 km and 540 km), the steady state stability margin decreased. This was because the pre-fault rotor angle increased as the wind farm transmission length increased. This is shown in Table 4.1, where the prefault power flow results of the power network are tabulated.

**Table 4.1:** Generator Reactive Power as Wind Farm Distance Increases

| $Q_{gen}$(MVAr) | Wind Farm Distance (km) | Rotor Angle (deg) | Terminal Voltage (kV) | $Q_{infiniteBus}$ (MVAr) | $P_{infiniteBus}$ (MW) |
|---|---|---|---|---|---|
| 8.22 | 1 | 25° | 13.8 | -5.03 | 72.16 |
| 5.14 | 20 | 25° | 13.8 | -5.42 | 72.16 |
| 1.90 | 40 | 26° | 13.8 | -5.82 | 72.16 |
| -1.36 | 60 | 26° | 13.8 | -6.26 | 72.16 |
| -7.92 | 100 | 28° | 13.8 | -7.06 | 72.16 |
| -42.55 | 300 | 38° | 13.8 | -11.41 | 72.20 |
| -84.19 | 500 | 54° | 13.8 | -16.63 | 72.33 |
| -94.15 | 540 | 56° | 13.8 | -17.88 | 72.38 |

It is evident that as the transmission line length increases, the synchronous generator generates less reactive power until it starts absorbing the excess reactive power delivered by the transmission line connecting the wind farm to the power network. The prefault rotor angle of the synchronous generator increases as the reactive power from the synchronous generator decreases as shown in Table 4.1.This can also be explained by observing the simplified expression which defines the reactive power supplied by the generator to the external network when the line's resistance and shunt admittance are neglected:

$$Q_{gen} = \frac{E \cdot V}{X_T} \cos\delta - \frac{V^2}{X_T} \tag{4.2-1}$$

where:

$Q_{gen}$ - the reactive power from the synchronous generator

$E$ - the internal voltage of the synchronous generator

$V$ - the voltage at the infinite bus

$X_T$ - the total reactance of the power network (refer to appendix 4)

$\delta$ - the rotor angle

The '-' sign in front of some reactive power values ($Q_{gen}$ and $Q_{infiniteBus}$) means that the generator or infinite bus is absorbing reactive power.

Table 4.2 enlists the prefault power flow results of transmission line 4 as its length increased with respect to Bus 2 and Bus 5.It is thus observed that the infinite bus consumed reactive power for all the different lengths of line 4. Thus, the only source of reactive power was the synchronous generator (for line length 1 km and 20 km) and the effect of increasing the length of line 4.

**Table 4.2:** Power in Transmission Line 4 as Wind Farm Distance Increases

| Wind Farm Distance (km) | P at Bus 2 (MW) | Q at Bus 2 (MVAr) | P at Bus 5 (MW) | Q at Bus 5 (MVAr) |
|---|---|---|---|---|
| 1 | -8.00 | 5.87 | 8.00 | -6.05 |
| 20 | -8.00 | 2.49 | 8.00 | -6.05 |
| 40 | -8.00 | -1.08 | 8.00 | -6.05 |
| 60 | -8.00 | -4.67 | 8.00 | -6.05 |
| 100 | -8.00 | -11.91 | 8.00 | -6.05 |
| 300 | -8.00 | -50.45 | 8.00 | -6.04 |
| 500 | -8.00 | -97.49 | 8.00 | -6.03 |
| 540 | -8.00 | -108.86 | 8.00 | -6.03 |

When line 4 is at length 1 km, 8 MW is fed onto Bus 2 through line 4. This 8 MW is generated by the wind farm and transmitted through line 4 to the power network. The reactive power supplied by the power grid to the wind farm is 5.87 MVAr through line 4 from Bus 2, while the wind farm absorbs 6.05 MVAr. Thus line 4 supplies 0.18 MVAr of reactive power in addition to the 5.87 MVAr from the grid to make the 6.05 MVAr consumed by the wind farm. It is observed in Table 4.2 that, as the transmission line 4 increases, the reactive power consumed by the wind farm remains fairly constant. This is due to having one SCIG drawing a constant 6 MVAr. However, the reactive power supplied by the grid to the wind farm decreases as the line 4 increases in length, until excess reactive power supplied by the transmission line is absorbed by the power grid. This occurs when the length of line 4 increases to about 40 km and the power grid takes in -1.08 MVAr. The transmission line is able to deliver more reactive power when the length of the line increases because the susceptance ($B$) of the transmission line increases as the length of the transmission line increases. The basis of the line delivering reactive power is that, the potential difference between the conductors of a transmission line causes the conductors to be charged. Therefore applying alternating voltages to the conductors causes charging currents to flow on the basis of alternate charging and discharging of the line capacitances [15]. Even though the reactance

($X_l$) of the transmission line also increases with line length, it appears that, the susceptance of the used transmission line model had a more significant impact on the power flow of the transmission line. The rationale for this is that, the characteristic impedance (SIL) of line 4 is $Z_c = 367.8\,\Omega$. The equivalent impedance of the wind farm $Z_{WF}$ = 12.1 Ω. Thus, the loading on line 4 from the wind farm is considered as a light load, since $Z_{WF}$ is much smaller than the SIL of line 4. As such, light loads which are significantly less than the SIL result in a rise of voltage at the receiving end. This is supported by data in table 4.3 below.

**Table 4.3:** Variation of Voltage on Bus 2 and Bus 5 as Length of Line 4 Increases

| **Length of Line 4 (km)** | **$V_{BUS\,2}$ (kV)** | **$V_{BUS\,5}$ (kV)** |
|---|---|---|
| 1 | 229.19 /_-2.85° | 229.18 /_-2.84° |
| 100 | 229.93 /_-2.84° | 230.52 /_-2.07° |
| 300 | 231.52 /_-2.84° | 245.34 /_-1.73° |
| 500 | 233.42 /_-2.84° | 288.96/_-1.25° |
| 540 | 233.87 /_-2.85 | 296.18/_-1.20° |

Bus 2 and bus 5 both have a voltage rating of 230 kV. It can thus be seen that, as the length of line 4 increases, the voltage magnitudes on both bus 2 and 5 increase. It can be concluded that active power flows from bus 5 to bus 2 since the voltage angle at bus 5 leads that at bus 2 for all the different lengths of line 4[49]. Theoretical analysis of voltage magnitudes at bus 5 and bus 2 for when line 4 is 100 km or longer shows that reactive power flows from bus 5 to bus 2 since voltage at bus 5 is greater than that at bus 2 [49]. This reactive power is delivered by the capacitance of the line. Since the wind generator could only draw a fixed 6 MVAr of reactive power, the excess reactive power was sent into the power network and absorbed by the conventional synchronous generator as shown in table 4.2. Furthermore, the reactive power delivered by line 4 caused the voltage on bus 5 to increase to levels as high as 1.29 p.u. when the length was at 540 km. It is in such situations that shunt reactors would be connected to reduce the high voltages under light loads.

Figures 4.2 and figure 4.3 depict the response of the synchronous generator's rotor angle and terminal voltage after the fault.

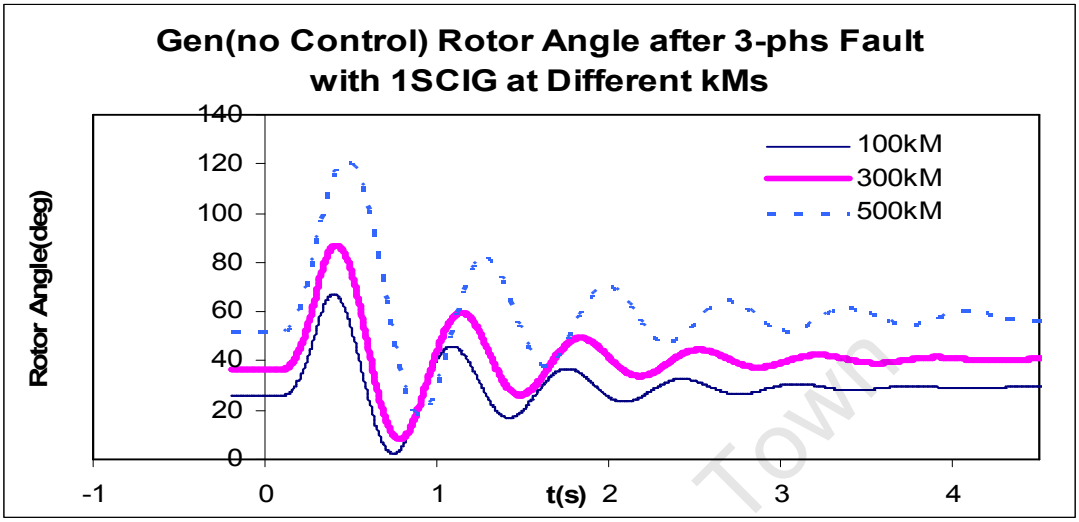


**Fig. 4.2:** Rotor responses with different line length of wind farm

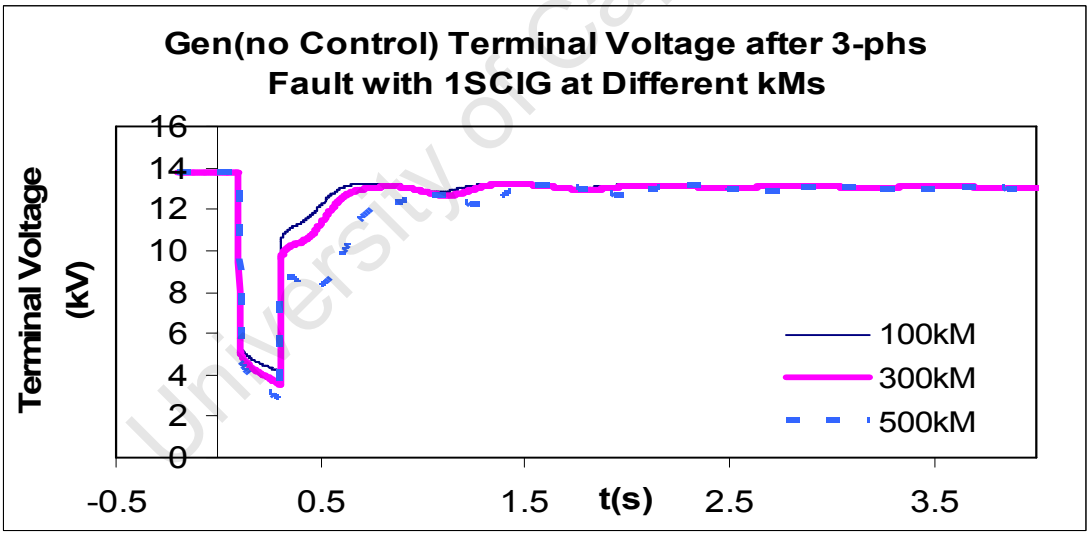


**Fig. 4.3:** Generator terminal voltage responses with different line length of wind Farm

As observed in Figure 4.2, the transient stability margin is smaller when the wind farm is at a distance of 500 km as compared with 300 km and 100 km. This is examined by observing the magnitude of the first swing of the rotor after the fault, which is much bigger with the wind farm distance of 500 km. The subsequent oscillations of the rotor to the first swing are also observed to take a longer time period (about 4.8 sec) to settle, whereas with the shorter

distances (100 km and 300 km) the rotor oscillations settle down quicker (3.1 sec and 3.6 sec). The reason for this is that the wind farm transmission line (line 4 in Figure 4.1) reactance is much higher when the distance is at 500 km. Hence, the total equivalent network reactance is highest compared with that of the shorter distances. The effect of this on the transient stability of the power network is that, when a fault occurs on the transmission line of the power system, the imbalance between the mechanical power and the electrical power produces a much higher acceleration power. This is the reason for the bigger magnitude of the first swing of the rotor and subsequent rotor oscillations. When the length of line 4 is increased to 540 km, the synchronous generator absorbs -94.06 MVAr, which is close to its minimum reactive power limit of -100 MVAr.

Figure 4.4 shows the operational limitations of the synchronous generator in relation to its active and reactive power. The active power generated by the generator of 80 MW coincides with the reactive power of -94.06 MVAr absorbed by the synchronous generator when line 4 was increased to 540 km.

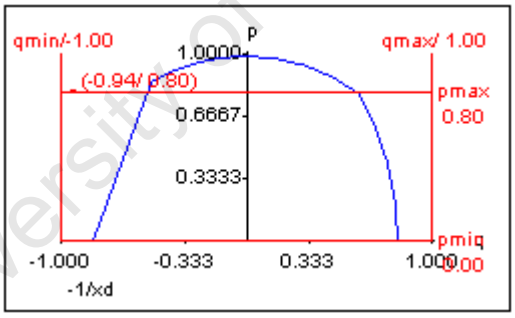


**Fig 4.4:** Operating P-Q curve of the synchronous generator with windfarm at 540 km

After the fault, the synchronous generator experiences instability as shown in figure 4.5 and 4.6.

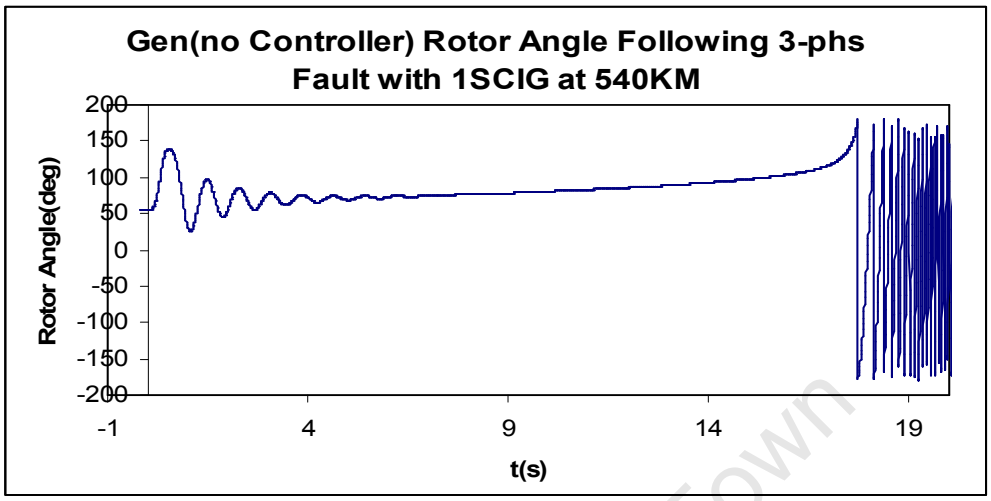


**Fig 4.5:** Generator rotor response after fault with wind farm at 540 km

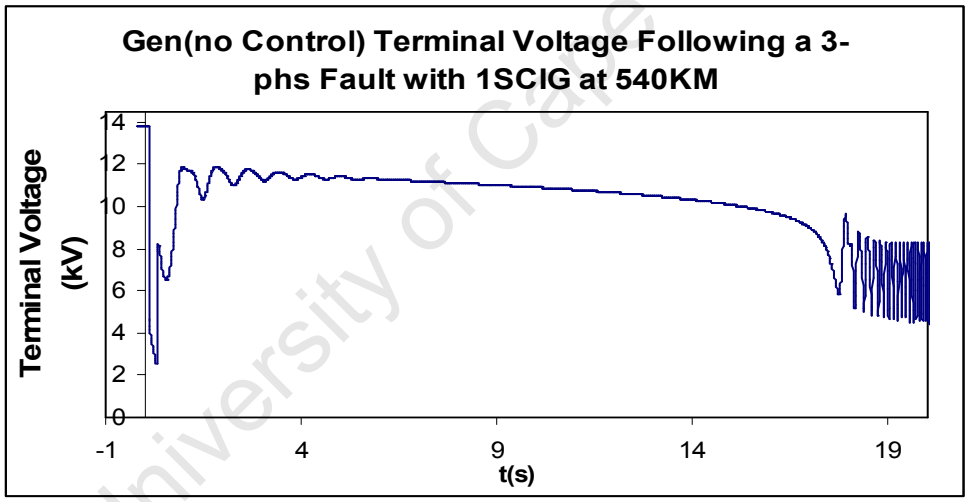


**Fig 4.6:** Response of generator terminal voltage with Wind Farm at 540kM

Once the fault is cleared, the oscillations of the rotor settle down after about 5 sec with an increasing magnitude of the rotor angle which leads to instability after 18 sec. The terminal voltage depicted in Figure 4.6 does not go back to its pre-fault level after the fault. The excitation voltage is not sufficient to support the increased reactive power demand of the power network due to a changed network topology of having taken the faulted line out of service. So, the voltage tries to recover, but gradually decreases to about 10 kV (which is 0.72 p.u. of 13.8 kV) before collapsing after 18 sec.

Table 4.4 shows the prefault and post-fault power flow results of the synchronous generator when line 4 had a length of 540 km.

**Table 4.4:** Prefault and Post-fault Power Flow of Synchronous Generator (no controller)

| $P_{gen\text{-}Prefault}$ (MW) | $Q_{gen\text{-}Prefault}$ (MVAr) | $P_{gen\text{-}Postfault}$ (MW) | $Q_{gen\text{-}Postfault}$ (MVAr) |
|---|---|---|---|
| 80.00 | -94.15 | 77.30 | -82.96 |

The post-fault power flow results represent that state of operation of the power system at the time when the simulation came to an end.The amount of real power delivered by the synchronous generator decreased after the fault had been cleared by permanently disconnecting the faulted line as shown in table 4.4. This can be explained by the following equation which defines the transferable electrical power from the synchronous generator into the power network when line resistance and shunt admittance are neglected:

$$P_{gen} = \frac{E \cdot V}{X_T} \sin \delta \tag{4.2-2}$$

where:

$P_{gen}$ - the active power from the generator

$E$ - the internal voltage of the generator

$V$ - the voltage at the infinite bus

$X_T$ - the total reactance of the power network

$\delta$ - the rotor angle.

When the fault is cleared by permanently disconnecting the faulted line, total network reactance increases and thus, the electrical power that is transferred to the power grid is reduced. In the same instance, this increase in the power network reactance results in a higher reactive power demand. The internal voltage of the generator maintained the same level after the fault as the prefault level because no controller was included on the synchronous generator.

### 4.2.1 Automatic Voltage Regulator (AVR) on Transient Stability of Network

The generator excitation system maintains synchronous generator terminal voltage at a specified level of during operation, controls the reactive power flow and also increases the synchronizing torque when required. When the terminal voltage of the generator drops due to an increase in the reactive power load or fault, the voltage magnitude is sensed through a potential transformer on one phase. This voltage is rectified and compared with a dc set point signal. The regulation error $\Delta V$ is amplified and used to control the AVR to increase the generator field current. This then leads to an increase in the transient emf $E'$ [23, 42]. Figure 4.7 shows a diagram of an IEEET1 AVR.

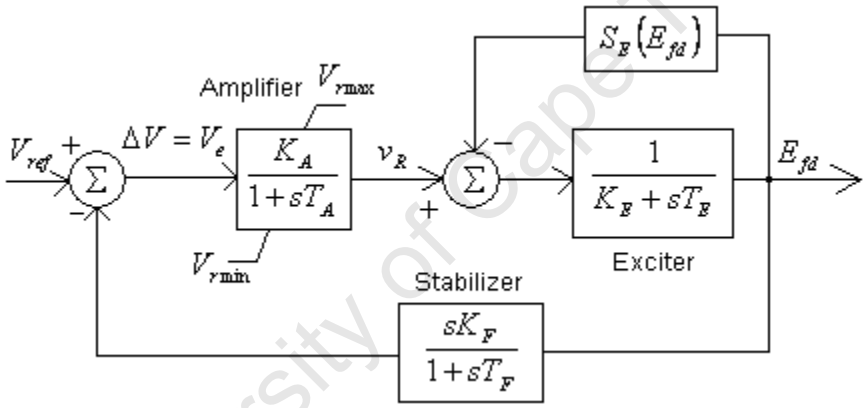


**Fig4.7:** Representation of an IEEET1 AVR

In Figure 4.7, $K_A$ is controller gain, $T_A$ is controller time constant, $K_F$ is stabilizer gain, $T_F$ is stabilizer time constant , $V_{r\max}$ is controller output maximum, $V_{r\min}$ is controller output minimum, $K_E$ is exciter constant , $T_E$ is exciter time constant, $S_E$ is the saturation factor and $E_{fd}$ is the field voltage.

It is worth noting that, ac and dc excitation systems consist of elements which have significant time delays and thus have poor inherent dynamic performance. As such, the excitation control mechanism through feedback of the generator stator voltage is unstable, unless a very low steady-state regulator gain is used. It is with this founded knowledge that, excitation control stabilization, comprising either series or feedback compensation is used to improve the

dynamic performance of the control system. The effect of the derivative feedback stabiliser shown in Figure 4.7 is to reduce the phase shift introduced by the time delays over a selected frequency range [15].

The IEEET1 AVR was deployed following the loss of synchronism of the synchronous generator as shown in Figures 4.5 and 4.6. The parameter settings of the AVR are listed in Appendix 9.

Table 4.5 registers the prefault and post-fault power flow results of the synchronous generator when the IEEET1 AVR was included. It is thus observed that the post-fault active power of the synchronous generator was relatively equal to the prefault active power flow due to the AVR. The post fault reactive power from the synchronous generator increased more when the AVR was included, compared with when there was no controller.

**Table 4.5:** Prefault and Post fault Power Flow of Synchronous Generator (AVR)

| $P_{gen\text{-}Prefault}$ (MW) | $Q_{gen\text{-}Prefault}$ (MVAr) | $P_{gen\text{-}Postfault}$ (MW) | $Q_{gen\text{-}Postfault}$ (MVAr) |
|---|---|---|---|
| 80.00 | -94.15 | 80.94 | -74.52 |

Figures 4.8 and 4.9 show that the stability of the system is maintained after the three phase fault is cleared by putting the faulted line out of service when the AVR is included. The rotor angle settles at about 48° after the fault. This is less than the pre-fault rotor angle which was about 58°. This is due to the increased reactive power supply to the power network by the synchronous generator because of the AVR, resulting with the decrease in the rotor angle.

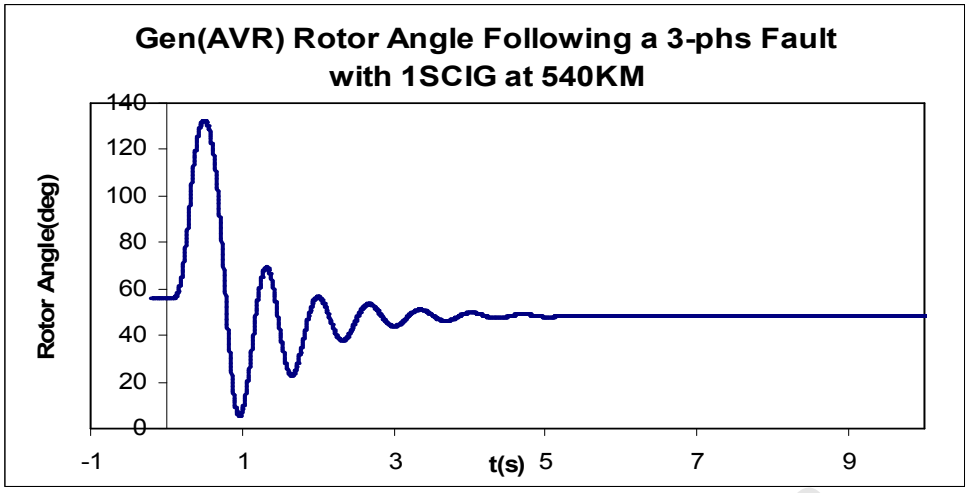


**Fig 4.8:** Rotor response with AVR with Wind Farm at 540 km

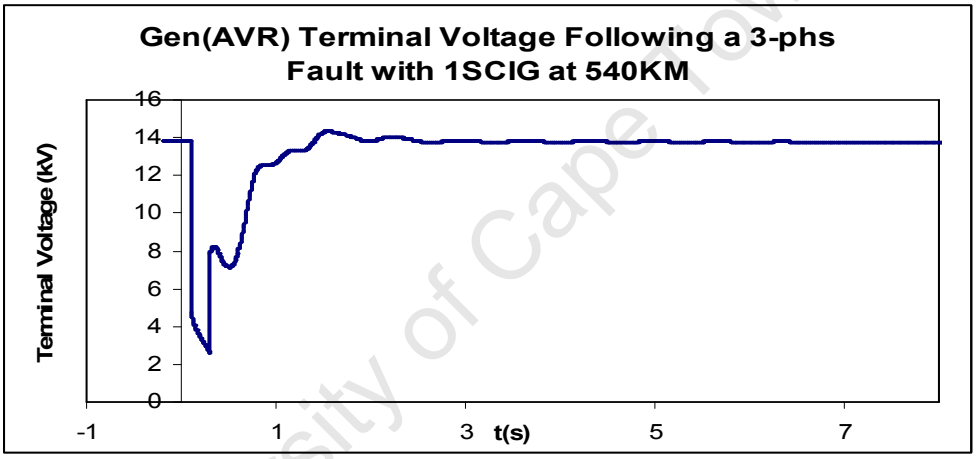


**Fig 4.9:** Terminal Voltage response with AVR and Wind Farm at 540 km

The terminal voltage is boosted back to its pre-fault level by the AVR as observed in Figure 4.9, which is the prime objective of the AVR. The slight overshoot as the voltage is recovering, can be attributed to the high gain of the AVR, as given in Appendix 9.

### 4.2.2 Effect of Speed Governor on the Transient Stability of the Power Network

The synchronous generator in Figure 4.1 was then fitted with an IEEEG2 speed governor only, i.e. The IEEET1 AVR was not included. The IEEEG2 speed governor is shown in Figure 4.10. The parameters of the speed governor are also given in Appendix 9.

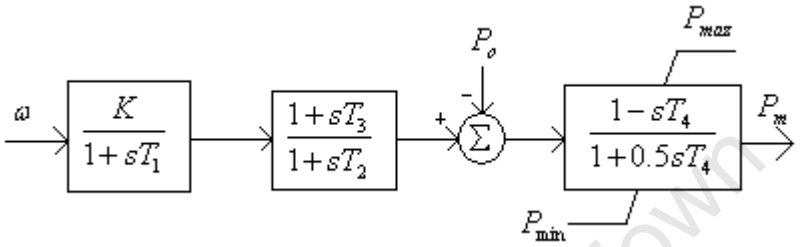


**Fig 4.10:** Representation of an IEEEG2 Speed Governor

In Figure 4.10 $K$ is controller gain, $T_1$ is governor time constant, $T_2$ is governor derivative time constant, $T_3$ is servo time constant, $T_4$ is water starting time, $P_{\max}$ is maximum gate limit , $P_{\min}$ is minimum gate limit and $P_m$ is the output mechanical power . After the fault occurs, there is a change in the electrical power output $P_e$ of the generator. This brings about a mismatch between the mechanical torque $T_m$ and the electrical torque $T_e$, which, in turn, results in speed variations [15].

A speed governor is a speed control mechanism which is responsible for controlling the throttle valves to the steam turbine or the gate position in hydro turbines and thereby adjusts the generator's mechanical power [23].

The transfer function in Figure 4.11 represents the change in rotor speed as a function of the electrical and mechanical power. This relationship characterises how the speed governor's operation of minimising the imbalance between mechanical power and the electrical power by changing the mechanical power accordingly, influences the degree of rotor speed variations $\Delta\omega_r$.

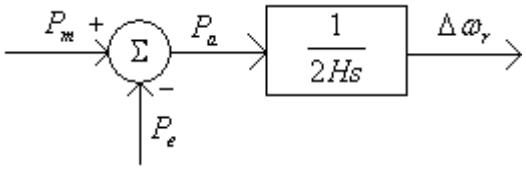


**Fig 4.11:** Transfer function relating speed and torques [15]

In Figure 4.11 $P_a$ is the acceleration power, $s$ is the Laplace operator and $H$ is generator inertia.

Table 4.6 shows the prefault and post fault power flow of the synchronous generator when the IEEEG2 speed governor was engaged. It is observed that in this case study, the post fault active power and reactive power were different to the prefault power flows.

**Table 4.6:** Prefault and Post fault Power Flow of Synchronous Generator (Governor)

| $P_{gen\text{-}Prefault}$ (MW) | $Q_{gen\text{-}Prefault}$ (MVAr) | $P_{gen\text{-}Postfault}$ (MW) | $Q_{gen\text{-}Postfault}$ (MVAr) |
|---|---|---|---|
| 80.00 | -94.15 | 77.08 | -83.06 |

Figures 4.12 and 4.13 show that after the fault was cleared with the generator fitted with the speed governor only, the power system did not maintain synchronism. This is evident after 18 seconds. The reactive power demand on the synchronous generator increased after isolating the faulted line. Furthermore the governor could only change the mechanical power of the generator, which was not sufficient to prevent instability.

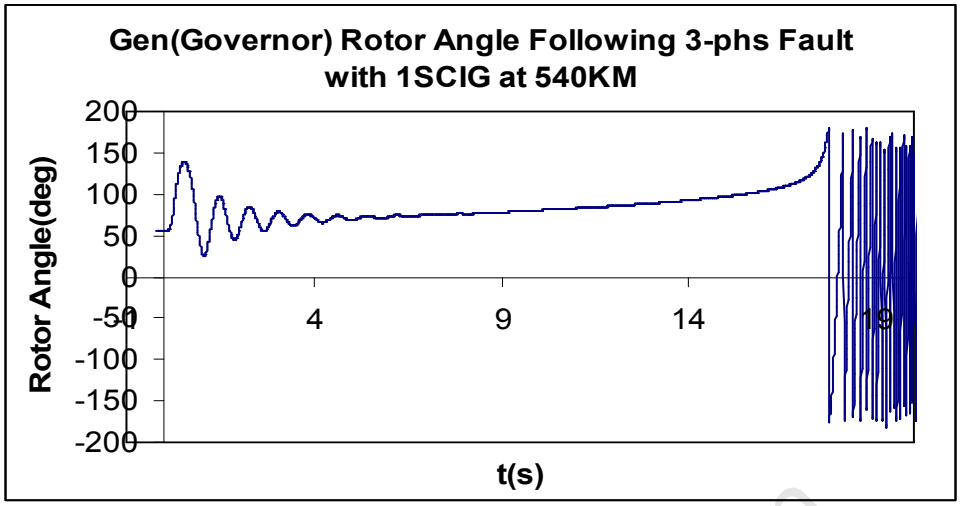


**Fig 4.12:** Rotor response of generator with governor to a 3-phs fault

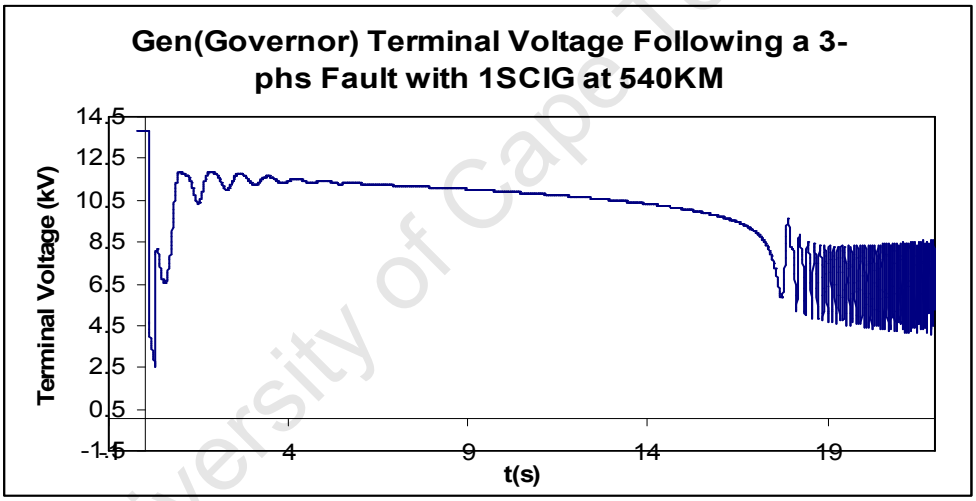


**Fig 4.13:** Generator terminal voltage response to a 3-phs fault



This kind of instability is not first swing instability, where the generator goes out of step within the first second after the fault is cleared. The magnitude of the rotor oscillations subside after the fault is removed as time progresses. However, the rotor's angle increases monotonically until stability is lost after about 18 seconds. When only the speed governor is included, the terminal voltage of the generator does not recover to the prefault value of 13.8 kV after the fault. The generator voltage recovers to about 11.5 kV before gradually decreasing with time to a point where the voltage collapses after 18 seconds. The IEEEG2 speed governor did not manage to reduce the degree of imbalance between the mechanical power and electrical power for the power system not to have lost stability using the given

parameters. However, the effect of change in the parameter values of the speed governor on the power system transient stability was not explored.

It is apparent that adding the IEEET1 AVR to the synchronous generator ended with a power system that was transiently stable in comparison with when only the IEEEG2 speed governor was connected. Nonetheless, the AVR and speed governor have complementary roles in practical systems, and both serve critical purposes with regard to controlling the power systems.

## 4.3 Impact of Increasing Squirrel Cage Induction Generators on System Transient Stability

It has been noted that, a longer transmission line connecting the wind farm to the power network has a negative effect on the transient stability of the power system. In order to distinctively investigate how increasing the number of squirrel cage induction generators connected on the power network will affect the transient stability of the power network, the transmission line connecting the wind farm was maintained at 1 km. The power system controllers were not included in this case, i.e. the AVR and the speed governor. The reactive power compensation (capacitor banks) for the SCIGs was also not included.

Figure 4.14 shows that, as the number of squirrel cage induction generators (SCIGs) increases within the wind farm, the magnitude of the first swing and subsequent oscillations of the synchronous generator's rotor angle also increases following the transient disturbance on the power network. Figure 4.15 shows that the normal operating slip($s$) of the wind farm before the fault is about -1 %, since the rotor speed of the squirrel cage induction generator is greater than that of the synchronous speed. When the fault occurs, the speed of the SCIG increases further, resulting in a more negative slip. Evidently as the wind farm capacity is increased to 40 MVA (4 SCIGs), the slip of the wind farm takes longer to recover after the transient fault is cleared. This is due to the cumulative inertia of the wind farm from the respective squirrel cage induction generators. The consequence of the SCIGs slip increasing is that the overall rotor resistance decreases $R_{rotor} = R_r / s$. Lower resistance leads to more current flowing

through the mainly inductive circuit of the SCIG , causing higher reactive power demand [43]. With a wind farm capacity of 40 MVA relative to 20 MVA and 10 MVA, there is a higher reactive power demand following the fault. This results in a much higher degree of imbalance between the mechanical power and electrical power of the synchronous generator, which brings about a higher acceleration power. The higher acceleration power is the reason for the bigger magnitude of the synchronous generator's first swing after the fault and subsequent oscillations thereof.

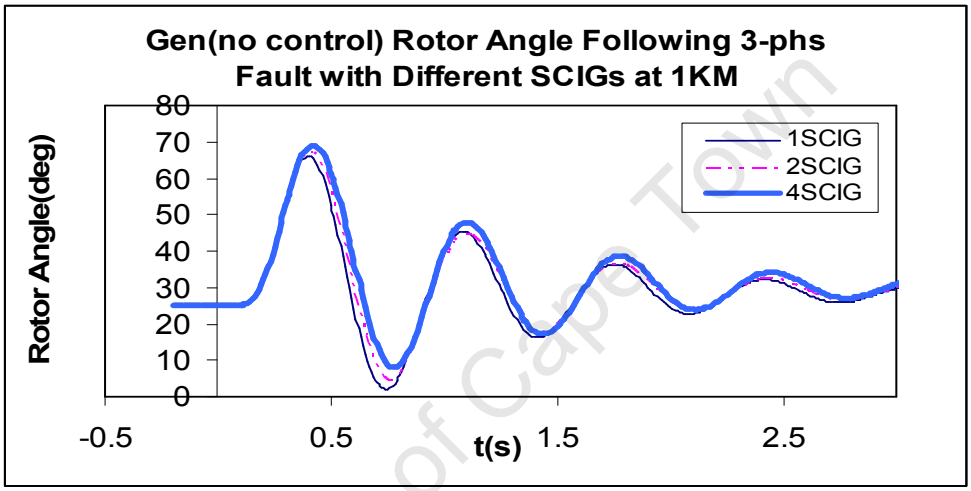


**Fig 4.14:** Rotor responses due to different number of wind generators (1,2 and 4)

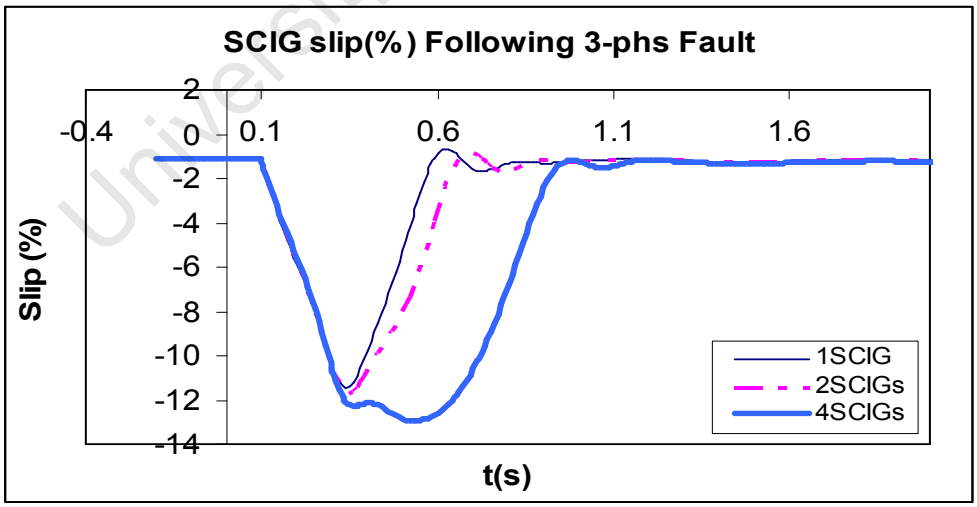


**Fig 4.15:** SCIG slip after a 3-phs Fault

The terminal voltage of the synchronous generator takes a much longer period to reach its post-fault level. This is about 13 kV when operating a 40 MVA wind farm on the power network, as shown in Figure 4.16. Because of an increased reactive power demand the

terminal voltage has a delay in recovering. When the wind farm capacity was increased to 50 MVA (5SCIGs), the rotor angle of the synchronous generator increased from 25° to about 52° after the fault, as shown in Figure 4.17 and 4.18. Since there is no AVR, the internal voltage of the synchronous generator is constant for all operating conditions. It then follows that, the rotor angle will increase as the reactive power demand on the synchronous generator increases and settles at a new operating point after the fault. The response of the generator's terminal voltage when the wind farm is increased to 50 MVA also highlights the effect of increased reactive power demand following the transient disturbance. The terminal voltage settles to about 9 kV as shown in Figure 4.18.

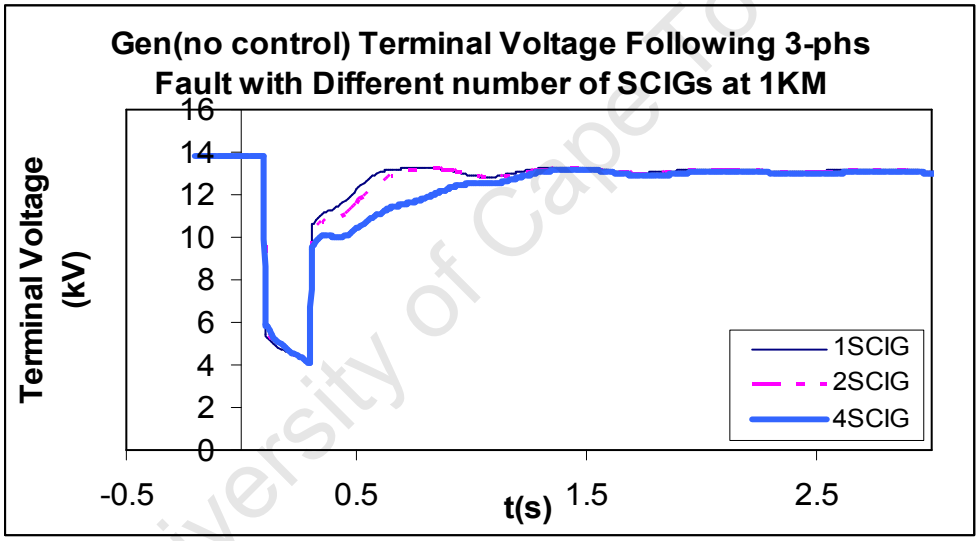


**Fig 4.16:** Terminal voltage due to different penetration of wind generators

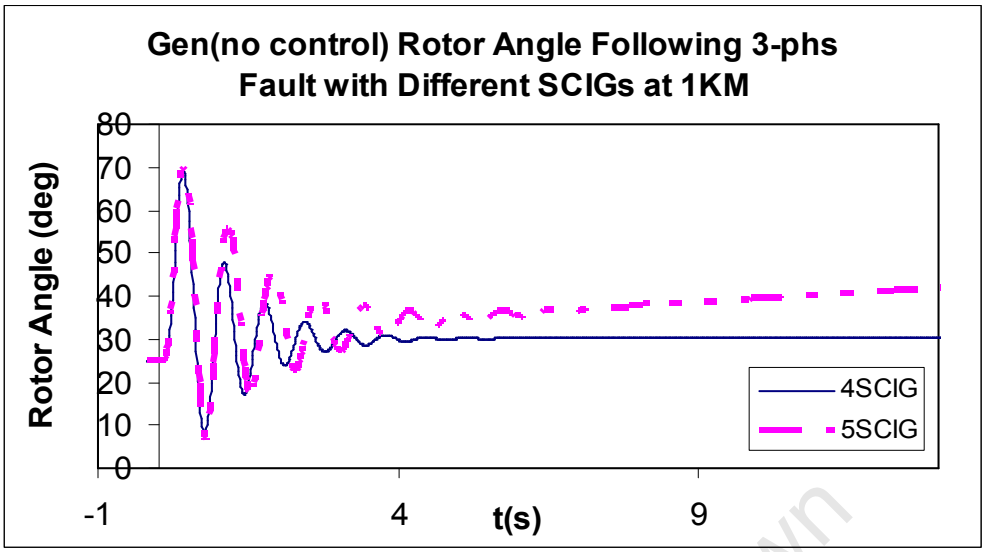


**Fig 4.17:** Rotor response due to different penetration wind generators (4 and 5)

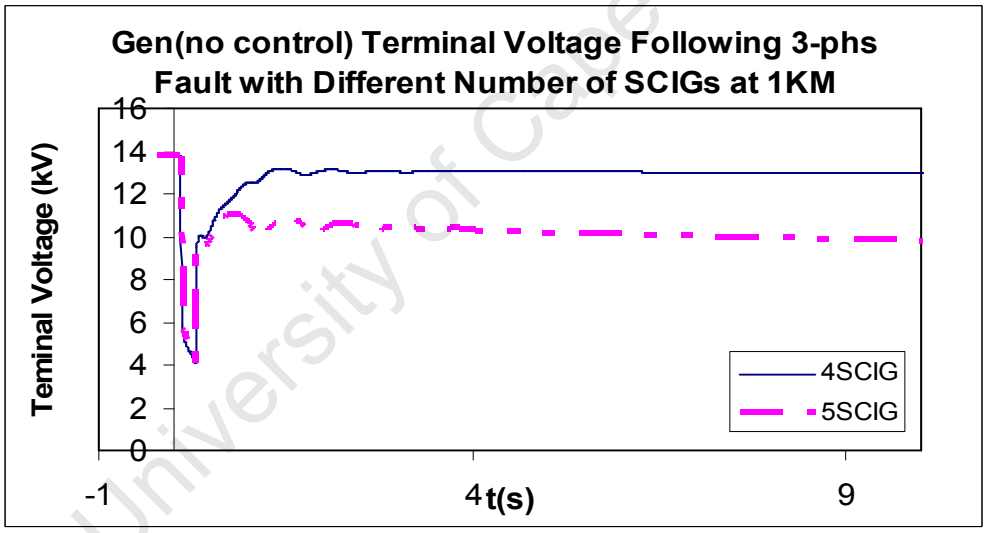




**Fig 4.18**: Generator terminal voltage response with different penetration of wind generators (4 and 5)

The power system remained stable with the 5SCIGs following the transient disturbance on the power network. This was with line 4 kept at 1 km. Reference is made to figures 4.17 and 4.18. These figures are supported by figures A 7.22 and A 7.23 in appendix 7.

## 4.4 The Effect of Capacitive Reactive Power Compensation of SCIGs on the System Transient Stability

The reactive power compensation generally used at the terminal of the SCIG was not included in the previous simulations. The capacity of the wind farm was set to 50 MVA (5 SCIGs) at a lagging power factor of 0.8. In the attempt to focus on the impact of compensating the SCIG wind farm with reactive power using capacitor banks. The case studies were investigated by setting the reactive power supplied by the capacitor bank to 15 MVAr, 20 MVAr and 30 MVAr under four different control scenarios, namely, without AVR and speed governor; with AVR only; with speed governor only and then with both AVR and speed governor. The wind farm was set to draw 30 MVAr from the power grid under normal operating conditions. The aforementioned different settings of the capacitor banks were chosen so that the impact on the power network's transient stability could be assessed when the reactive power demand of the wind farm was satisfied by having capacitor banks set to 30 MVAr. The 15 MVAr setting was to analyse how setting the capacitor banks to supply half of the wind farm's reactive power demand would affect the transient stability of the power grid. The capacitor bank setting of 20 MVAr was a choice setting between 15 MVAr and 30 MVAr, whereby 20 MVAr is approximately 0.67 p.u. of the rated reactive power that the wind farm is supposed to draw.

Tables 4.7, 4.8 and 4.9 list the voltage levels on the respective nodes of the power network when the capacitor banks were set to 15 MVAr, 20 MVAr and 30 MVAr under normal operating conditions.



**Table 4.7:** Voltage Levels on Power Network with Qcomp 15 MVAr in Steady-state

| | **V(kV)** | **$\delta$ (deg)** |
|---|---|---|
| Bus 1 | 13.80 | 1.07 |
| Bus 2 | 228.75 | 0.18 |
| Bus 3 | 229.67 | -1.80 |
| Bus 4 | 230.00 | 0.00 |
| Bus 5 | 228.72 | 0.20 |
| Bus 6 | 10.85 | 1.37 |

**Table 4.8:** Voltage Levels on Power Network with Qcomp 20 MVAr in Steady-state

| | **V(kV)** | $\delta$ **(deg)** |
|---|---|---|
| Bus 1 | 13.80 | 1.07 |
| Bus 2 | 228.97 | 0.18 |
| Bus 3 | 229.77 | -1.80 |
| Bus 4 | 230.00 | 0.00 |
| Bus 5 | 228.94 | 0.20 |
| Bus 6 | 10.98 | 1.37 |

**Table 4.9:** Voltage Levels on Power Network with Qcomp 30 MVAr in Steady-state

| | **V(kV)** | $\delta$ **(deg)** |
|---|---|---|
| Bus 1 | 13.80 | 1.08 |
| Bus 2 | 229.40 | 0.18 |
| Bus 3 | 229.99 | -1.80 |
| Bus 4 | 230.00 | 0.00 |
| Bus 5 | 229.39 | 0.20 |
| Bus 6 | 10.97 | 1.35 |

It is noted that voltage levels at bus 6, 5, 2 and 3 increased as the level of reactive power compensation was increased according to the given capacitor settings under steady-state conditions. This can be attributed to the relationship between the bus voltage and the reactive power supplied onto a respective bus, which is defined by equation 3.2-48. As the reactive power supplied by the capacitor banks to the SCIGs was increased from 15 MVAr to 20 MVAr and to 30 MVAr, more of the reactive power supplied by line 4 was transferred into the power network. This resulted with the voltage on bus 5, 2 and 3 increasing accordingly. The negative voltage angle on bus 3 brought to light the fact that active power flowed from bus 2 to bus 3 since active power flows from a leading voltage angle to a lagging voltage angle. The conventional synchronous generator supplied 80 MW for all levels of SCIG Qcomp (reactive power compensation) to load 1 on bus 2. The SCIG wind farm and infinite bus each supplied about 40 MW for all levels of the SCIG Qcomp. The cumulative active power (80 MW) from the infinite bus and the SCIGs was then supplied to load 2 on bus 3.

### 4.4.1 The Effect of Reactive Power Compensation (No AVR and No Speed Governor)

Figure 4.19 shows the responses of the generator's rotor angle after the three phase fault was applied on line 2 for 0.2 sec, whereby the fault was removed by taking the faulted line out of service. The system experiences instability. When compensation is 15 MVAr, the instability shows up only after 90 sec. This kind of instability is also not a first swing type of instability where the system goes out of step within 1 sec. As the level of compensation is increased, the time span before the instability occurs is shortened. For the 15 MVAr compensation, the instability occurs in about 100 sec, while in the case of 30 MVAr compensation, the instability occurs in about 47 sec. These results were rather surprising as there was no expectation that the system was to take more than 30 sec before showing signs of instability.

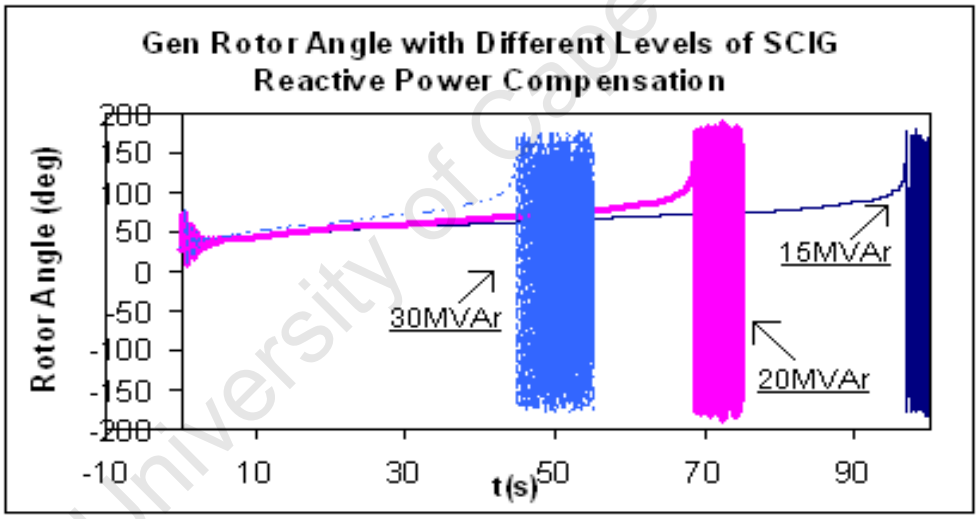


**Fig 4.19:** Rotor responses (no AVR and Governor)

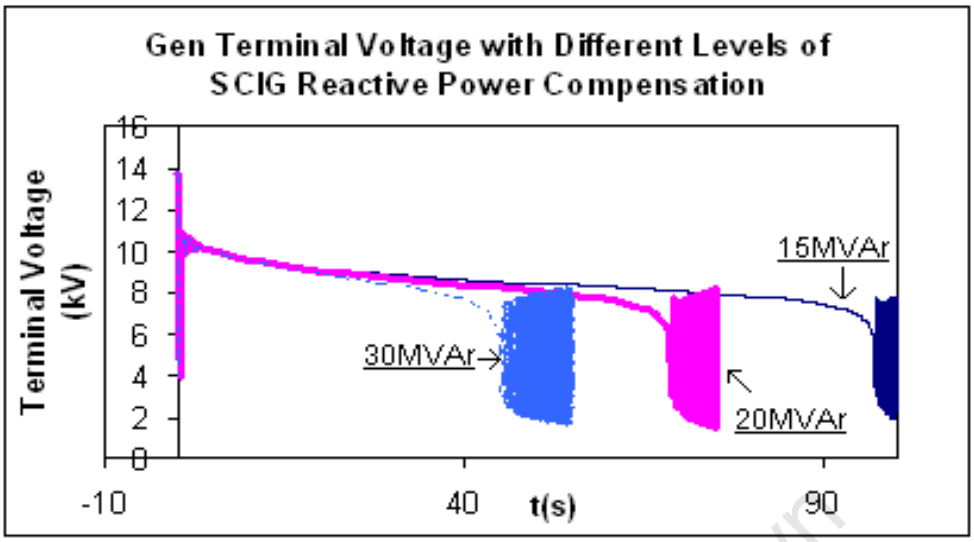


**Fig 4.20:** Generator terminal voltage (no AVR and no Speed Governor)

The results suggest that, even though increasing the reactive power compensation to 30 MVAr improved the voltage level in steady-state, this level of reactive power compensation is not good for improving the power system's transient stability. Figure 4.20 shows the response of the terminal voltage of the generator. The pattern is similar to that of the rotor angle responses. The instability of the system is evident in the responses. There is inadequate excitation voltage to support the increased reactive power demand from the power network with a changed topology. The voltage levels decrease further with time. When 30 MVAr compensation is used, the voltage level drops to about 8 kV after the fault was cleared before collapsing.

### 4.4.2 The Effect of Reactive Power Compensation (with AVR only)

When the generator is equipped with an AVR, which performs the function of changing the synchronous generator's internal voltage in an effort of maintaining a constant terminal voltage for different operating conditions of the power network, the system remains stable for all levels of reactive power compensation as can be seen in Figures 4.21 and 4.22.The responses of the terminal voltage in Figure 4.22 shows that the voltages return to their prefault level of 13.8 kV after the fault is cleared. This is in contrast with Figure 4.20, where the voltage levels seemed to drop significantly after the fault was cleared. This shows the effectiveness of the AVR in improving the transient stability of the system. Again, the 20

MVAr compensation level gives the best responses followed by that at 15 MVAr. The 30 MVAr compensation level produces the worst responses. In this case, the terminal voltage response is slugging, and the voltage returns to it initial value only after about 3 sec.

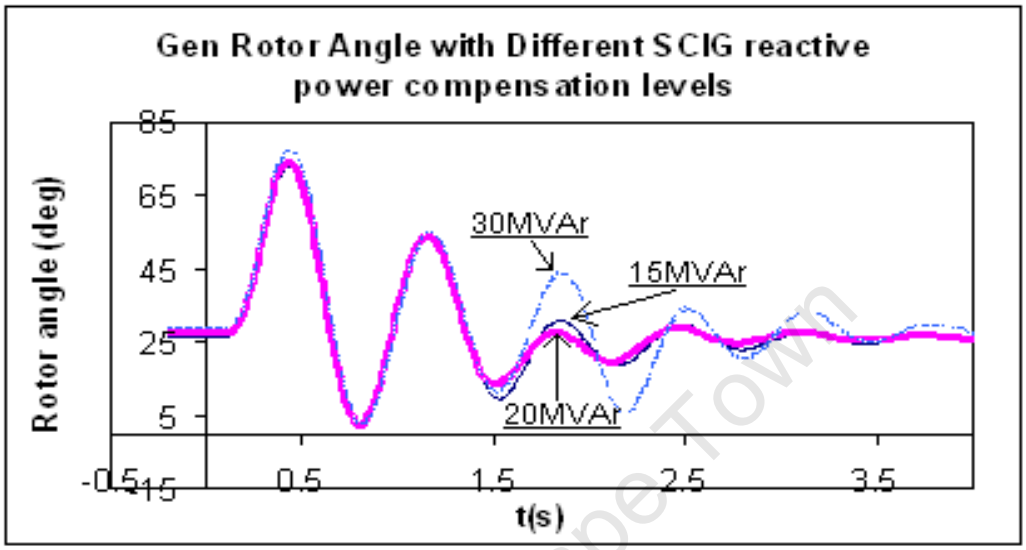


**Fig 4.21:** Rotor angle response (with AVR only)

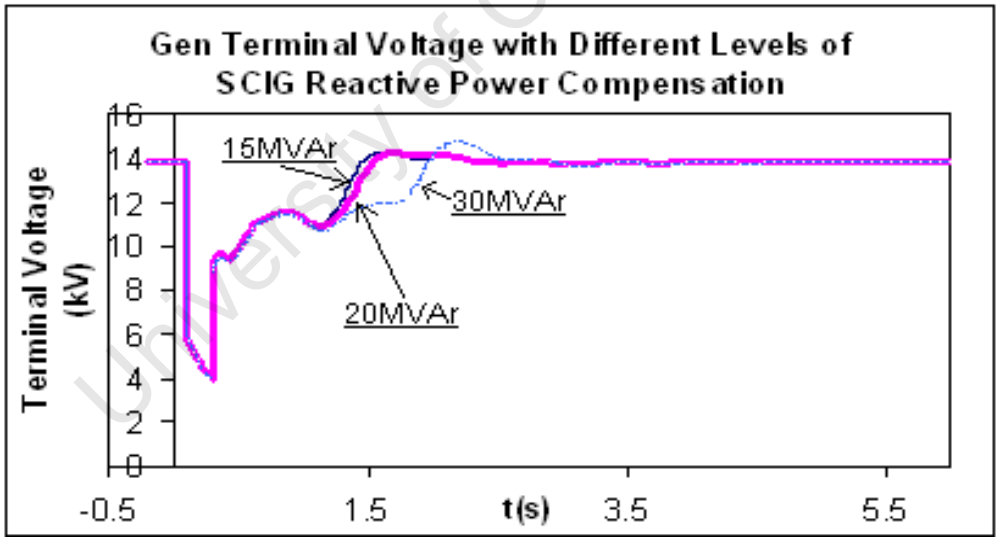


**Fig 4.22:** Generator terminal voltage with AVR

### 4.4.3 The Effect of Reactive Power Compensation (with Governor only)

When the governor is included, the system still experiences instability as can be seen in Figures 4.23 and 4.24. The governor's main function is to sense a speed deviation and or power change command, and convert it into appropriate valve action to restore the generator speed [18]. So, when the state of equilibrium between mechanical and electrical power is disturbed by the fault on the power network, the speed governor will act to minimise the resultant acceleration power by decreasing and increasing the generator's mechanical power. The reactive power demand increased after isolating the faulted line, and the governor could only change the mechanical power of the generator, which was not sufficient to prevent instability as shown in Figure 4.23. The power network experienced instability much more quickly with reactive power compensation of 30 MVAr level followed by the 20 MVAr and then 15 MVAr compensation level. Based on theoretical understanding of the functionality of the speed governor, it was expected that, if instability occurred following the fault with the IEEEG2 speed governor included, the period leading to instability in this particular case study would have been longer for the different levels of SCIG reactive power compensation. This is compared with the case study in which there were no system controllers for the different levels of SCIG reactive power compensation. However, the simulation results suggest that the IEEEG2 speed governor model used did not have much significant impact to the transient stability of the power system. This was because the periods of instability when there were no controllers appeared to be similar to when only the speed governor was included.



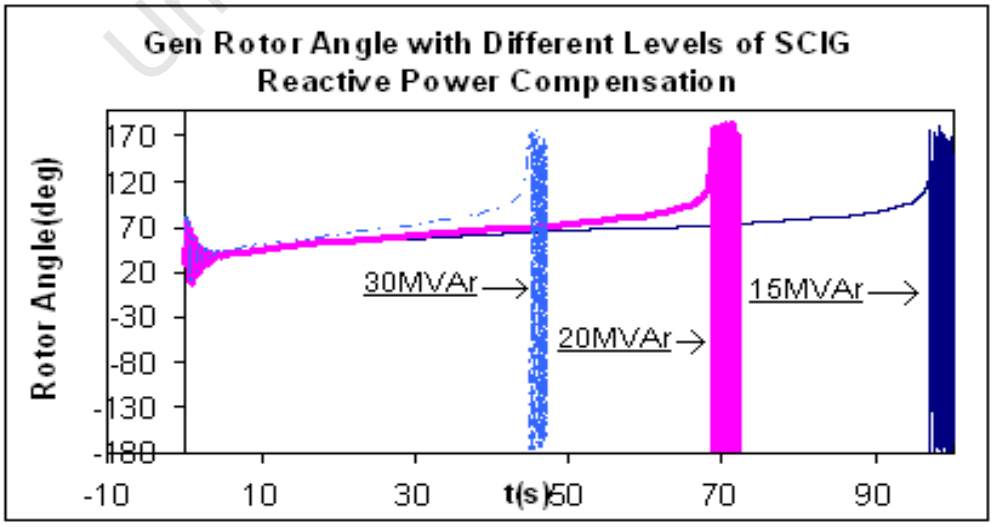


**Fig 4.23:** Rotor angle responses (with governor only)

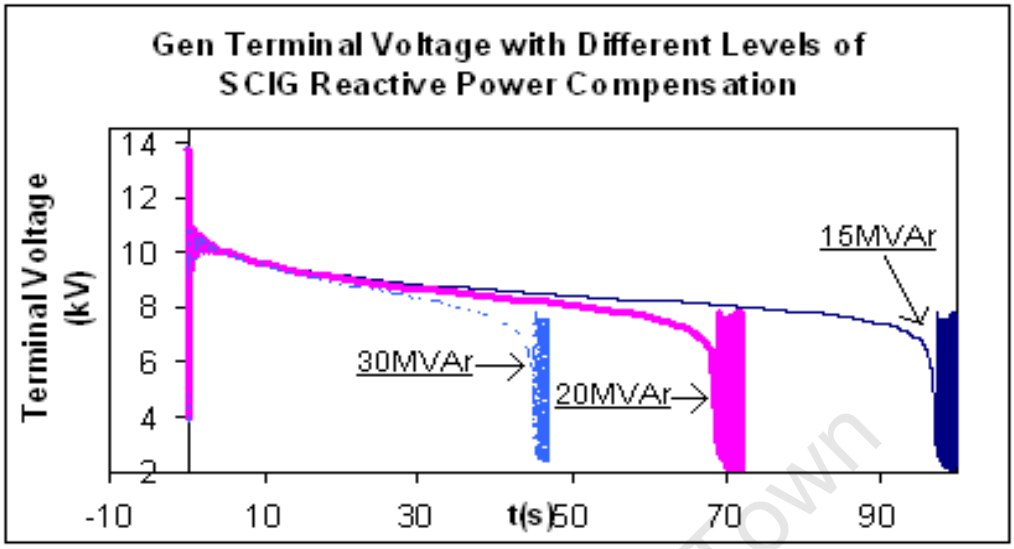


**Fig 4.24:** Terminal voltage (with governor only)

### 4.4.4 The Effect of Reactive Power Compensation (with AVR and Governor)

Both the AVR and governor were activated for different levels of compensation. The power system's response to the fault is much the same as in the cases where only the AVR was included. The system is transiently stable as shown in Figures 4.25 and 4.26. The subsequent oscillations of the generator to the first swing, with compensation of 30 MVAr, have a much bigger amplitude than those of 15 MVAr and 20 MVAr compensation levels. This effectively highlights the negative influence that Qcomp (reactive power compensation) of 30 MVAr has on the damping of the rotor oscillations of the generator. Figure 4.28 show cases that the Qcomp of 30 MVAr results in the terminal voltage of the generator taking a bit longer to get to its prefault value compared with the other two compensation levels.

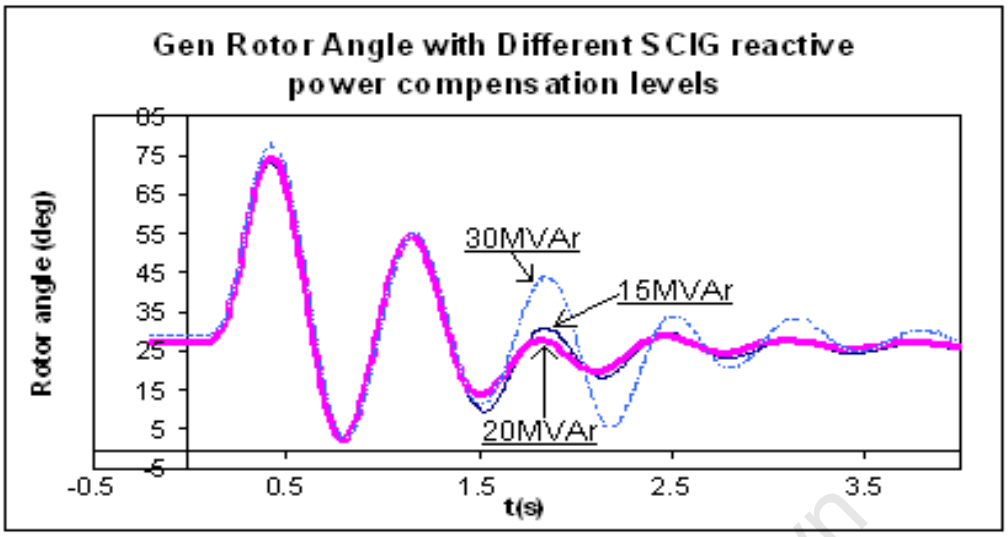


**Fig 4.25:** Rotor response (with AVR and governor)

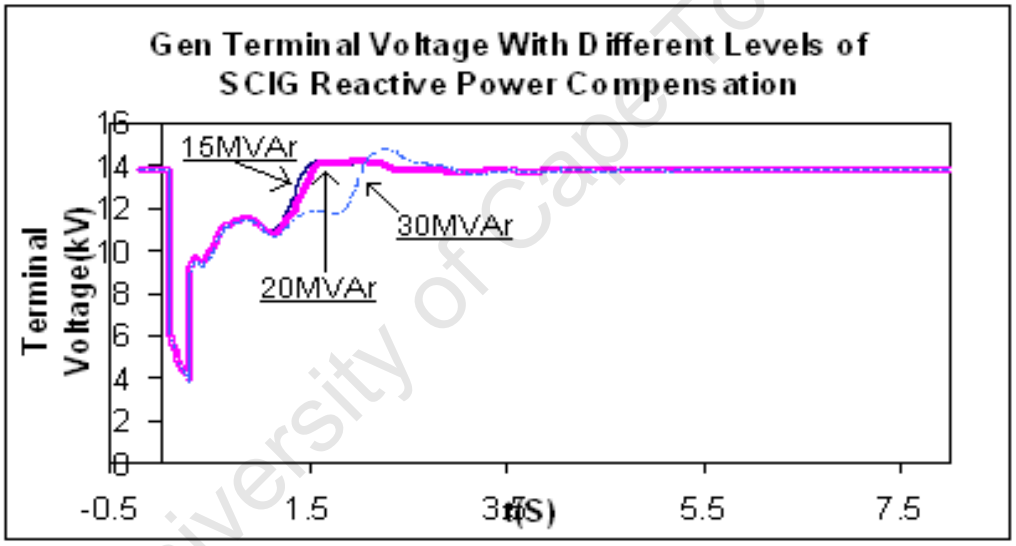


**Fig 4.26:** Terminal voltage with AVR and governor



### 4.4.5 The Effect of Reactive Power Compensation on AVR Excitation Voltage and Speed Governor Output

The effect of the different levels of Qcomp on the excitation voltage is shown in Figure 4.27. The excitation voltage rises for all levels of reactive power compensation to its maximum limit, following the fault on the power network. At 30 MVAr compensation level, the excitation voltage stays at the maximum value longer than the other two compensation levels. Also, at 30 MVAr compensation level, the minimum value of the excitation voltage is lower than that of the other two levels. This goes to show how 30 MVAr compensation impacts on the excitation system following the transient fault.

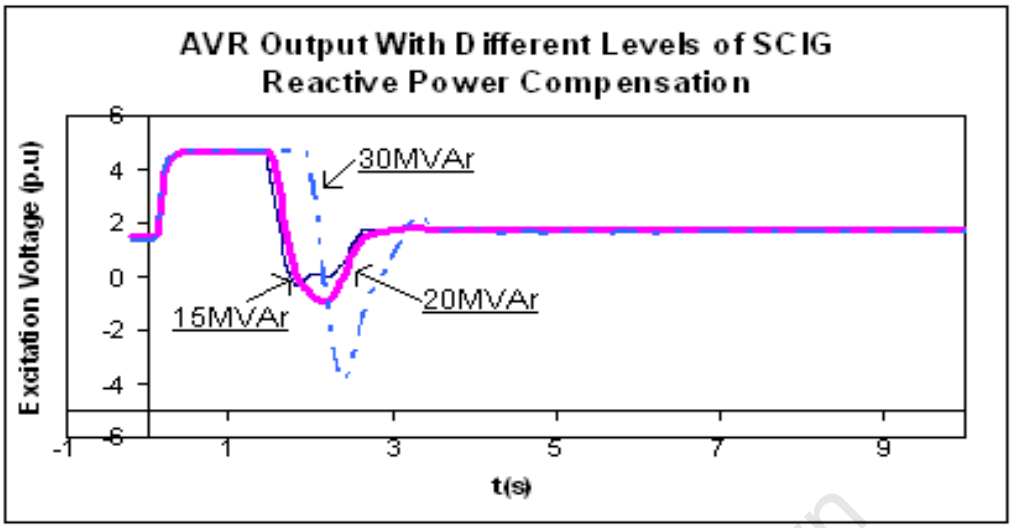


**Fig 4.27:** Excitation voltage with different levels of compensation

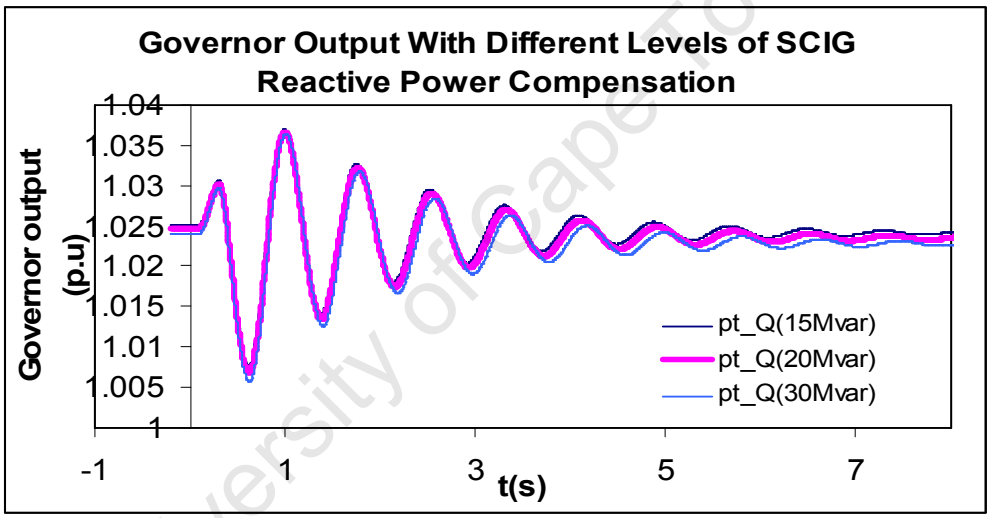


**Fig 4.28:** Governor output with different levels of compensation

The speed governor is evidently not affected in a particular way by any of the reactive power levels which were explored. The mechanical power of the governor increases and decreases accordingly in effort of minimising the imbalance between the mechanical and the electrical power of the generator as shown in Figure 4.28.

## 4.5 The Effect of Squirrel Cage Induction Generator Inertia on System Transient Stability

The squirrel cage induction generator based wind farm was then maintained at a generating capacity of 50 MVA at a lagging power factor of 0.8 with no capacitor banks. The length of the transmission line connecting the wind farm to the power network was kept at 1 km for all case studies in which the inertia of the squirrel cage induction generators was altered for every three-phase fault that was applied. The fault had a duration of 0.2 sec and was cleared by placing the faulted line out of service. In all the case studies, the AVR and speed governor were not activated.

Figures 4.29 and 4.30 compare the effect of increased SCIG inertia from 1.21 sec to 1.87sec on the transient stability of the power system. When the SCIG inertia was at 1.87 sec, the rotor angle of the synchronous generator settled at 30° after the fault was cleared by removing the faulted line from the power network indefinitely. Whereas, when the SCIG inertia was at 1.21 sec, the rotor angle increased to about 52° as seen from Figure A 7.22 in Appendix 7 after the fault was cleared. Increasing the inertia of the induction generators brought about a higher resistance towards the increment of the SCIGs speed after the fault occurred. With a lower inertia, the SCIGs would speed up more following the transient disturbance. This would lead to higher magnetising currents flowing through the SCIGs leading to a higher reactive power demand from the grid. Figure 4.30 shows how the terminal voltage of the synchronous generator only recovers to about 11 kV when the inertia of the SCIGs is 1.21 sec after the fault is cleared, as an indication of increased reactive power demand. Thus, it recovers to about 13 kV when the inertia of the SCIGs is increased to 1.87 sec, indicating that the reactive power demand on the synchronous generator after the fault was cleared, was not as much as in the previous case.

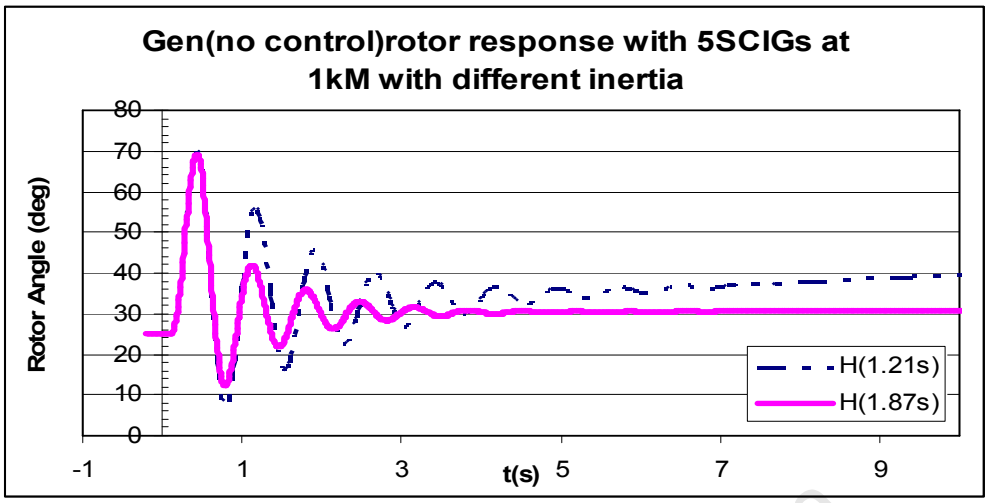


**Fig 4.29:** Generator rotor response due to different SCIG inertia

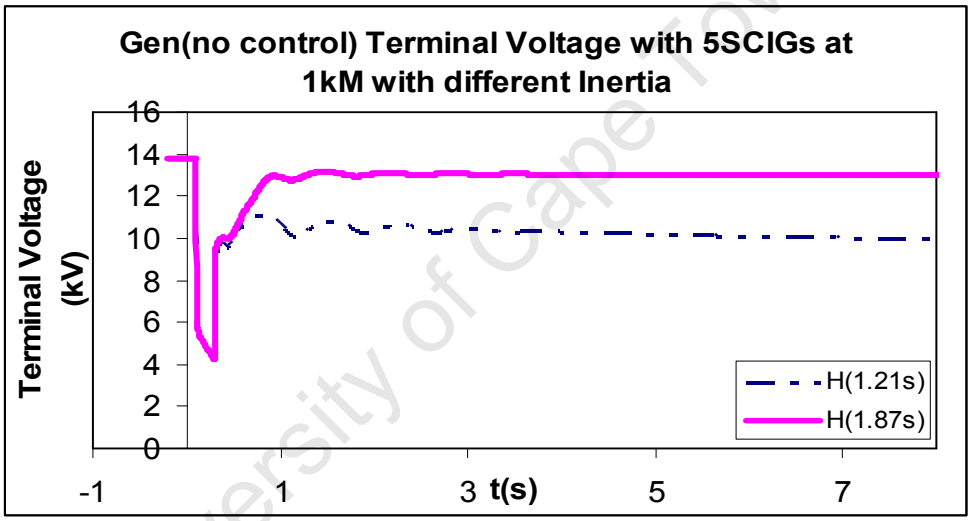


**Fig 4.30:** Generator terminal voltage due to different SCIG inertia

Figure 4.31 shows that, when the fault occurs, the imbalance of mechanical power of the SCIG and its generated electrical power will cause the SCIG to speed up, especially when the inertia of the SCIG is relatively low (i.e. 1.21 sec). Once the fault is cleared, the SCIGs reactive power consumption from the power grid increases due to its high rotational speed. If the rotor accelerates faster than the terminal voltage of the SCIG is restored, the SCIGs reactive power consumption continues to increase, leading to a further decrease of the SCIGs terminal voltage and balance between the mechanical and electrical power, and a further acceleration of the rotor. Depending on the design and the settings of its protection system, the wind turbine will either be stopped by its under voltage protection or be stopped and disconnected by its overspeed protection [27].

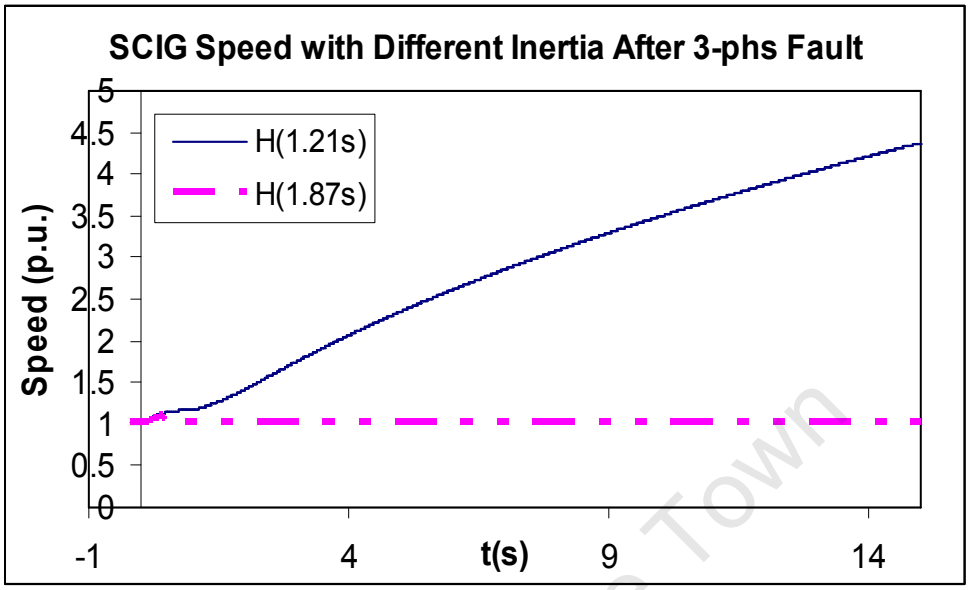


**Fig 4.31:** SCIG speed following the 3-phs fault with different inertia

# THE IMPACT OF A DOUBLY-FED INDUCTION GENERATOR (DFIG) ON THE TRANSIENT STABILITY OF A POWER NETWORK

# 5

## 5.1 Introduction

Wind turbines based on doubly – fed induction generators (DFIG) are currently the most popularly used in the field of wind power, and thus deserve some attention [32]. The case studies presented below focus on the responses of the grid to a transient disturbance (i.e. a three phase fault), when doubly-fed induction generators are connected to the grid. The DFIGs are connected to the same network as that shown in Figure 4.1 having the same parameters. Figure 5.1 shows the power network model to which the doubly-fed induction generators were connected. The applied three-phase fault on line 1 is cleared by putting the faulted line out of service after 0.2 sec. One doubly-fed induction generator is rated at 10 MVA with a lagging power factor of 0.8. The voltage source converter (VSC) had a power rating of 3 MVA and initially had its reactive power set to 0 MVAr. The chosen control mode of the VSC model was that of Vdc-Q, which specifies the dc-voltage and reactive power. The transmission line connecting the doubly-fed induction generators (line 4) to the power network was kept at a length of 1 km.

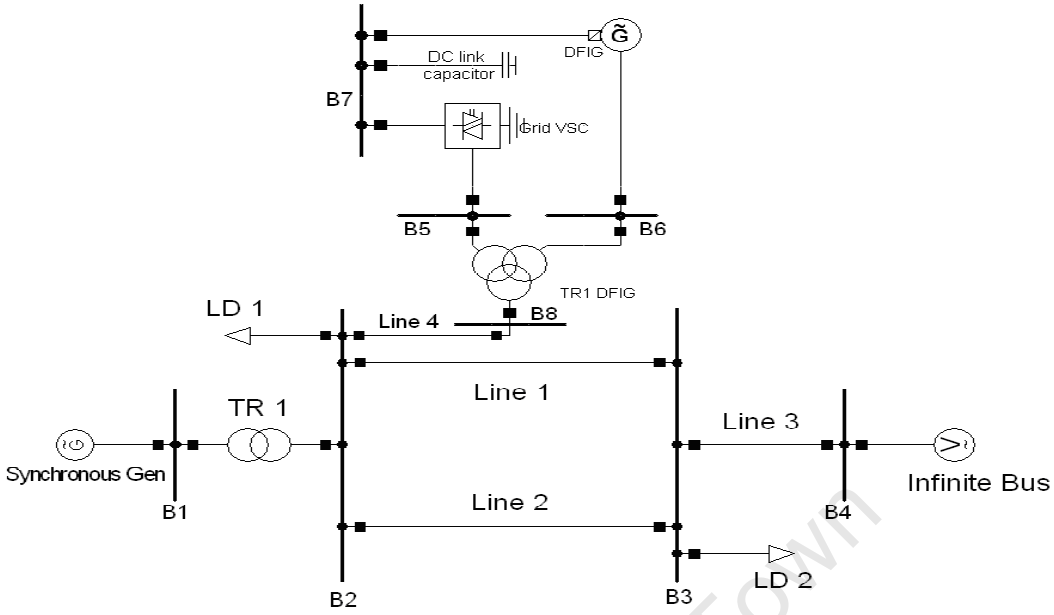


**Fig 5.1:** Power network model connected to a doubly-fed induction generator

## 5.2 The Effect of Penetration of Doubly-Fed Induction Generators on the Power System Transient Stability

Focus was initially placed on the impact on the power system's transient stability when the number of doubly-fed induction generators connected to the power grid was increased. Figure 5.2 shows how the synchronous generator rotor responds after the fault is cleared when the number of DFIGs connected to the power network increased. The magnitude of the first swing of the synchronous generator increases as the number of DFIGs connected increases. This is due to the fact that, when a short circuit occurs on the power grid, the voltage drop at the DFIG terminal results in a drop in the active power through the stator. This then causes the electrical torque to drop, as shown in Figure 5.3, which, in turn causes the DFIG to accelerate. An increased acceleration causes an increase in the reactive power consumption of the DFIG through the stator. Thus, with a higher number of DFIGs there will be an increase in this reactive power consumption, which would effectively result in a higher imbalance between mechanical power and the electrical power of the synchronous generator. Hence, the transient stability margin of the system will be negatively affected. However, in this particular case, the DFIGs protection system (i.e. the Crow bar), was not set to operate when the short circuit occurred on the power grid. This crowbar protection system would in actual fact, block the rotor side converter when high rotor currents are detected and have the DFIG behaving as a squirrel cage induction generator. This would imply that the controllability of the DFIG would be lost during crowbar coupling and the DFIG wind park would consume more reactive power during the crowbar coupling as the number of DFIGs on the power network increased [12]. Nonetheless, the grid side converter stays active during grid faults, whether the rotor side converter is blocked by the crow bar or not. The grid side converter can then contribute supplementary reactive power to the grid. Moreover, this reactive power will be limited to the rating of the VSC, which is about 25 % - 30 % of the rated power of the DFIG.

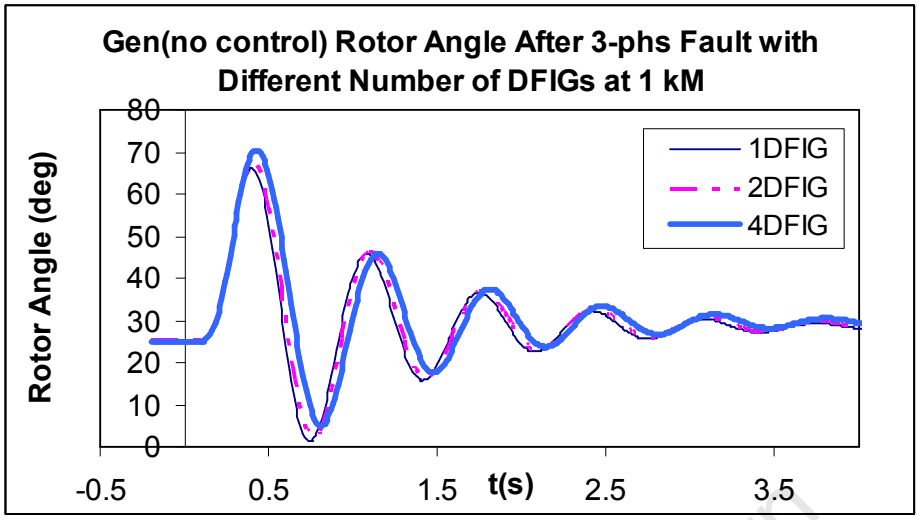


**Fig 5.2:** Rotor response with increased penetration of DFIGs on power network

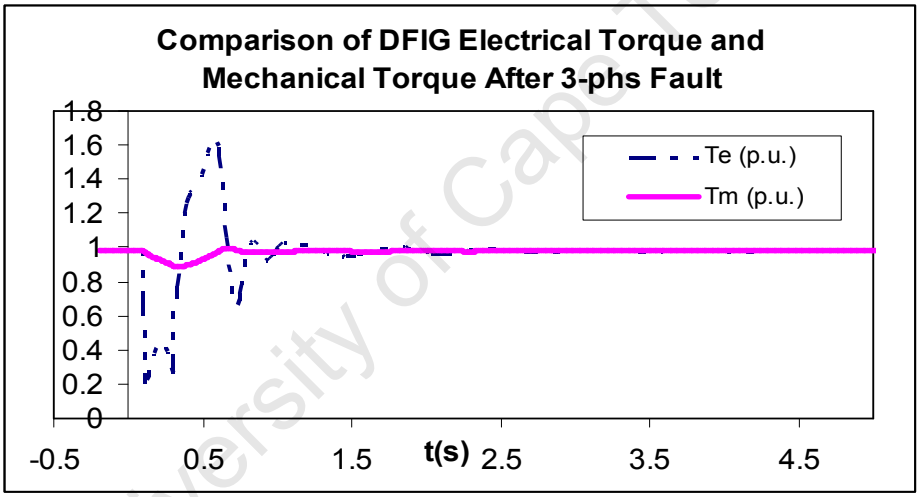


**Fig 5.3:** Comparison of DFIG electrical torque and mechanical torque after 3-phs fault

Figure 5.4 shows, the negative consequences of increasing the number of DFIGs connected to the power grid, which is, the terminal voltage of the synchronous generator experiences a delayed recovery to its post-fault level. In this particular case, when there were 4 DFIGs connected, the terminal voltage of the synchronous generator recovered to 13 kV slightly longer than when there was 1 DFIG and 2 DFIGs connected to the power network. This was due to an increased reactive power demand on the synchronous generator after the fault, when there were 4 DFIGs compared with when there was a smaller number of DFIGs on the power network.

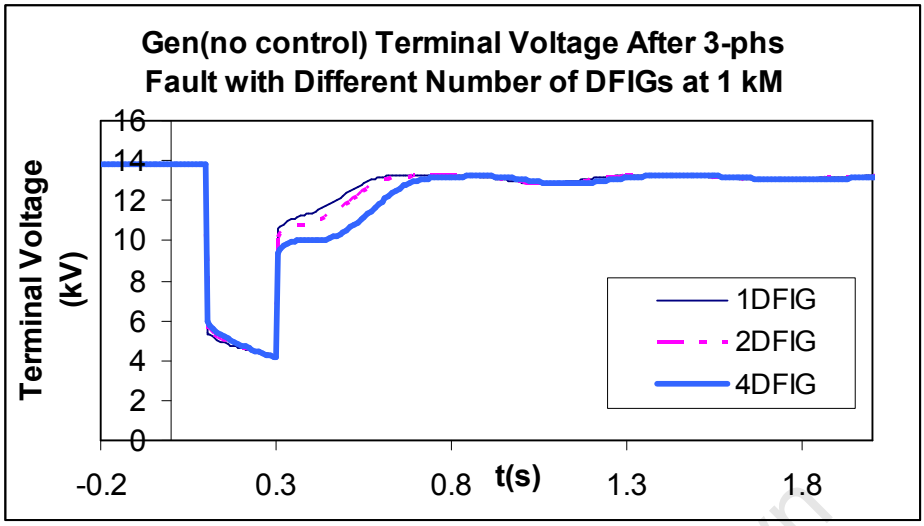


**Fig 5.4:** Terminal voltage response with increased penetration of DFIGs on power network

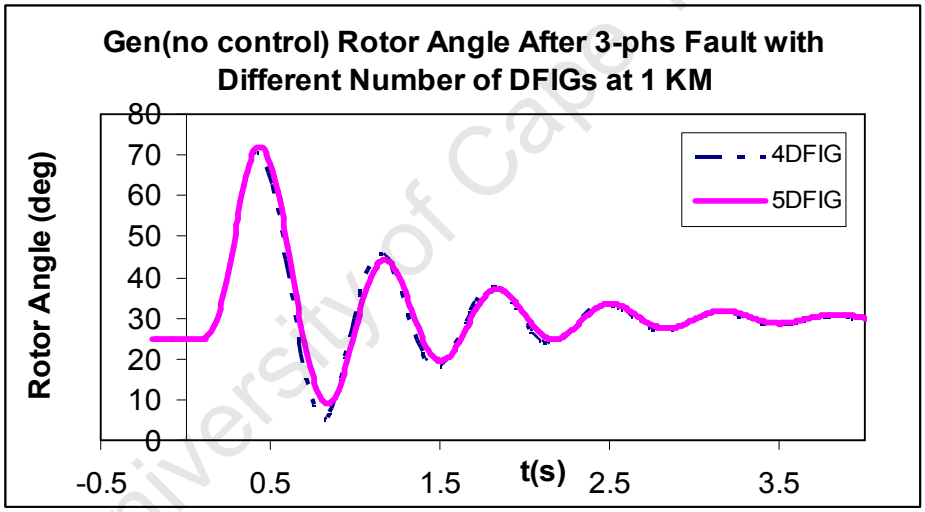


**Fig 5.5:** Rotor response with increased penetration of DFIGs on power network

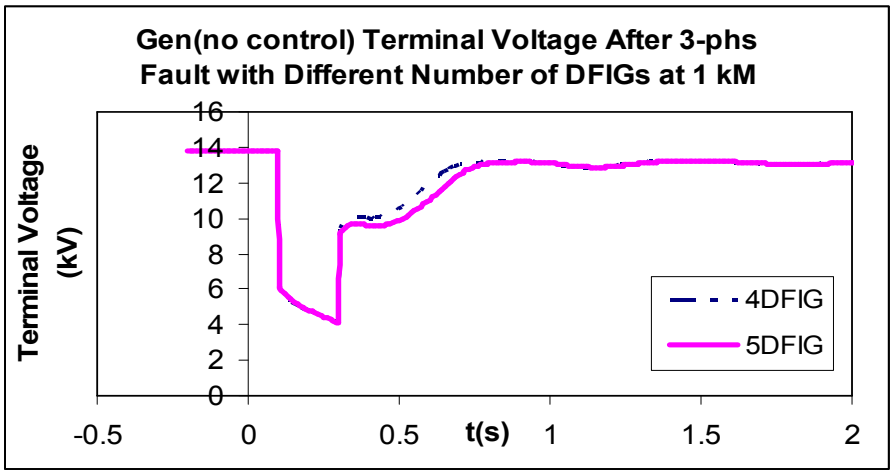


**Fig 5.6 :** Terminal voltage response with increased penetration of DFIGs on power network

### 5.2.1 The Effect of AVR on Power System Transient Stability with 5DFIGs

Figure 5.7 highlights the fact that, when an AVR is included, the synchronous generator's rotor angle settles at about 25° after the fault is cleared. This is the same angle as the pre-fault angle. However, when there was no controller included, the rotor angle of the synchronous generator settled at about 30° after the fault was cleared. The settling of the rotor angle at its prefault rotor angle when the AVR is included is because the synchronous generator is able to generate enough reactive power to meet the total reactive power demand from the power network after the fault was cleared by removing the faulted line out of service. This is supported by equation (4.2-1), which governs the relationship of the synchronous generator's reactive power and its rotor angle.

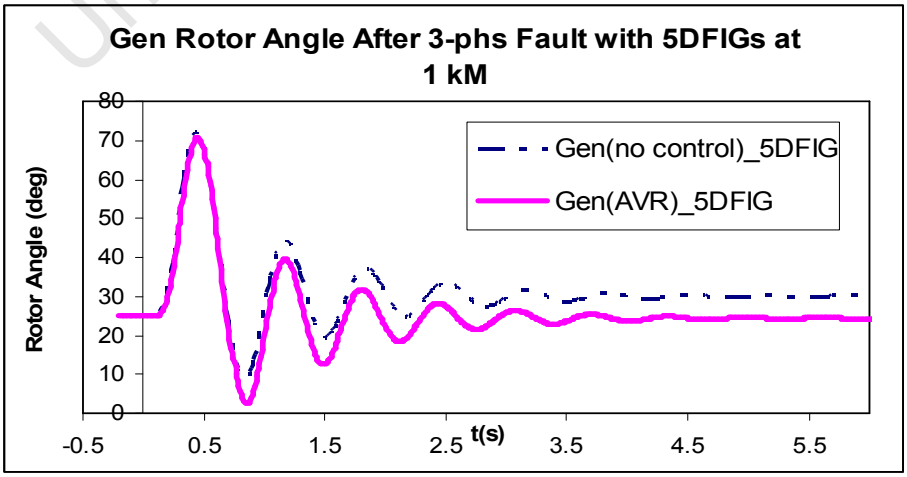


**Fig 5.7:** Rotor response with AVR and no controller after fault with 5DFIG connected

Figure 5.8 shows that, with the inclusion of an AVR, the terminal voltage of the synchronous generator is restored to its prefault level following the fault. Based on the reactive power demand from the power network on the synchronous generator after the fault, the excitation system increased its excitation current to inject more reactive power into the power network and thus supporting the terminal voltage of the synchronous generator. This resulted in the terminal voltage recovering back to its prefault level of 13.8 kV. With no AVR, the post-fault terminal voltage settled at around 13.2 kV.

An observation made here is that, the difference is relatively small between the terminal voltage of synchronous generator when the AVR is included compared to when it is not included. The voltage difference is about 0.6 kV, which highlights the fact that, the DFIGs grid side converters offered reactive power support to the power network after the fault. This effectively reduced the total amount of reactive power demand on the synchronous generator from the power network, and thus, when there was no AVR included, the terminal voltage recovered to 13.2 kV after the fault.

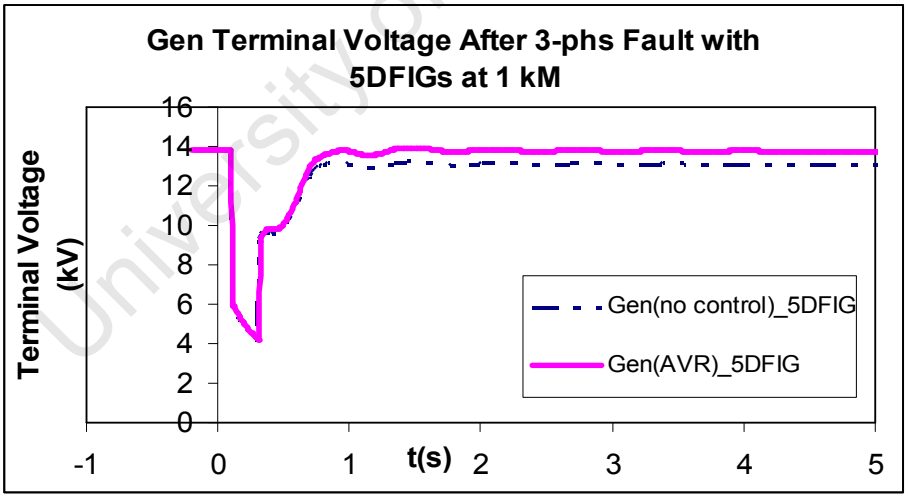


**Fig 5.8:** Terminal voltage response with AVR and no controller after fault with 5DFIG connected

## 5.3 The Effect of Different Reactive Power Set-points of the VSC on the on the Power System Transient Stability

In this case study, the capacity of the DFIG wind farm was kept at 50 MVA (i.e. 5 DFIGs). The voltage source converter's (VSC) reactive power exchanged with the grid depends on the control strategy and the converter rating, but often equals zero. This means that the grid side converter operates at unity power factor [27]. It was on this premise that, the VSCs reactive power set-point was initially set to 0 MVAr. Each induction generator was set to generate 8 MW and draw 6 MVAr through the stator terminals. No generator controllers (i.e. AVR and speed governor) were used in the ensuing case studies.

Table 5.1 tabulates the amount of reactive power generated by the synchronous generator as the reactive power set point (Qsetpoint) of the VSC is varied between -3 MVAr and 3 MVAr under steady state operation.

Table 5.1 Generator Reactive Power as VSC Qsetpoint Varies

| $Q_{gen}$ (MVAr) | VSC Qsetpoint (MVAr) |
|---|---|
| 45.51 | -3 |
| 40.75 | -2 |
| 31.35 | 0 |
| 22.10 | 2 |
| 17.53 | 3 |

It is evident that, as the VSC injects more reactive power into the grid, the synchronous generator generates less reactive power. A three-phase short-circuit was then applied on line 1 for 0.2 sec before taking the faulted line out of service. The response of the synchronous generator to the transient disturbance was observed under three different settings of the VSC Qsetpoints (-3 Mvar, 0 Mvar and 3 Mvar). Qsetpoints 2 MVAr and -2 MVAr were not explored in effort of focusing on the effect of unity power factor setting of the VSC and the effect of maximum and minimum reactive set points of the VSC on the transient stability of the power system. In Figure 5.9, the transient response of the rotor angle is depicted. It is seen that with Qsetpoint at -3 MVAr, the magnitude of the first swing of the rotor is relatively smaller compared with the other reactive power set points. However, the subsequent swings

are higher than the other two Qsetpoints (i.e. 0 MVAr and 3 MVAr). Qsetpoint 3 MVAr resulted in the biggest magnitude of first swing after the fault, nevertheless, subsequent oscillations to the first swing were smaller in amplitude and settled much quicker when compared with Qsetpoint of 0 MVAr and Qsetoint of -3 MVAr. A high reactive power set point seems to have a negative effect on the initial response of the synchronous generator after the fault. With the VSC reactive set point at 0 MVAr, the first swing of the synchronous generator after the fault was higher than when the Qsetpoint was -3 MVAr and smaller than when the Qsetpoint was 3 MVAr. The subsequent oscillations to the first swing appeared to be similar to those when Qsetpoint was at 3 MVAr, i.e. smaller compared with when Qsetpoint was at -3MVAr.

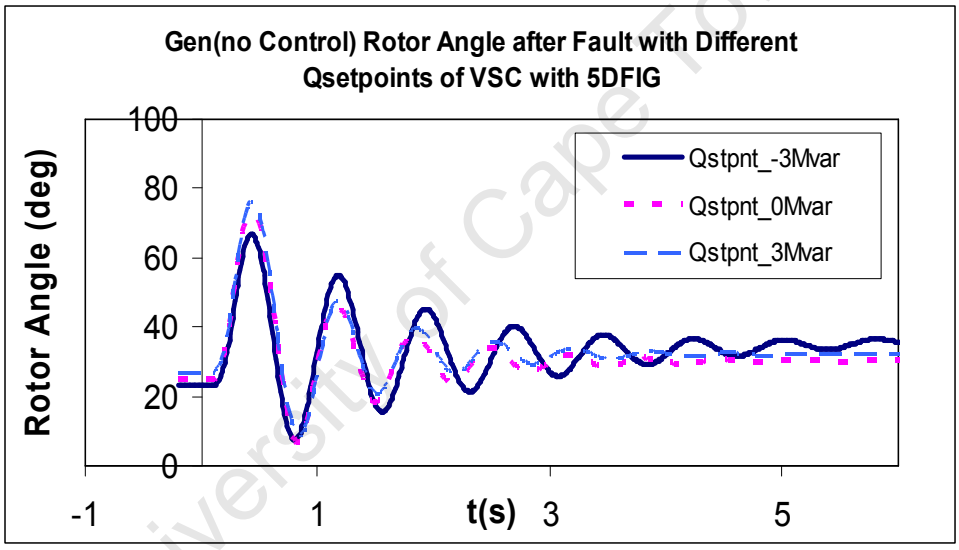


**Fig 5.9:** Rotor response due to different VSC Qsetpoints

From Figure 5.10, it can be seen that Qsetpoint of -3 MVAr does not result with an acceptable voltage level following the fault since the voltage drops from 13.8 kV to 10 kV, which is about 0.72 p.u. of the prefault voltage. Both Qsetpoints 3 MVAr and 0 MVAr have a similar effect on the terminal voltage of the synchronous generator following the fault as observed in Figure 5.10.

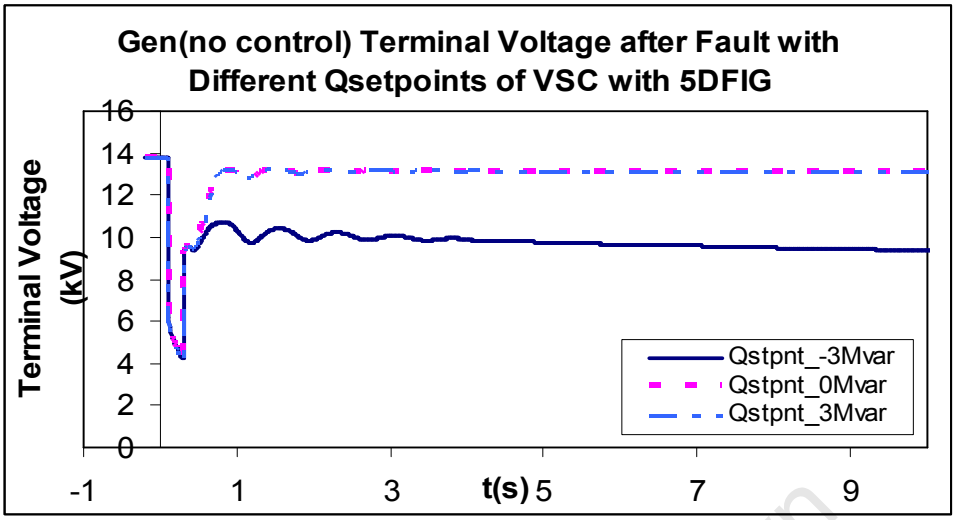


**Fig 5.10:** Terminal Voltage due to different VSC Qsetpoints

Figure 5.10 shows that after the fault, the reactive power demand on the synchronous generator is highest with Qsetpoint at -3 MVAr. The high reactive power demand is due to the change in the network topology of putting the faulted line out of service as well as the reactive power drawn by the converter. It is observed in Figure 5.11, that, immediately after the fault was cleared, the synchronous generator experienced the highest reactive power demand with Qsetpoint -3 MVAr, followed by 0 MVAr and a relatively better reactive power demand with Qsetpoint 3 MVAr. This can be attributed directly to the VSC supplying reactive power to the power grid (i.e. Qsetpoint 3 MVAr), and thus resulting in a positive effect on the voltage recovery rate the synchronous generator. With Qsetpoint -3 MVAr, the VSC draws reactive power from the grid and contributes to the reactive power demand on the synchronous generator.

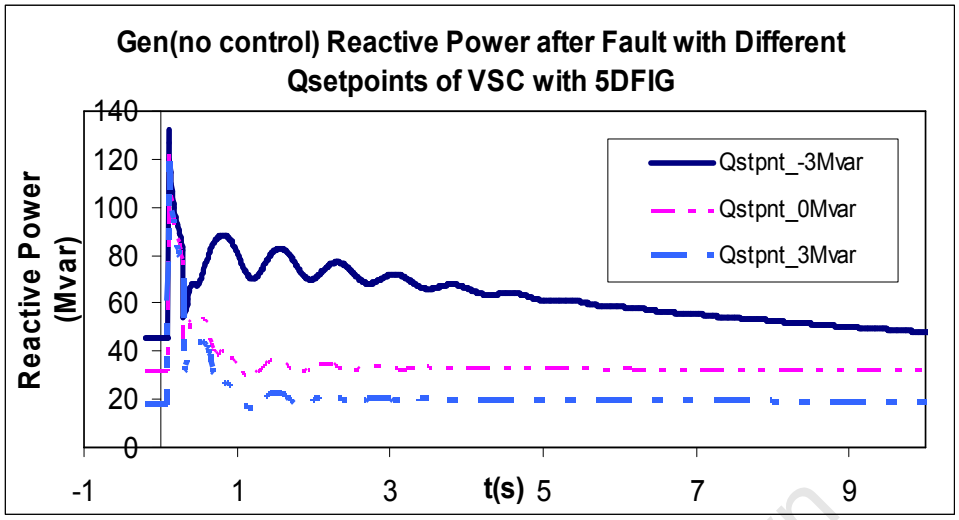


**Fig 5.11:** Gen reactive power with different Qsetpoints of VSC

However, Figure 5.12 shows that the active power of the synchronous generator was affected but not too differently by the different Qsetpoints of the VSC. Of interest, is the fact that, the oscillatory behaviour of the synchronous generator's active power following the fault, took a bit longer to settle down with Qsetpoint -3 MVAr, as compared with the other two Qsetpoints (i.e 0 MVAr and 3 MVAr).

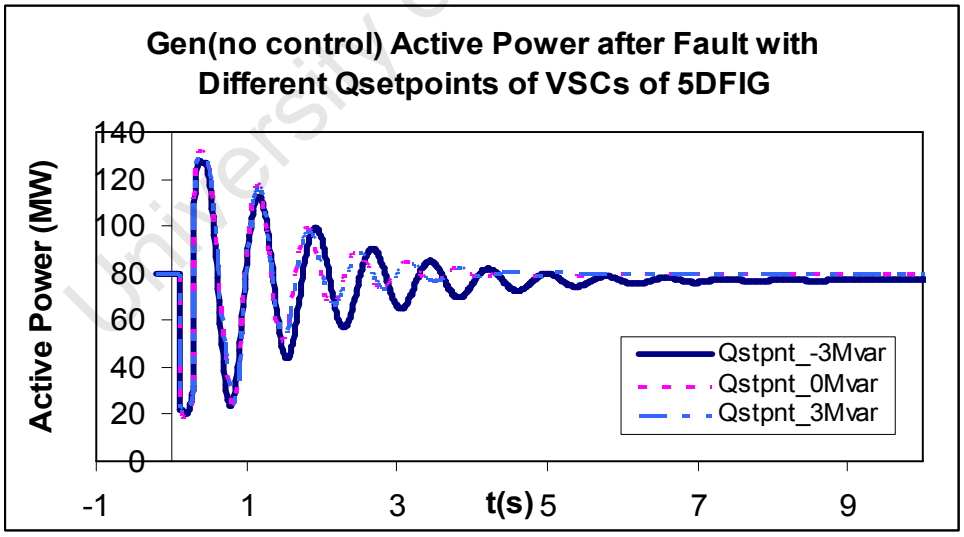


**Fig 5.12:** Gen active power with different Qsetpoints of VSC

## 5.4 The Effect of VSC Current Controller on the Power System Transient Stability

Figure 5.13 is a block diagram of the integrated current controller of the voltage source converter. The VSC operates in a stator voltage oriented reference frame, hence, the d-axis represents the active current and the q-axis the reactive current component [44]. The dq – current controller forms the fastest stage of a PWM-converter-controller [45]. The controller regulates the d and q axis current components of the grid-side PWM converter. Current references are defined by a slower outer control-loop regulating active and reactive power [44]. The reference of the control currents is set from desired active and reactive power references. A dynamic reactive power reference can be set following the requirements of the grid management service. In particular, the reactive power reference can be cancelled if a unit power factor is required.

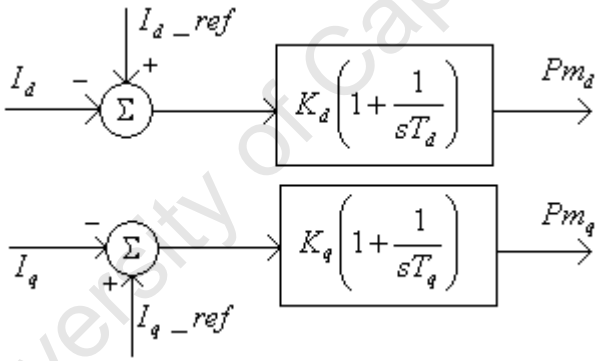


**Fig 5.13:** Representation of the VSC current controller

Where $I_{d,q}$ are the converter's ac-currents, $I_{d\_ref,q\_ref}$ are the current references, $K_{d,q}$ are the proportional gains, $T_{q,d}$ are the integration time constants and $Pm_{d,q}$ are the output signals.

The grid current references are deduced from the equations between the grid voltages, active and reactive power in the (d, q) reference frame synchronized to the grid network. By imposing an active power reference $P_{ref}$ and a reactive power reference $Q_{ref}$, the current references can be deduced as follows [46]:

$$I_{d\,ref} = \frac{P_{ref} \cdot V_d + Q_{ref} \cdot V_q}{V_d^2 + V_q^2} \tag{5.4-1}$$

$$I_{q\,ref} = \frac{P_{ref} \cdot V_q - Q_{ref} \cdot V_d}{V_d^2 + V_q^2} \tag{5.4-2}$$

Where [14]:

$$V_d = \frac{2}{3} \cdot \left[\cos \omega t \cdot V_a + \cos(\omega t - 120) \cdot V_b + \cos(\omega t + 120) \cdot V_c\right] \tag{5.4-3}$$

$$V_q = \frac{2}{3} \cdot \left[-\sin \omega t \cdot V_a - \sin(\omega t - 120) \cdot V_b - \sin(\omega t + 120) \cdot V_c\right] \tag{5.4-4}$$

Where $V_{a,b,c}$ is voltage of phase a, b and c respectively. The impact of the grid-side voltage source converter current controller on the transient stability of the power network was initially explored by setting the proportional gains $K_{d,q}$ to 0.01, 0.1 and 1.0. The default setting was maintained at 0.1 .The power network was then exposed to a transient disturbance for the three different gain settings, whereby the electromechanical dynamics of the system were observed. This is shown in figures 5.14 and 5.15. Increasing the proportional gain from 0.01 to 1.0 seems to not have brought much of a significant difference on the rotor response and terminal voltage response of the synchronous generator following the fault. However, with a gain of 0.01 the rotor oscillations following the first swing seem to have had a relatively slightly smaller magnitude in comparison with the other higher gain settings.

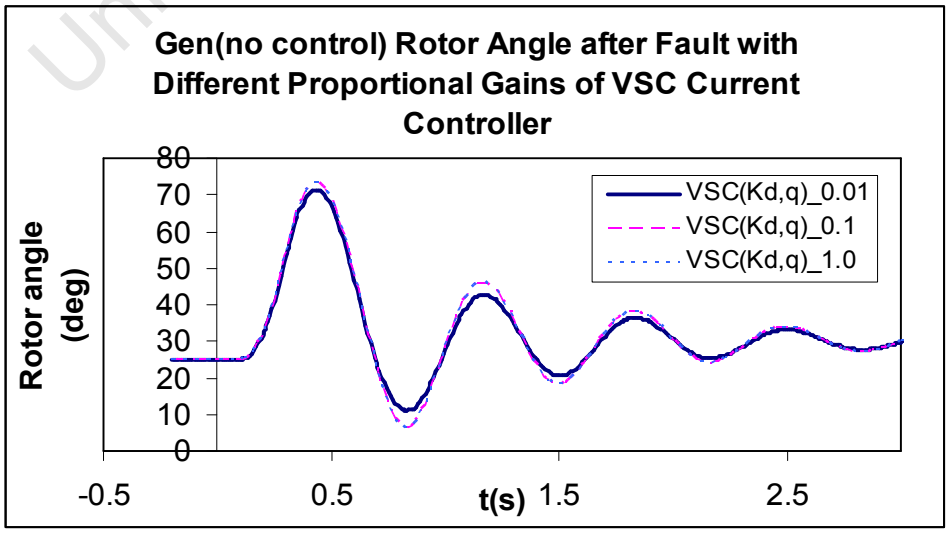


**Fig 5.14** Rotor response with different proportional gain values of VSC current controller

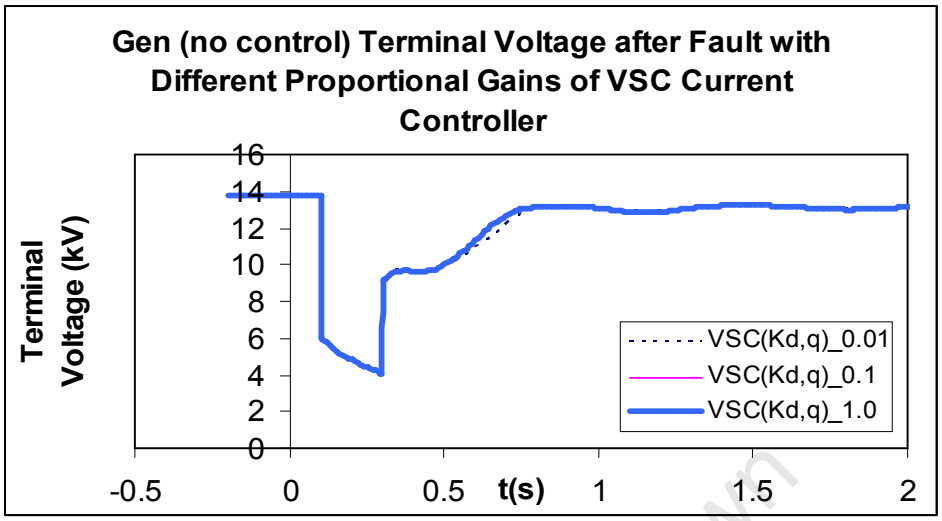


**Fig 5.15:** Terminal voltage with different proportional gain values of VSC current controller

## 5.5 The Effect of Doubly-Fed Induction Generator Slip on Transient Stability of the Power System

The effect of the DFIG slip on the transient stability of the power system was explored by setting the slip to -30 %, -16 %,-8 %, 8 %,16 % and 30 %, where the initial slip was at -0.1 %. The chosen slip settings are well within the speed range of the DFIG since the DFIG's variable speed range is + / - 30 % of synchronous speed [32]. The parameters of the VSC were set as in Appendix 2 where the reactive power was set to 0 MVAr. The capacity of the DFIG wind farm was kept at 50 MVA, and each doubly-fed induction generator was set to generate 8 MW and draw 6 MVAr on the stator terminals. Conventionally, a negative slip means that the rotor speed of the induction machine is higher than synchronous speed, and this speed range is technically referred to as the super synchronous speed. When the rotor speed of the wind generator is below synchronous speed but within operational limits, then the wind generator is said to operate in the sub-synchronous speed range. Here, it is worth noting that for the models of the DFIGs used in DIgSILENT, a negative slip translates to the rotor speed of the wind generator being less than that of synchronous speed. A positive slip effectively means the rotor speed of the wind generator is greater than that of synchronous speed. The slip of the DFIG models has been deduced to be governed by equation (5.5-1).

$$s = \frac{n_g - n_s}{n_g} \tag{5.5-1}$$

Where; $s$ is generator slip, $n_g$ is generator speed and $n_s$ is synchronous speed.

Figure 5.16 shows the response of the synchronous generator's rotor after the fault was cleared. It is seen that with a less negative slip, the acceleration power of the synchronous generator after the fault is highest. This is verified by the first swing and subsequent oscillations of the synchronous generator's rotor when the DFIG slip was set to -8 % in comparison with -16 % and -30 % slip. The reaction of the synchronous generator's terminal voltage after the fault is shown in Figure 5.19. The period of voltage recovery is relatively short for the given DFIG slip settings. The voltage overshoot for slip values -30 % and -16 % results from a high reactive power injection from the VSC with respect to the required amount

to meet nominal. Herein, the synchronous generator was not equipped with an AVR and speed governor, thus the only source of reactive power after the fault was the VSC.

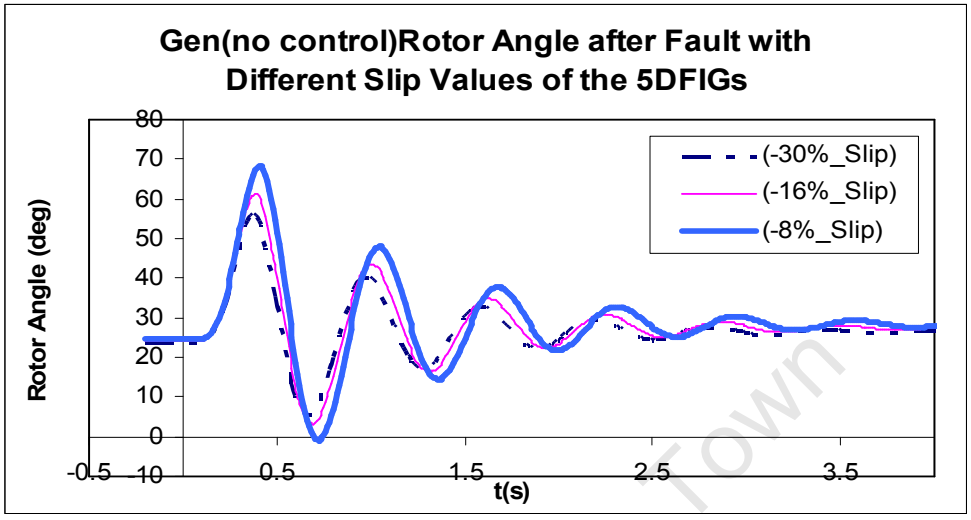


**Fig 5.16:** Rotor response with DFIG slip less than 0

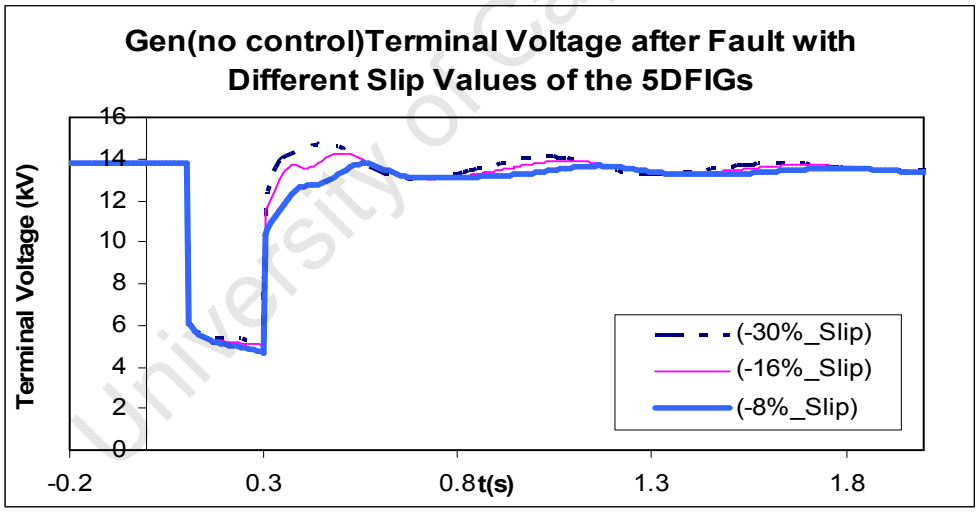


**Fig 5.17:** Terminal voltage with DFIG slip less than 0

Figure 5.18 shows that when the slip of the DFIG is greater than 0, i.e. when the rotor speed of the DFIG is greater than synchronous, the rotor angle of the synchronous generator increases to about 55°. This rotor angle is a new operating point following the fault. The steady state stability margin of the synchronous generator is decreased when the rotor angle increases. Figure 5.19 shows that the terminal voltage of the synchronous generator does not

recover to its prefault level. The voltage recovers to about 10.5 kV and gradually decreases and settles at about 9.7 kV which is 0.70 p.u. of 13.8 kV.

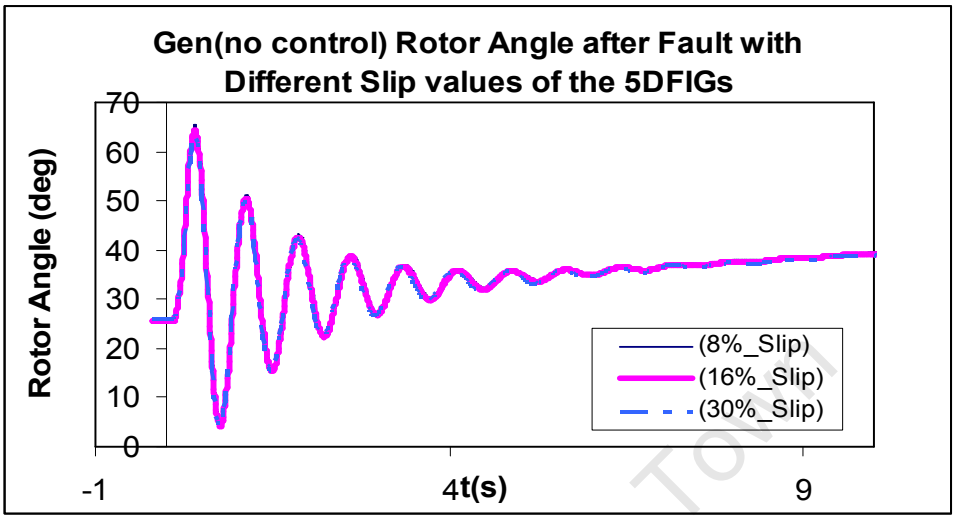


**Fig 5.18:** Rotor response with different slip settings

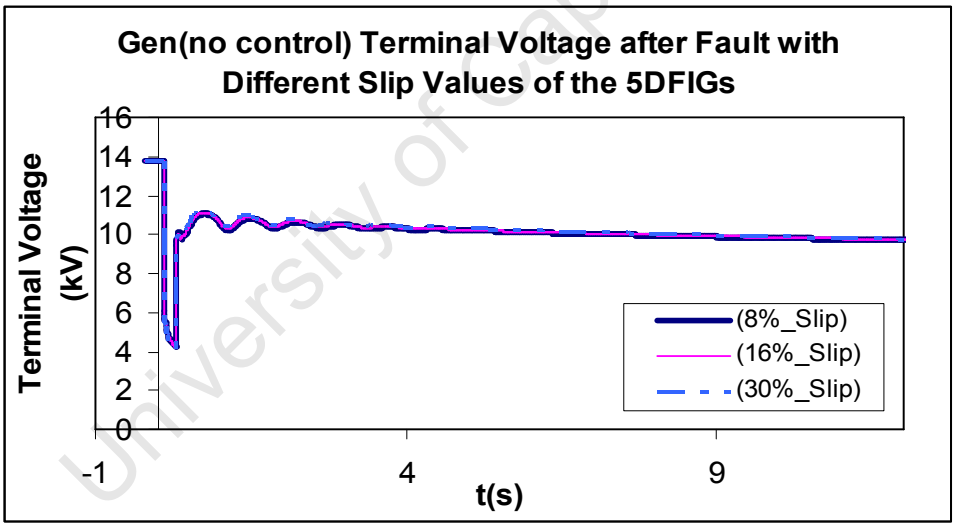


**Fig 5.19:** Terminal Voltage for different slip values

Figure 5.20 illustrates the angle at which the rotor angle of the synchronous generator settles at following the transient fault on the power network when the DFIG slip is set to 8 %, as observed, this angle is about 55°.

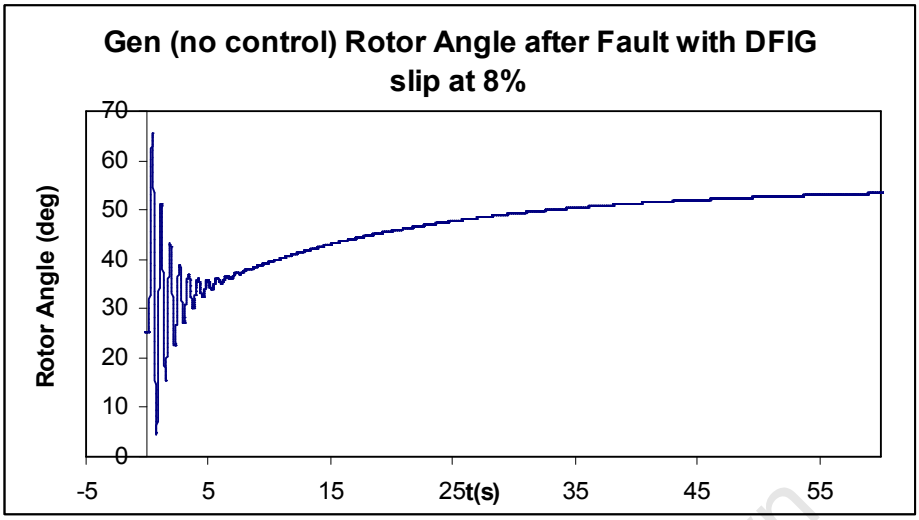


**Fig 5.20:** Rotor response with DFIG slip at 8%

Figure 5.21 depicts shows an extended simulation time for the terminal voltage of the synchronous generator following the fault with DFIG slip set to 8%.

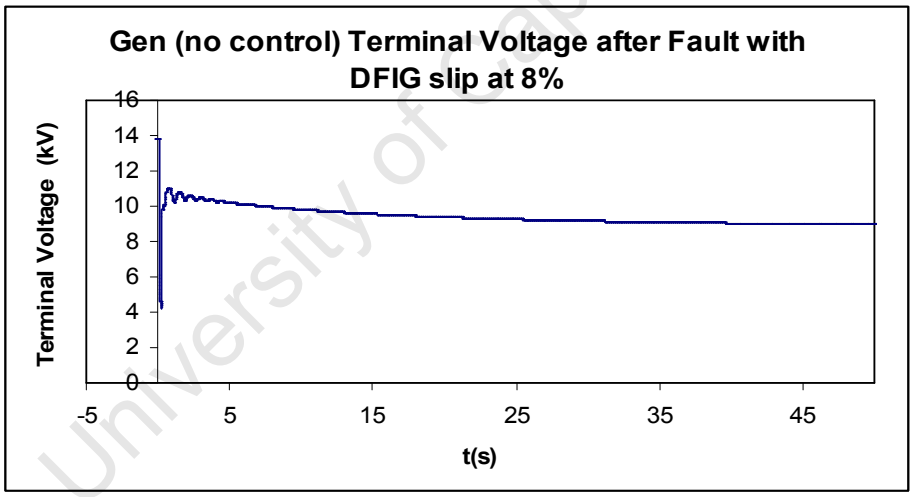


**Fig 5.21:** Terminal voltage with DFIG slip at 8%

When the DFIG is running at a speed which is lower than the synchronous speed, a fault on the power network results in an increase of the DFIGs rotor speed. This is shown in Figure 5.22. The speed increases and decreases back to normal prefault after the fault is cleared. However, when the DFIG's speed is above synchronous, a fault on the power network results with a high increase of the DFIG's rotor speed as seen in Figure 5.23.

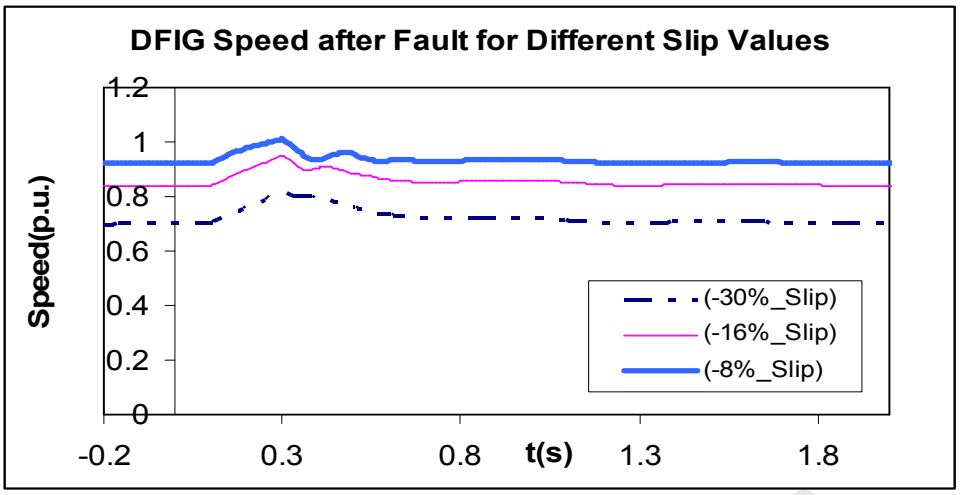


**Fig 5.22**: DFIG speed with negative slip

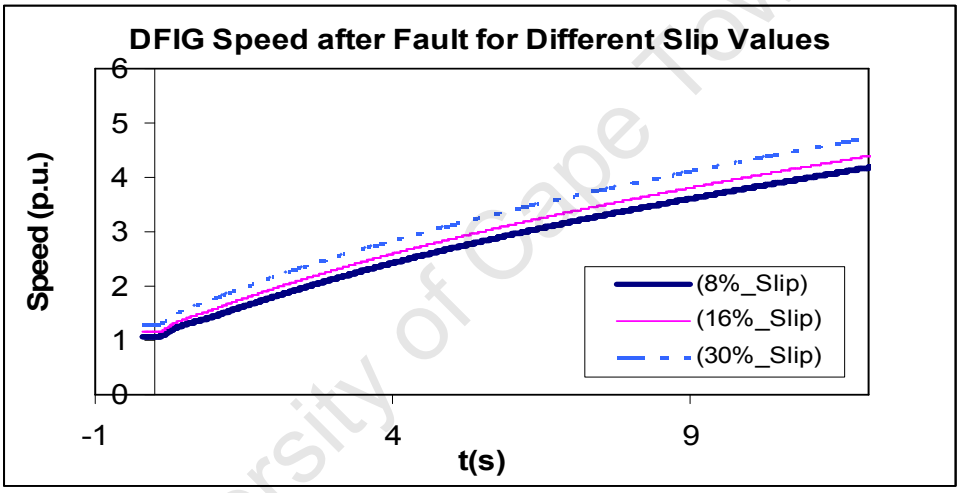


**Fig 5.23:** DFIG speed with positive slip

This high speed increase results with the induction machine drawing more reactive power as the slip increases. This is due to the decrease in the rotor resistance, which thus causes high reactive currents to flow in the machine. Figure 5.24 shows that, due to the high reactive power demand of the DFIG the terminal voltage of the synchronous generator did not recover to atleast 0.95 p.u. of the prefault voltage as seen in Figure 5.19.

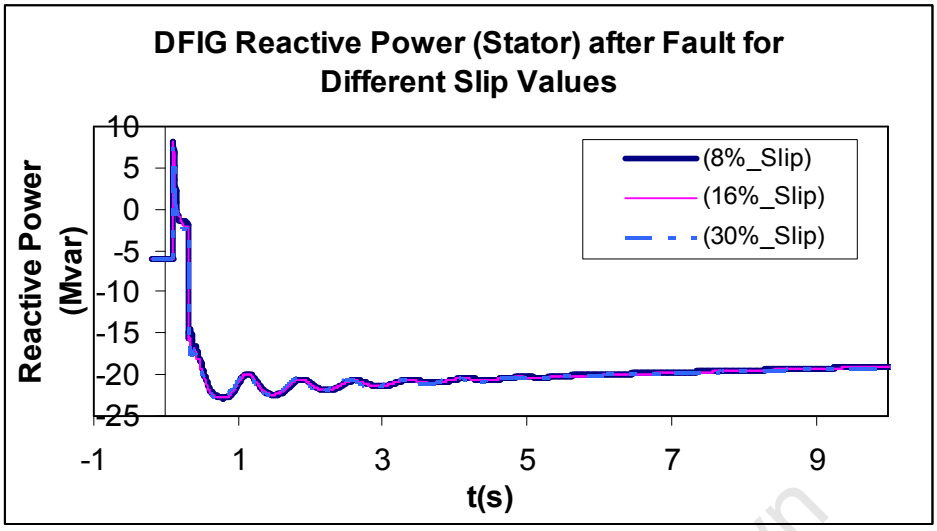


**Fig 5.24:** DFIG stator reactive power for positive slip

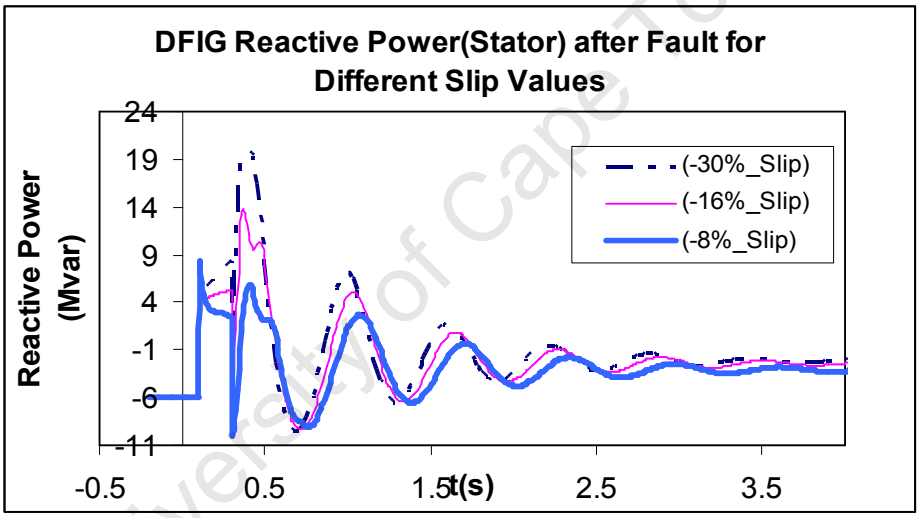


**Fig 5.25:** DFIG stator reactive power for negative slip



When the speed of the induction generator exceeds a set limit in practical systems, an over speed switch will fully pitch the blades and apply the disk brake in case of an emergency [47]. Thus, the reactive power demand of the DFIG would not exceed its power rating as seen in Figure 5.25.

The synchronous generator was then equipped with an IEEET1 AVR, while having the DFIG slip set to 8 %. Figure 5.26 shows that, after the fault on the power network was cleared, the rotor angle settled at about 8°. The steady state stability margin of the synchronous generator was significantly improved with the rotor angle being at this angle, since the rotor angle

moved further away from the theoretical critical stability point. This stability limit is greater than 90° in salient pole synchronous machines [23]. However, in Figure 5.20 the rotor angle had increased to 52°. The terminal voltage as shown in Figure 5.27 recovered to 13 kV after 6 sec. The delay draws attention to the fact that, when the fault occurred with the DFIG operating at a high speed, the reactive power demand on the synchronous generator was relatively higher. In Figure 5.17, it can be seen that the terminal voltage recovered within 1sec after the fault when the DFIG slip was set to -8 %.

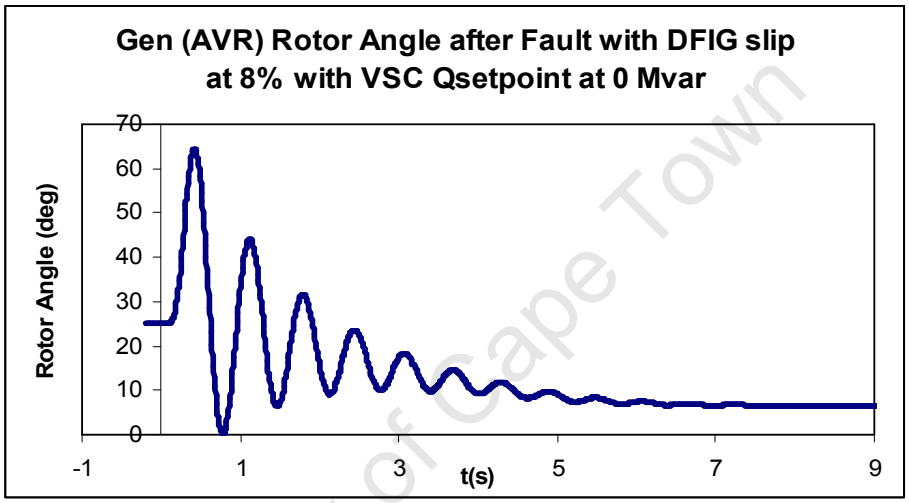


**Fig 5.26:** Rotor response (AVR) with DFIG slip at 8 %

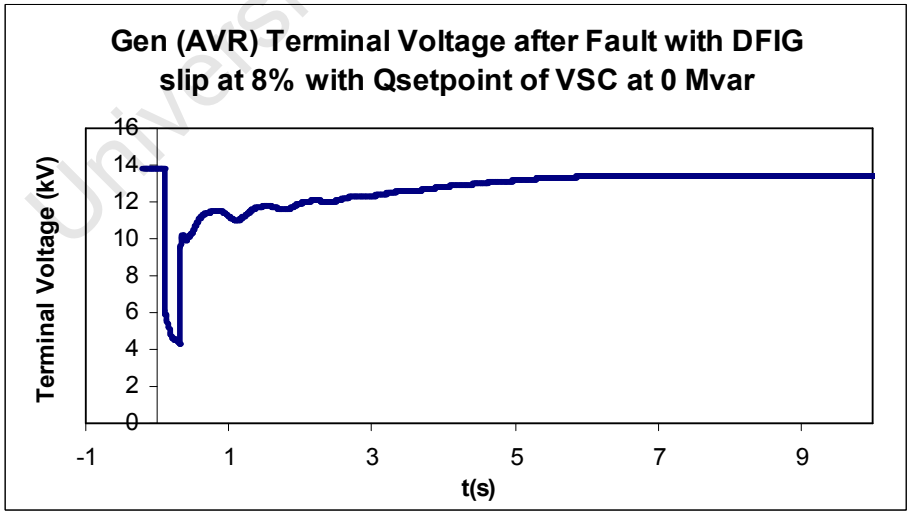


**Fig 5.27:** Terminal Voltage (AVR) with DFIG slip at 8 %

# 5.6 A Comparison of the Impact of DFIG and SCIG on the Transient Stability of the Power System (With and without AVR)

## 5.6.1 The Impact on Transient Stability without AVR

Figure 5.28 and Figure 5.29 shows the response of the synchronous generator's rotor angle and terminal voltage following a fault, when the 50 MVA DFIG based wind farm and the 50 MVA SCIG wind farm were each connected at a time. The dynamic behaviour of the power system after a fault when connected to DFIGs is compared with when SCIGs are connected. This is to distinctively show the impact of doubly-fed induction generators on the power system's transient stability. In this case, the SCIG wind farm was not connected with any capacitor banks, and no power system controllers were activated for both cases.

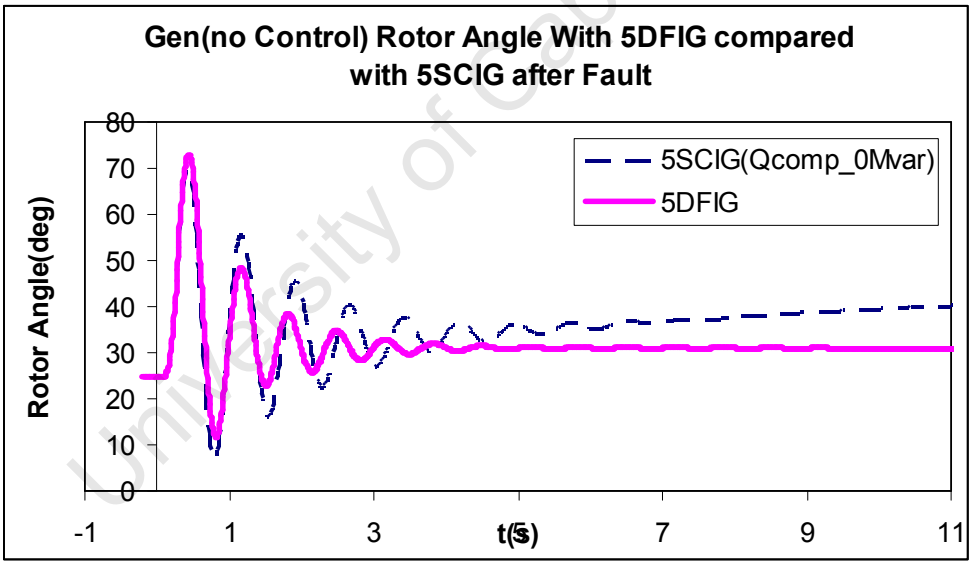


**Fig 5.28:** Generator rotor response with 5SCIGs and 5DFIGs

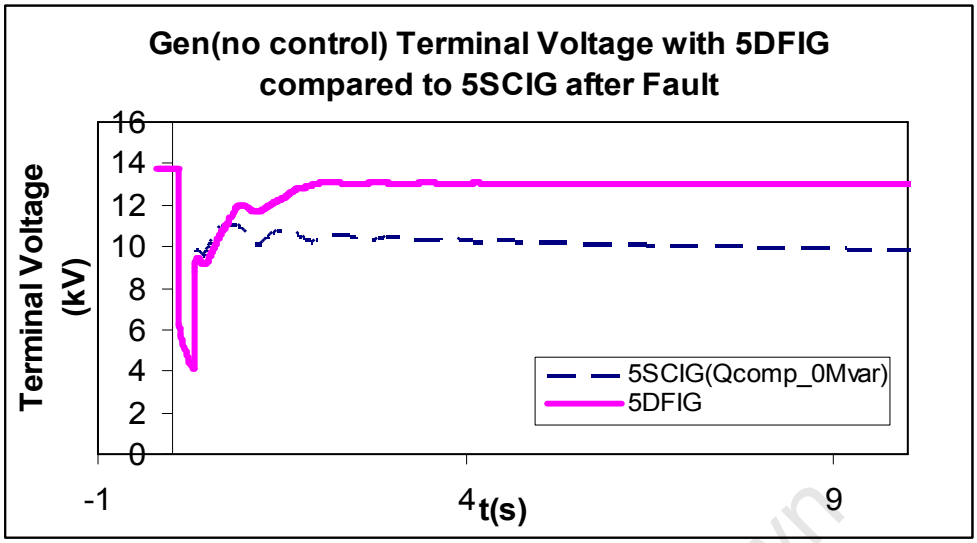


**Fig 5.29:** Generator terminal voltage with 5SCIGs and 5DFIGs

It is observed that when the DFIGs were connected, the magnitudes of the subsequent oscillations to the first swing of the generator's rotor are significantly smaller in comparison to when SCIGs were employed. The rotor angle settles to a value of about 30° following the fault when DFIGs were utilized, whereas with the SCIGs, the rotor angle increased to about 52° as shown in Figure 4.18. The increase of the rotor angle when SCIGs were used is indicative of the high reactive power demand on the synchronous generator after fault, since the AVR was not connected. It is evident that, the doubly-fed induction generators were able to give reactive power support to the power network following the fault. This is on the basis that the line-side converter (LSC) was able to supply reactive power which is utilized during grid faults only [48]. The small increase of the rotor angle when DFIGs were connected relative to when SCIGs were connected is because the synchronous generator did not have to increase as much generation of reactive power following the fault. Figure 5.29 shows that, the terminal voltage of the synchronous generator was restored to about 13 kV following a transient fault when DFIGs were connected compared with it settling at 9 kV when connected to SCIGs as shown in Figure 5.29.

The response of the power system after a fault when connected with 5DFIGs was then compared to when the power network was connected with 5SCIGs with a preferred reactive

power compensation of 20 MVAr using capacitor banks. This is shown in Figures 5.30 and 5.31.

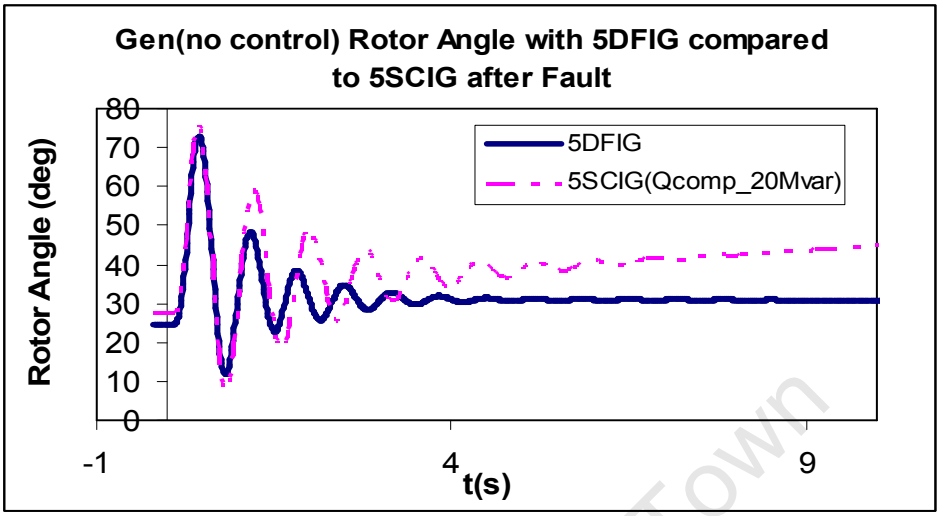


**Fig 5.30:** Rotor response with 5DFIGs and 5SCIGs

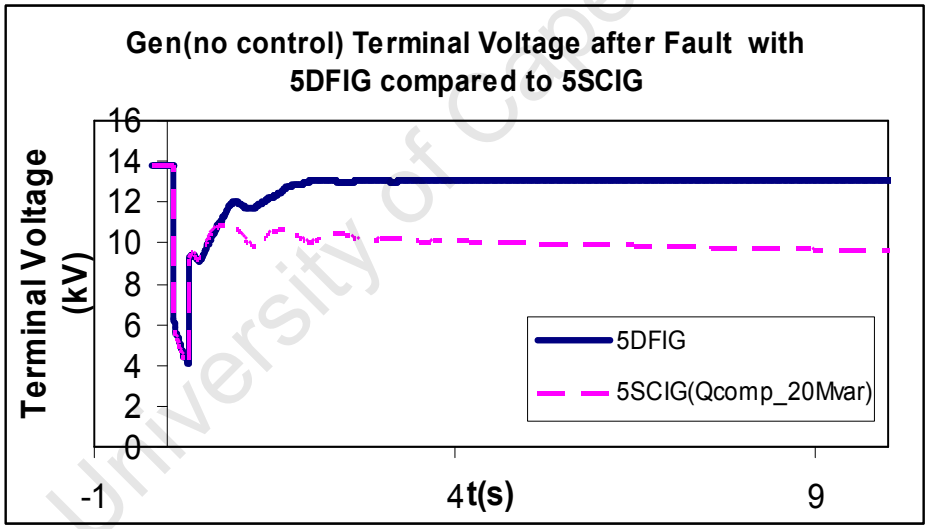


**Fig 5.31:** Terminal Voltage with 5DFIGs and 5SCIGs

The prefault rotor angle when the DFIGs were connected is relatively smaller due to a reduction in reactive power generation of the synchronous generator. The first swing of the synchronous generator's rotor is greater with SCIGs after the fault. With the DFIGs, the synchronous generator's rotor oscillations subsequent to the first swing die out relatively quickly, and the rotor angle increased slightly from 26° to 30° following the fault. However, with the SCIGs, the rotor angle of the synchronous generator increases beyond 90° until stability is lost after 1 min 10 sec as already presented in Figure 4.21. The terminal voltage of

the synchronous generator is restored to about 13 kV after the fault when DFIGs were connected. With SCIGs, the terminal voltage of the conventional generator decreased to about 8 kV before the voltage collapsed after 1 min 10 sec as shown in Figure 4.22.

The results show that, when doubly-fed induction generators are connected, the period taken to minimize the imbalance between the mechanical power and electrical power is relatively shorter when compared with that when SCIGs are connected. It can thus be said that the DFIG wind farm complied with the German grid code. This states that, wind farms not only have to supply active power but also reactive power into the grid [48]. That is how the terminal voltage of the synchronous generator was restored to 0.94 p.u. of the prefault voltage of 13.8 kV after the fault, and moreover, the synchronous generator was not equipped with an AVR and also with no speed governor.

### 5.6.2 The Impact on Transient Stability with AVR

The impact of the 50 MVA DFIG wind farm on the transient stability of the power network was then compared with the impact of the 50 MVA SCIG wind farm on the power system transient stability when the synchronous generator was equipped with an AVR. The SCIG wind farm had the preferred reactive power compensation of 20 MVAr via capacitor banks. A three-phase fault was applied on line 1 and cleared by removing line 1 from service after 0.2 sec. Figure 5.32 compares the rotor response of the synchronous generator when each type of wind generator concept was connected to the power network at a time. It is observed that, when the DFIGs were connected, the power system had a better transient response compared with when the SCIGs were connected even when the synchronous generator had an AVR in both cases. The first swing and subsequent swings are relatively smaller with the DFIG. The magnitude of the swings is defined by the degree of imbalance between the mechanical power and electrical power of the synchronous generator. This imbalance was minimized much quicker when DFIGs were used, than when the SCIGs were employed. This goes to show that, the DFIG did provide reactive power support to the power network following the fault.

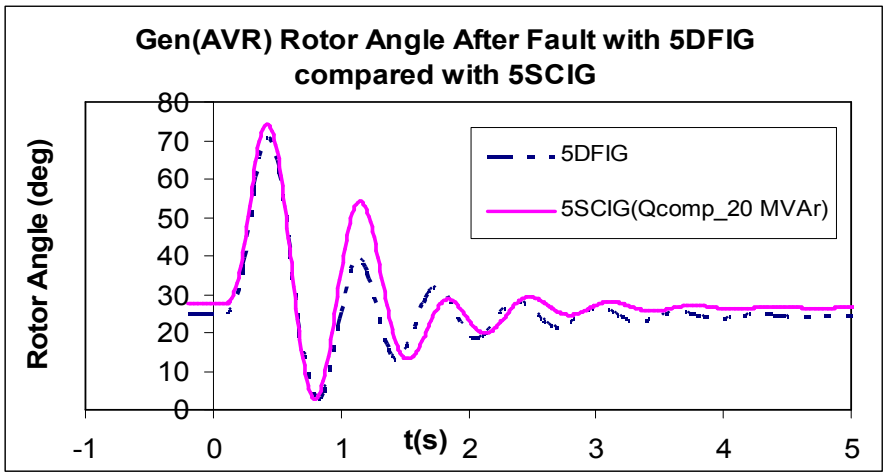


**Fig 5.32:** Rotor response with 5DFIGs compared with 5SCIGs

Figure 5.33 shows how the terminal voltage of the synchronous generator responded following the three-phase short circuit on the power grid when the SCIGs were connected, and then when the DFIGs were connected while the AVR was active. It is seen that, the terminal voltage of the synchronous generator recovered more quickly when the DFIGs were used. This is because of the supply of reactive power support during grid faults by the line side converter of the DFIG. This decreases the amount of reactive power demand on the synchronous generator when the faulted line is put out of service. Furthermore, this enables the exciter system to restore the synchronous generator's terminal voltage relatively quicker when compared with when SCIGs are connected. SCIGs consume more reactive power during grid faults since their rotors speed up and decrease the resistance in the rotor circuit as the slip increases. This results in more reactive currents flowing through the SCIG. In this particular case, the SCIG based wind farm with a capacity of 50 MVA, was set to draw a rated 30 MVAr of reactive power from the power grid. The capacitor banks supplying reactive power compensation to the SCIG wind farm, were set to inject 20 MVAr only. Thus, when the fault was cleared, the SCIG consumed more reactive power from the power grid which resulted with the terminal voltage of the synchronous generator taking a bit longer to get to its pre-fault level as shown in Figure 5.33.

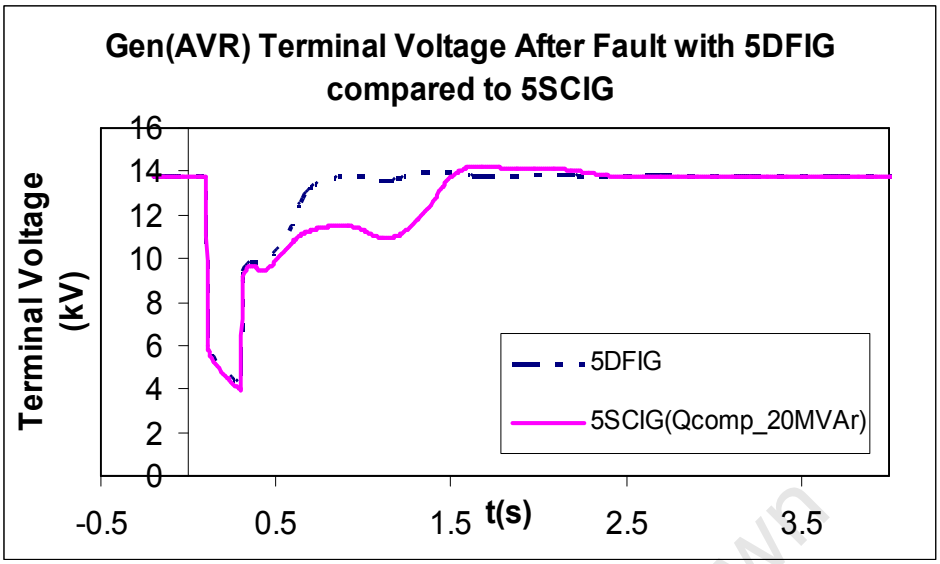


**Fig 5.33:** Terminal Voltage with 5DFIGs compared with 5SCIGs

# THE IMPACT OF A CONVERTER DRIVEN SYNCHRONOUS GENERATOR (CDSG) ON THE TRANSIENT STABILITY OF THE POWER NETWORK

# 6

## 6.1 Introduction

The case studies presented in this chapter are based on a converter driven synchronous generator (CDSG) wind farm operating at a lagging power factor of 0.8.The capacity of 1 CDSG was 10 MVA. Figure 6.1 shows the connection of the converter driven synchronous generator to the power network. The transmission line (line 4) connecting the wind farm to the power network was kept at a length of 1 km. The power network's transient stability was explored with the connection of the CDSGs by applying a three-phase short-circuit on line 1 for 0.2 sec. The fault was then cleared by putting the faulted line out of service. Buses 8, 7, 6 and 5 have nominal voltages of 3.3 kV, 6.6 kV (dc), 3.3 kV and 230 kV respectively. Transformer TR2 is used to step up the 3.3 kV voltage on bus 6 to 230 kV onto bus 5. Loads 1 (LD 1) and load 2 (LD2) were both set to use 80 MW and 40 MVAr. Each full scale voltage source converter connected to each wind generator was rated at 15 MVA in order to handle the rated power of each wind generator, which was set to 10 MVA. The wording line side converter (LSC) will thus be used interchangeably with grid side converter. However, the acronym GSC will be reserved for generator side converter.

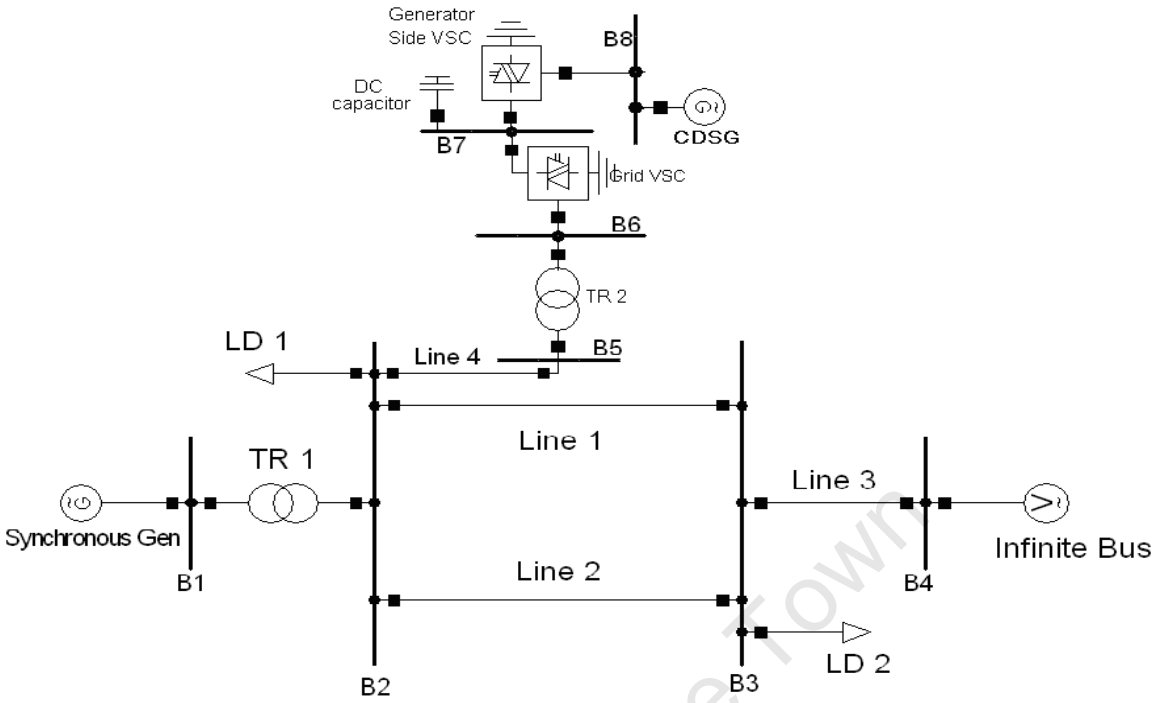


**Fig 6.1:** Power Network Model connected to converter driven synchronous generator

## 6.2 The Effect of Penetration of Converter Driven Synchronous Generators on the Transient Stability of the Power Network

Figure 6.2, illustrates, the transient response of the conventional synchronous generator's rotor response when there is an increased penetration of converter driven synchronous generators (CDSGs) on the power grid. Based on the observation regarding the results, it is seen that, as the penetration level of CDSGs increases on the power network, the first and subsequent swings of the synchronous generator following a grid disturbance become bigger.

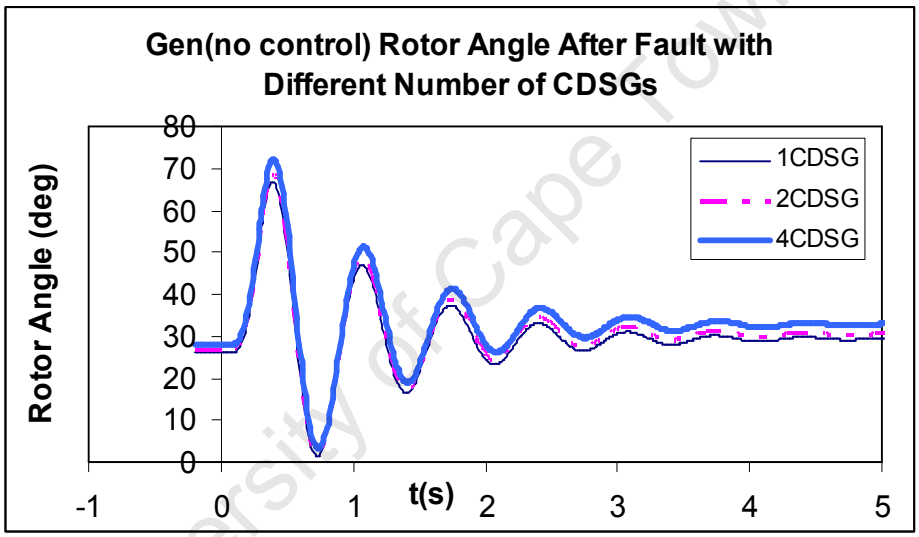


**Fig 6.2:** Rotor response after fault with different number of CDSGs

Figure 6.3 depicts that, when the level of CDSG penetration increases, the transient response of the synchronous generator's terminal voltage after the fault is cleared, does not differ much with the rise in penetration. This can be attributed to the fact that, the stator of the CDSG is coupled to a full scale converter. This effectively decouples the CDSG from the grid to which it is connected to. This ultimately eliminates any electromechanical influence the CDSG would have on the power grid following a transient fault. The grid side converter of the CDSGs interaction with the power grid serves to offer grid support during grid disturbances and to deliver active and reactive power during steady-state operation.

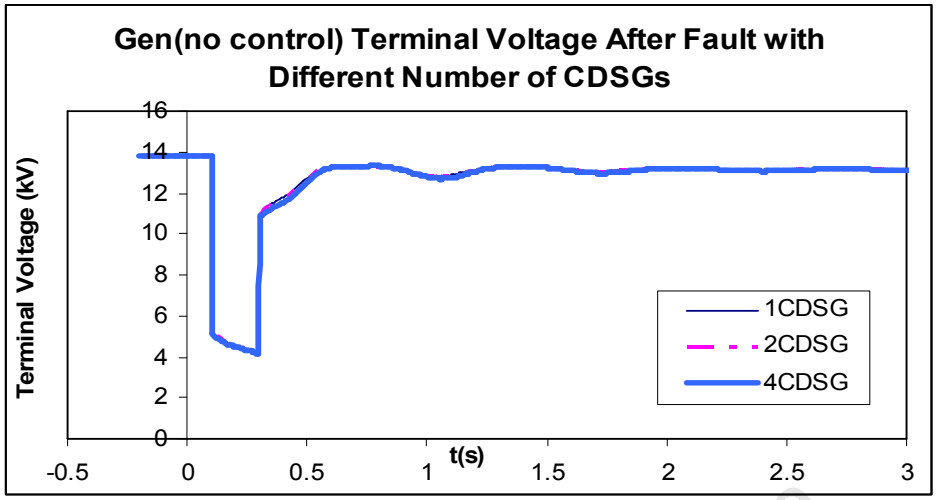


**Fig 6.3:** Terminal voltage response after fault with different number of CDSGs

## 6.3 The Effect of Different Reactive Power Set-Points of the VSC on the Power Network

Tables 6.1 and 6.2 tabulate the effect on synchronous generator's reactive power generation due to different reactive power set points (Qsetpoints) of the line side converter (LSC) and the generator side converter (GSC) under steady state conditions. The reactive power setpoint of the generator side converter was initially set to 0 MVAr. Then the reactive power setpoint of the line side converter was set to the different reactive power setpoints (i.e -9 MVAr, -5 MVAr, 0 MVAr, 5 MVAr, 9 MVAr ). The maximum and minimum reactive setpoints were chosen as 9 MVAr and -9 MVAr, on the basis that the CDSG was rated at 10 MVA and the respective maximum and minimum settings would cause an excessive overload on the synchronous generator. A power flow simulation was run to acquire the reactive power from the conventional synchronous generator for each reactive setpoint, as tabulated in Table 6.1. The reactive power setpoint of the line side converter was then maintained at 0 MVAr. From there, the reactive setpoints of the generator side converter were then changed accordingly as was done for the line side converter. For each reactive setpoint setting of the generator side converter, a power flow simulation was run and the respective reactive power output of the synchronous generator was attained thereof, as listed in Table 6.2.

Table 6.1: Effect of LSC Qsetpoint

| $Q_{gen}$(Mvar) | LSC Qsetpoint (Mvar) |
|---|---|
| 49.82 | -9 |
| 28.96 | -5 |
| 5.04 | 0 |
| -17.01 | 5 |
| -30.26 | 9 |

Table 6.2: Effect of GSC Qsetpoint

| $Q_{gen}$(Mvar) | GSC Qsetpoint (Mvar) |
|---|---|
| 5.04 | -9 |
| 5.04 | -5 |
| 5.04 | 0 |
| 5.04 | 5 |
| 5.04 | 9 |

The results bring to light the fact that the grid side converter plays a critical role in relation to the reactive power exchange between the CDSG and the power network. This is on the basis of how the amount of reactive power from the LSC being injected into the power network affects the reactive power generation of the synchronous generator. Thus more focus will be placed on the line side converter (LSC) of the full scale voltage source converter in the following case studies.

## 6.4 The Effect of System Controllers on the Transient Stability of the Power Network

The parameter settings of the VSC current controller are given in Appendix 2. The influence of the VSC current controller on the transient stability of the power network was explored under three different control scenarios of the power system. Firstly, no controllers were included, then only the AVR was added, and lastly the speed governor was added alone. Figure 6.4 suggests that, the power system is transiently stable for the three control scenarios. The rotor angle settled to its prefault angle after the fault was cleared by placing the faulted line out of service, when the synchronous generator was equipped with an AVR. This is due to the increase in the internal voltage of the synchronous generator from the exciter system. This in turn enhanced the amount of electrical power transferable from the synchronous generator to the power network after the fault. As observed in Figure 6.5, the terminal voltage of the synchronous generator recovered to its prefault level when the AVR was operational. The recovery time of the terminal voltage of the synchronous generator when no controllers were included was similar to that when the speed governor was used, as seen in Figure 6.5
In the figures below *nctrl* stands for no controller included.

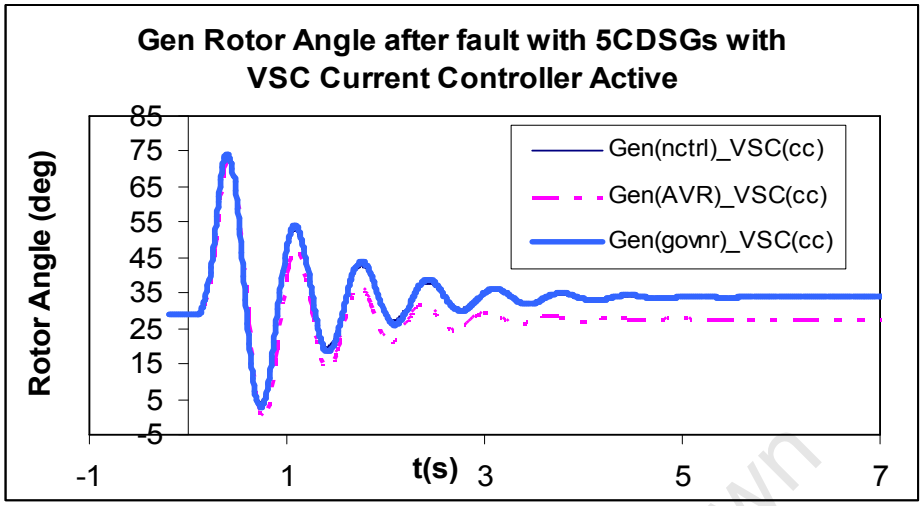


**Fig 6.4:** Rotor response with VSC current controller active

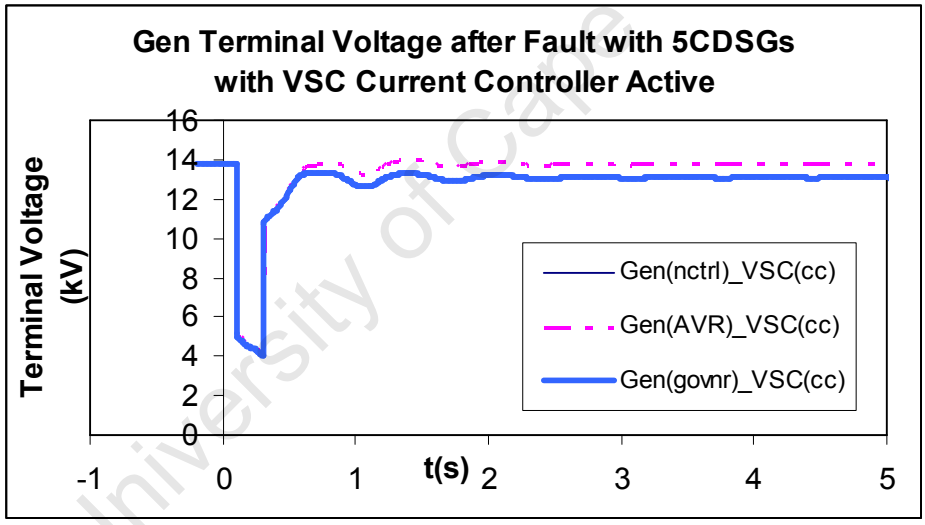


**Fig 6.5:** Terminal voltage with VSC current controller active

## 6.5 The Effect of the Reactive Power Set Points of the LSC on the Transient Stability of the Power Network

The reactive power setpoints (Qsetpoints) of the line side converter which were explored were -9 MVAr, -5 MVAr, 0 MVAr, 5 MVAr and 9 MVAr. These parameter settings were well within the operational limits of the line side converter since it had a rating of 15 MVA. The changes in the rotor angle of the synchronous generator due to different Qsetpoints of the LSC before the fault have been listed in Table 6.3.

Table 6.3: Effect of LSC Qsetpoints on the Generator Prefault Rotor Angle

| LSC Qsetpoint (MVAr) | $Q_{gen}$ (MVAr) | PreFault Rotor Angle (deg) |
|---|---|---|
| 9 | -30.26 | 38° |
| 5 | -17.01 | 34° |
| 0 | 5.04 | 29° |
| -5 | 28.98 | 25° |
| -9 | 49.82 | 22° |

It is clear from table 6.3 that, as the amount of reactive power supplied by the line side converter to the power network decreases from 9 MVAr to -9 MVAr, the prefault rotor angle of the synchronous generator also decreases.

It can be seen from Table 6.3 that , the generator absorbs reactive power for positive values of the Qsetpoints. In these cases the generator is under excited, which means the stability margin of the generator is reduced. The higher the positive value of the Qsetpoint, the more the generator is absorbing reactive power and the less stable (steady-state) the system becomes. On the other hand, negative values of the Qsetpoint means that the generator is required to supply reactive power. The smaller the Qsetpoint, the higher the reactive power generated, and the higher the initial stability margins. For 0 MVAr Qsetpoint, the reactive power generated is the lowest and the initial rotor angle is in the middle (29°), with acceptable stability margin

The power network was exposed to a three-phase short-circuit on line 1 of figure 6.1. The fault was cleared after 0.2 sec by taking line 1 out of service. The AVR and speed governor were not used in the following study case. Figure 6.6 shows the rotor response of the synchronous generator for different reactive power setpoints (9 MVAr, 5 MVAr, 0 MVAr). It is observed from the rotor responses that, with reactive power injection of 9 MVAr from the line side converter, the power system had the most pessimistic transient response. This can be explained by the fact that, the magnitude of the first and subsequent swings of the rotor was the highest, followed by the setpoint of 5 MVAr . The 0 MVAr setpoint has the smallest first swing and subsequent swings. From Figure 6.7, it can be seen that the transient responses for -5 MVAr and -9 MVAr setpoints are better than that of 0 MVAr setpoint with -9 MVAr giving the preferred transient response.

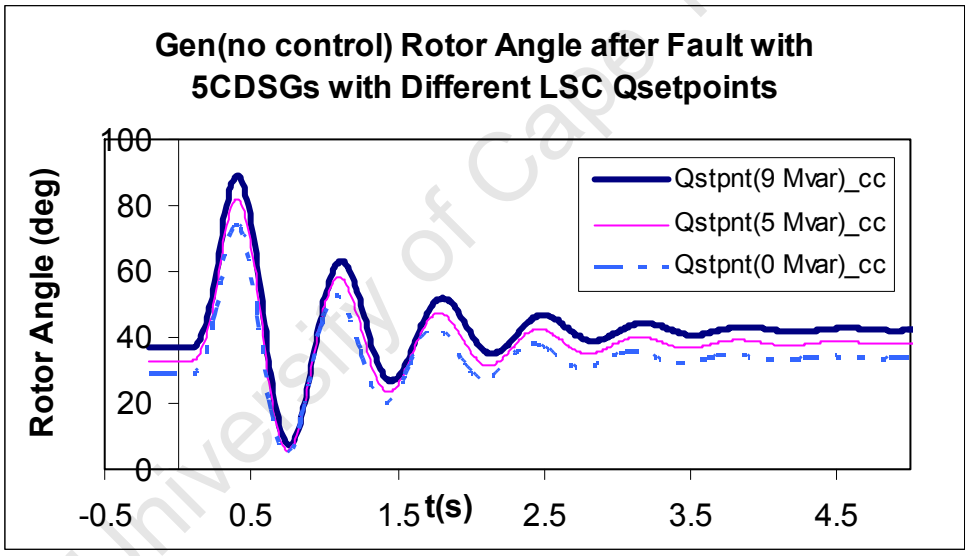


**Fig 6.6:** Rotor response with different LSC reactive power set points $\geq 0$

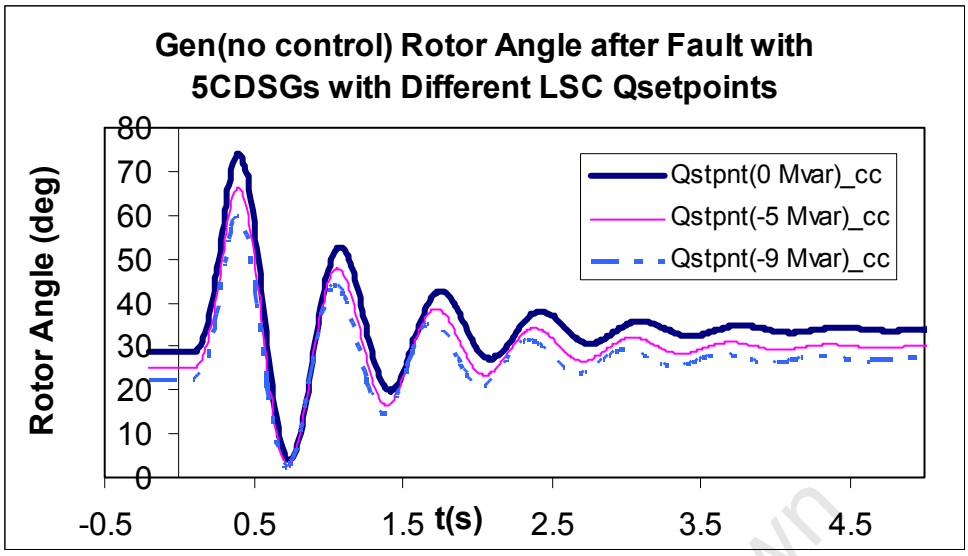


**Fig 6.7:** Terminal voltage with different LSC reactive power set points $\leq 0$

Figures 6.8 and 6.9 show that, for the different reactive power setpoints of the LSC, the transient response of the terminal voltage of the synchronous generator was more or less similar. The voltage recovery time for all the different Qsetpoints of the LSC was short.

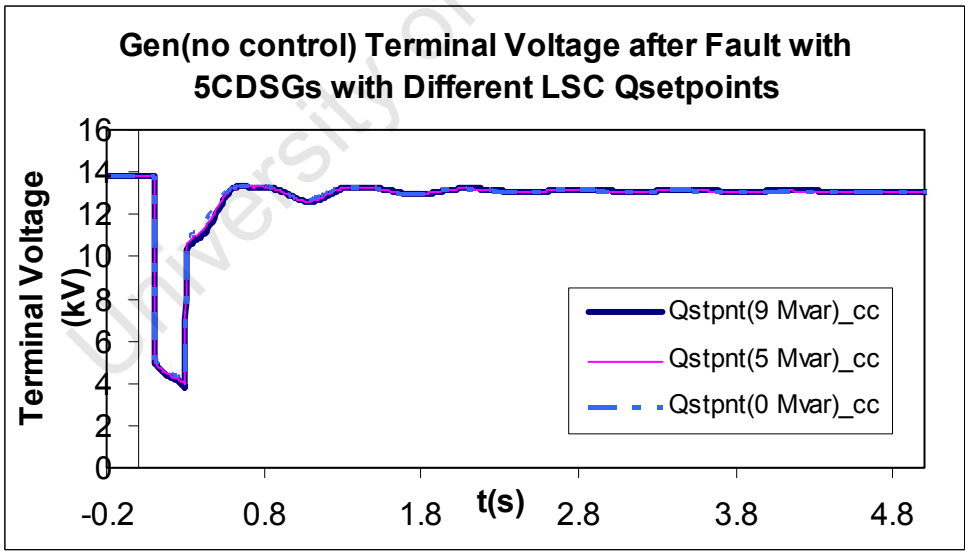


**Fig 6.8:** Terminal voltage with LSC reactive power set points $\geq 0$ and active current controller

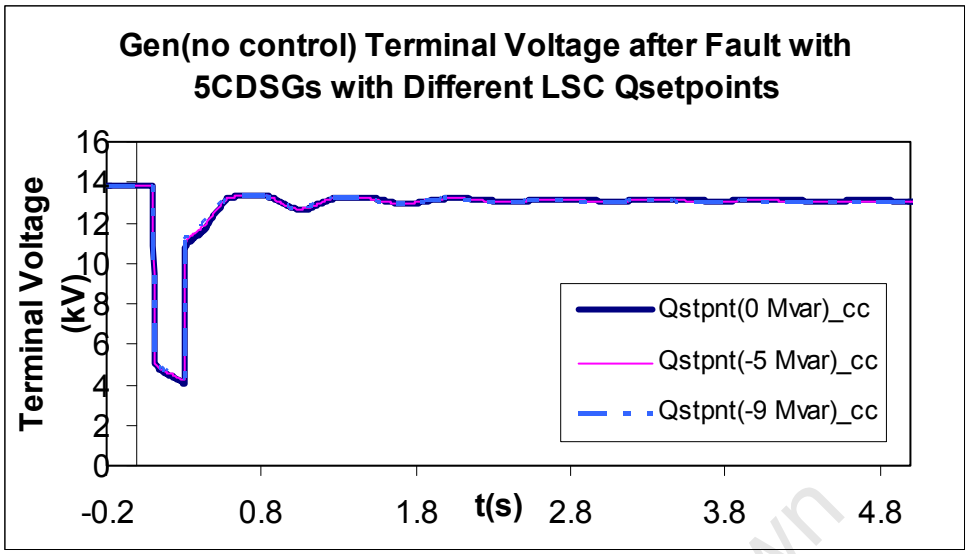


**Fig 6.9:** Terminal voltage with LSC reactive power set points ≤ 0 and an active current controller

## 6.6 A Comparison of the Effect of CDSG vs DFIG on the Transient Stability of the Power Network

The transient response of the power system with 5 DFIGs and 5 CDSGs was compared by connecting each wind generator concept at a time. The conventional synchronous generator was not equipped with an AVR and speed governor. The grid side converter of the DFIG was kept at a unity power factor, while that of the CDSG was also set to unity power factor. The current controller was operational for both the DFIG and the CDSG. Figure 6.10 shows the rotor response of the synchronous generator following the three-phase short circuit on the power network, which was cleared after 0.2 sec by taking line 1 out of service. When the LSCs Qsetpoint was 0 MVAr for both the DFIGs and CDSGs, the power system had a fairly similar response with regards to the different wind generator technologies. The first swing of the synchronous generator's rotor for both types of wind generators with the Qsetpoints at 0 MVAr settings had a similar magnitude. It is thus observed that, when the LSCs of the DFIG and that of the CDSG are both set to operate at 0 MVAr, the resultant acceleration power of the synchronous generator's rotor due to the imbalance of the mechanical power and electrical power is more or less the same. Moreover, the prefault rotor angle of the synchronous generator when the DFIGs were connected with the grid side converter set to 0 MVAr was lower than when the CDSGs were connected with similar settings. This is explained by the

fact that, the DFIGs stator terminals are directly connected to the power network, and thus there was some reactive power which was being drawn from the grid resulting in the lower prefault rotor angle .It is in this context, that the synchronous generator was supplying 31.35 MVAr to the rest of the power network before the fault. When the CDSGs were connected, the synchronous generator supplied 5.04 MVAr to the power system before the fault. The significant difference in the reactive power supplied by the synchronous generator when CDSGs were connected compared with when the DFIGs were connected can be attributed to the rotor side converter of the DFIG providing minimal excitation current to the rotor circuit of the DFIG. Furthermore, this resulted with the power network having to supply some magnetizing current. Also, the grid side converter of the DFIG was set to unity power factor and thus did not provide any reactive power to the power grid, thus the synchronous generator had to increase its reactive power supply. When the CDSGs were connected to the power network, the reactive power supplied by the synchronous generator was lower. This is due to the fact that the grid side converter was set to unity power factor and thus did not inject or absorb any reactive power from the power network. It follows that, the higher the reactive power supplied by the synchronous generator, the smaller the prefault rotor angle.

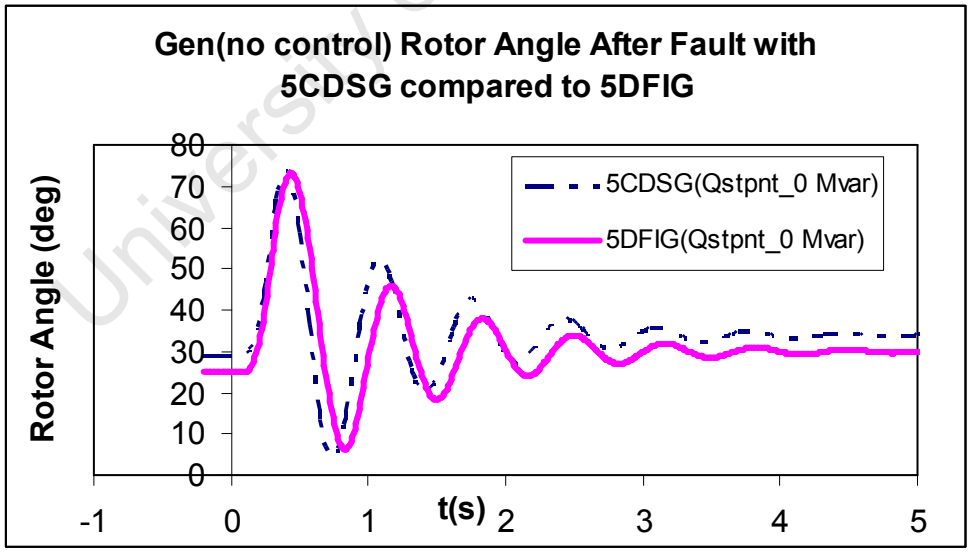


**Fig 6.10:** Rotor angle response from 5CDSG vs 5DFIG

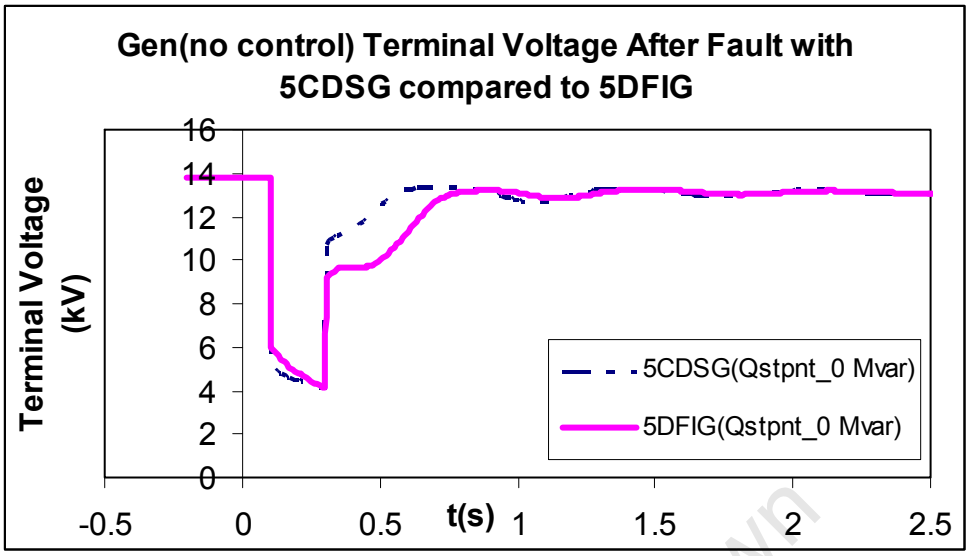


**Fig 6.11:** Terminal voltage response from 5CDSG vs 5DFIG

Figure 6.11 depicts the transient response of the synchronous generator's terminal voltage when connected to the different wind generator technologies. The terminal voltage recovers much quicker when the CDSGs were connected as compared with when the DFIGs were connected. This is due to the characteristic difference between the DFIG design and that of the CDSG. Since the stator terminals of the DFIG are directly coupled to the power network, it follows that its electromechanical dynamics after the fault will have some effect on the power system. The design of the converter driven synchronous generator is such that, the mechanical dynamics of the CDSG following the fault are completely decoupled from the grid owing to the full scale voltage source converter. The effect of the CDSG on the power network after a transient disturbance will be primarily characterized by the electrical response of the line side converter of the CDSG. It is therefore due to the response of the LSC following a fault that the terminal voltage of the synchronous generator recovered quicker compared with when the DFIG was connected.

# CONCLUSIONS & RECOMMENDATIONS

# 7

- A wind farm which is much further away from the grid requires a long transmission line to connect it to the power network. The negative consequence of this is that, the stability of the synchronous generator connected to the grid may be compromised since its steady state operating rotor angle increased as the length of the transmission line increased. A high prefault rotor angle means that the synchronous generator has its rotor angle moved closer to its operating limits.

- Having a fully operational AVR (i.e. IEEET1) enhances the transient stability of the power network.

- In practical power systems, the speed governor plays a complementary control role with the AVR. The governor controls the generator's mechanical torque in effort of maintaining frequency within set limits. However, the IEEEG2 speed governor with the given parameters did not manage to support the power network to maintain stability following a transient disturbance. This can further be supported by the case study wherein, the length of the transmission line connecting the squirrel cage induction generator based wind farm was increased to 540 km. At this length, the power system was transiently unstable when no power system controllers (i.e. IEEET1 AVR and IEEEG2 speed governor) were included and when only the IEEEG2 speed governor was included. However, when only the IEEET1 AVR was included, the power system was transiently stable.

- Furthermore, the power system was transiently unstable when power system controllers were not included, and also when only the IEEEG2 speed governor was included for the case study of he three different levels of reactive power compensation. Conversely, when the IEEET1 AVR was used for the same case study, the power system was stable for all three levels of reactive power compensation following the grid disturbance. This brought to light that the AVR is more critical than the speed governor in as far as transient stability is concerned.

- An increase in the number of wind generators connected in a wind farm could possibly negatively affect the transient stability of the power grid to which the wind farm is connected to. This is based on the observation that when the number of SCIGs, DFIGS and CDSGs connected to the power network is increased, the first swing of the synchronous generator became bigger following the fault on the power network, wherein, no system controllers were included.

## 7.1 The Effect of SCIGs on the Power System Transient Stability

It has been noted, based on the simulation results that, to best compensate the reactive power of a wind farm using SCIG technology with capacitor banks, the reactive power drawn by the wind farm cannot be looked at simply as a measure of rule. This is in reference to the case study in which, a SCIG wind farm capacity was at 50 MVA and different levels of reactive compensation were explored, these being; 15 MVAr, 20 MVAr and 30 MVAr. The simulation results have shown that in the cases explored, reactive power compensation of 20 MVAr resulted with a power system which had the most preferred response to a transient disturbance.

Increasing the amount of reactive power compensation to 30 MVAr resulted in a power system which had the best steady state operation with respect to the reactive power limits of the synchronous generator and voltage levels on the bus bars of the power network. This level of reactive power compensation culminated in a power network which had the least demand of reactive power from the synchronous generator and hence the exciter system was operated well within its limits.

Choosing SCIGs which have a relatively high inertia constant will prove prudent on the basis that, the power network to which they will be connected will have a better transient response compared with having wind generators with lower inertia.

## 7.2 The Effect of DFIGs on Transient Stability

The use of variable speed wind generators, such as doubly-fed induction generators brings about a power network which has a better transient response compared with using fixed speed wind generators with capacitive reactive power compensation. Variable speed wind generators are interfaced with voltage source converters and are able to supply reactive power and thus support the grid during transient disturbances.

Maintaining the reactive power set point of the doubly-fed induction generators line side converter at 0 MVAr is better than at 3 MVAr in relation to the power system's transient stability, since the rotor angle's first swing is bigger after the fault with 3 MVAr. Keeping the reactive power set point at 0 Mvar is also better than at -3 MVAr on the basis that, when the reactive set point is set to -3 MVAr the synchronous generator's terminal voltage dropped to an unacceptable voltage level of 0.63 p.u. after the fault.

Line side converters of the back-to-back PWM voltage source converter are more critical when it comes to the influence that variable speed converters have on the power system. This is in relation to reactive power exchange between the wind farm and the grid.

The integrated current controller of the voltage source converter is significant to the stable operation of the VSC and thus has a positive influence on the transient stability of the power network to which the variable speed wind generator is connected to. This is founded on the premise that the transient RMS simulations required an active current controller of the VSC to run.

Increasing the proportional gain of the grid side current controller by a factor of a 100 did not result with a significant difference to the transient response of the power system. Thus, setting

the proportional gain to a value within set limits will not affect the transient stability of the power system in a noteworthy manner.

When a grid disturbance occurs at a time when the speed of the DFIGs is above synchronous speed, the transient stability of the power system will be negatively affected. This is governed by fact that the speed of the DFIGs will increase further beyond synchronous speed due to the fault. This will result in an increase in reactive power demand from the DFIG in context with the VSC set to unity power factor. Then, the terminal voltage of the synchronous generator settles at 0.70 p.u. of the prefault voltage when no power system controllers were used.

## 7.3 The Effect of CDSGs on Transient Stability

The line side converter of the CDSG is more critical than the generator side converter in relation to reactive power exchange between the CDSG and the power grid. This was founded on the realization that the line side converter's reactive power setting had an influence on the amount of reactive power supplied by the conventional synchronous generator. However, the rotor side converter employs rotor speed control and can also control the frequency on the stator of the wind generator.

Increasing the reactive setpoint of the line side converter of the CDSG from -9 MVAr to 9 MVAr resulted in the rotor angle of the conventional synchronous generator increasing. Thus, the rotor angle moved towards its stability limits. Reactive setpoint of 0 MVAr of the VSC proved to be the most preferred reactive setpoint since the conventional synchronous generator supplied the least amount of reactive power to the power grid. This in turn meant that, the excitation system would be operated well within its limits.

By comparing the effect of CDSGs and DFIGs on the transient stability of the power system when the respective VSCs had their reactive power set points set to 0 MVAr , CDSGs proved more favorable over the doubly-fed induction generator. This is based on establishing that, the terminal voltage of the local conventional synchronous generator will have a rapid recovery following a transient disturbance on the power network in relation to when using a DFIG. This can be attributed to having a full scale converter interfacing with the grid when using a

CDSG in comparison with the partial-scale converter of the DFIG. However, the cost implication of using a full-scale voltage source converter could be a deterring factor to choosing the converter driven synchronous generator over the doubly-fed induction generator

## 7.4 Recommendations for Future Work

The wind generator models used did not incorporate the mechanical transmission system of the wind turbine since only the standard electrical models from the DIgSILENT library were used. Hence the model of the wind generators used incorporated one inertia mass, that being of the wind generators rotor. In some research studies, two mass models are used. These models incorporate the inertia mass of the turbine and would be implemented by using dynamic simulation language (DSL) in DIgSILENT. Thus the results are subject to a possibility of change with the inclusion of the wind turbine model and its mechanical controllers. This would require an extensive use of the DSL language in DIgSILENT. Models of wind generators including the transmission system would expand the scope of analysis and assess to what degree does:

- A two mass model mechanical system compared with a one mass model with increased inertia, impact on the power system transient stability.

- The speed rate at which turbine blades pitch impact on power system transient stability.

- The flexibility of the drive train of the wind turbine affect the transient stability.

- A serial connection of wind turbines in a wind farm impact on a power network's transient stability.

- A combination of different wind generator concepts connected to the same power network affect the transient stability of the power system.

# 8
# REFERENCES


[1] A.D. Hansen, L.H. Hansen, "Market Penetration of Wind Turbine Concepts over the Years," *risoe,* 2007.

[2] T. T. Chuong, P.V. Hoa, "Study of Grid Integrated System", *International Symposium on Electrical & Electronics Engineering*,Oct 24, 2007.

[3] Z. Chen, Y. Hu, F. Blaabjerg, "Stability Improvement of Induction Generator-Based Wind Turbine Systems", *IET Renew, Power Gener*, 2007.

[4] http://www.wwindea.org/home/index.php?option=com_content&task=view&id=223&Itemid=40

[5] G. Ramathran, J.B Ekanayake, N. Jenkins, "Frequency Support from Doubly-Fed Induction Generator Wind Turbines", *IET Renew, Power Gener*, 2007.

[6] N. Dinic, B. Fox, D. Flynn, L. Xu, A. Kennedy, "Increasing Wind Farm Capacity", *IEE Proc.-Gener. Transm.Distrib*, Vol 153, No. 4, 2006.

[7] Eltra, "Specifications for Connecting Wind Farms to the Transmission Network", *Eltra doc.no. 74174, Eltra*, 2000.

[8] I. Erlich, M. Wilch, C. Feltes, "Reactive Power Generation by DFIG Based Wind Farms with AC Grid Connection", *EPE*, Aalborg, 2007.

[9] M. Kayikçi and J.V. Milanović ,"Reactive Power Control Strategies for DFIG – Based Plants,"*IEEE Trans. Energy Conversion*, Vol.22, No. 2, June 2007

[10] M.A. Pöller, "Doubly-Fed Induction Machine Models for Stability Assessment of Wind Farms," *IEEE PowerTech,*2003.

[11] V. Akhmatov, "*Analysis of Dynamic Behaviour of Electric Power Systems with Large Amount of Wind Power,"* Ph.D Thesis, Technical University of Denmark, 2003.

[12] P. Bousseau, "Grid Impact of Different Technologies of Wind Turbine Generator Systems (WTGS,)"*Dispower, Energy Environment and Sustainable Development*, 2000.

[13] C. Abbey, B. Khodabakhchian, F. Zhou, S. Dennetiere, J. Mahseredjian, G. Joos, "Transient Modeling and Comparison of Wind Generator Topologies", *IPST'05*, Montreal, Canada, June 19-23, 2005

[14] S.B. Papaefthimiou, S. A. Papathanassiou, "Simulation and Control of variable Speed Wind Turbine with Synchronous Generator," *stpapath,* 2008.

[15] P .Kundur , *Power System Stability and Control.* McGraw-Hill, Inc. 1994

[16] " *DIgSILENT Technical Documentation – Synchronous Generator* " DIgSILENT GmbH , Germany, 2007.

[17] http://www.eskom.co.za/eia/Enviro%20assessments/Hydra-Gamma/CH01.pdf

[18] A.R Bergen, V.Vittal, *Power System Analysis*. 2nd Edition, Prentice Hall, Inc. 2000.

[19] P.C. Sen ,*Principles of Electric Machines and Power Electronics*. 2nd Edition, John Wiley & Sons, Inc. 1997.

[20] "*DIgSILENT Technical Documentation – Two Winding Transformer(3- Phase)* " DIgSILENT GmbH, Germany, 2007.

[21] J.D. Glover, M.S. Sarma, *Power System Analysis and Design*. 3rd Edition, Brooks/Cole , 2002.

[22] K.A. Folly, "Power Transmission Lines-Steady State Operation," *EEE 3057S Notes*, *University of Cape Town*, 2007.

[23] K.A. Folly, "Transient Stability," *EEE 4090F notes, University of Cape Town*, 2007.

[24] A.R Katančević "*Transient and Dynamic Stability on Wind Farms*" M.Sc. Thesis, Helsinki University of Technology, March 2003.

[25] O. Samuelsson "*Electric Power Systems-Laboratory Exercise 2, The Synchronous Generator,*" 2007.

[26] S. Ayusun , Y. Liang, C.O Nwankpa "A Sensitivity Approach for Computation of the Probability Density Function of Critical Clearing Time and Probability of Stability in Power System Transient Stability Analysis," *Science Direct, Applied Mathematics and Computation*, 2006.

[27] T. Ackerman, *Wind Power in Power Systems*. John Wiley & Sons, Ltd , 2005.

[28] Poul Sorensen, Anca D. Hansen, Florin Iov , Clemens Jauch and Frede Blaabjerg, "Dynamic Wind Turbine Models in Power System Simulation Tool DIgSILENT," *Riso National Laboratory, Roskilde*, December 2003.

[29] D. Naimi, T. Bouktir, "Impact of Wind Power on the Angular Stability of a Power System," *Leonardo Elctronic Journal of Practices and Technologies*, Issue 12, 2008.

[30] A. D. Hansen, P. Sørensen, F.Blaabjerg, J. Becho, "Dynamic Modelling of Wind Farm Grid Interaction," *Wind Engineering*, Volume 26, No.4, 2002.

[31] "*Dynamic Modelling of Doubly Fed Induction machine Wind Generators,*" DIgSILENT GmbH, Germany , 2003.

[32] I. Erlich, H. Wrede, C. Feltes, "Dynamic Behavior of DFIG-Based Wind Turbines During Grid Faults," *IEEJ Trans.IA,*vol.128,No.4,pp.369-401, 2008.

[33] C. Chompoo-inwai, C. Yingvivatanapong, K. Methaprayoon and W. J. Lee, "Reactive Compensation Techniques to Improve the Ride-Through Capability of Wind Turbine During Disturbance", *IEEE Transactions on Industry Application,* vol. 41, No.3,pp.666-672,2005.

[34] M V.A. Nunes, J. A. Peças Lopes, H. H Zürn, U.H Bezerra and R. G. Almeida, "Influence of Variable- Speed Wind Generators in Transient Stability Margin in Electrical Grids*," IEEE Transactions on Energy Conversion,* vol. 2, 2004.

[35] " *DIgSILENT – Technical Documentation- Doubly –fed Induction Machine*," DIgSILENT GmbH, 2007.

[36] L Holdsworth, X.G Wu, J.b Ekanayake and N. Jenkins , " Comparison of Fixed Speed and Doubly-Fed Induction Wind Turbines during Power System Disturbances," *IEE Poceedings-Gener, Transmission. Distribution,* May 2003.

[37] http://www.digsilent.de/Consulting/Publications/DirectDrive_Modeling.pdf

[38] L.H Hansen, L. Helle, F.Blaabjerg, E. Ritchie, S. Munk-Nielsen, P. Sørensen , B. Bak-Jensen, *Conceptual Survey of Generators and Power Electronics for Wind Turbines.* Risø National Laboratory , Roskilde , Denmark , 2001.

[39] S. Seman, "*Transient Performance Analysis of Wind – Power Induction Generators,*" Ph.D thesis, Helsinki University of Technology, 2006.

[40] N. Mohan, T.M. Undeland, W. P. Robbins, *Power Electronics*. 3rd Edition, John Wiley & Sons, 2003.

[41] V. K. Khanna , *The Insulated Gate Bipolar Transistor*. IEEE press, John Wiley & Sons, 2003.

[42] http://www.eolss.net/ebooks/Sample%20Chapters/C05/E6-39A-05-03.pdf

[43] C. Jauch, P. Sørensen, I. Norheim , "Simulation of the Impact of Wind Power on The Transient Fault Behavior of the Nordic Power System, " *Science Direct, Electric Power Systems Research*, 2007.

[44] " *DIgSILENT-Technical Documentation-PWM Converter*", DIgSILENT GmbH, Germany, 2007.

[45] S. C. Patel, K. A. Stephen, "Performance of Generator Protection During Major System Disturbances, " *IEEE paper No. TPWRD-00370*, 2003.

[46] http://www.ecowerc.com/products/pdf/nexgen-specs.pdf

[47] M.Wilch, V.S. Pappala, S.N. Singh, I. Erlich , "Reactive Power Generation by DFIG Based Wind Farms with AC Grid Connection, " *Power Tech, IEEE ,* 2007.

[48] T. Gönen , *Electric Power Transmission System Engineering,* 1st ed., John Wiley & Sons, 1988.

[49] K.A. Folly, "Active and Reactive Power Transfer," *EEE 3057S Notes*, *University of Cape Town*, 2007.

[50] M.T. Ameli, S. Moslepour, V. Sotudehnegad, "Reducing the Undesirable Effects of Wind Farms High Penetration on Frequency," *Proc.IAJC-IJME International Conference*, 2008.

[51] T.T Chuong, P. V. Hoa, "Effect of Wind Generators in Voltage Dips," *International Symposium on Electrical & Electronics Engineering*, 2007.

# 9

# APPENDIX 1

**Table A.1** Typical overhead transmission line parameters

| **Nominal Voltage** | 230 kV | 345kV | 500kV | 765kV | 1,100kV |
|---|---|---|---|---|---|
| $R(\Omega/km)$ | 0.050 | 0.037 | 0.028 | 0.012 | 0.005 |
| $x_L = \omega L(\Omega/km)$ | 0.488 | 0.367 | 0.325 | 0.329 | 0.292 |
| $b_C = \omega C(\mu s/km)$ | 3.371 | 4.518 | 5.200 | 4.978 | 5.544 |
| $\alpha(nepers/km)$ | 0.000067 | 0.000066 | 0.000057 | 0.000025 | 0.000012 |
| $\beta(rad/km)$ | 0.00128 | 0.00129 | 0.00130 | 0.00128 | 0.00127 |
| $Z_C(\Omega)$ | 380 | 285 | 250 | 257 | 230 |
| SIL(MW) | 140 | 420 | 1000 | 2280 | 5260 |
| Charging MVA/ $km = V_o^2 b_C$ | 0.18 | 0.54 | 1.30 | 2.92 | 6.71 |

N:B 1) Rated frequency is assumed to be 60Hz

2) Bundled conductors used for all lines listed, except for 230kV line

3) $R, x_L$ and $b_C$ are per-phase values.

4) SIL and charging MVA are three – phase values

# APPENDIX 2

## Network Parameters

Synchronous Machine (Type Info)
Srated : 100 MVA, V rated 13.8 kV
Power factor : 0.8
Rotor type :Salient Pole

RMS Simulation

- Inertia Time Constant 2.5 s
- Stator resistance 0.03 p.u.
- Stator leakage reactance 0.13 p.u.

- Synchronous reactance

Xd : 1.2 p.u.
Xq : 0.7 p.u.

- Transient time constants
Td' : 5s

- Transient reactances
Xd': 0.3 p.u.

- Stransient time constants

Td'' : 0.04s

Tq" : 0.05s

- Subtransient reactances

Xd" : 0.22 p.u
Xq" : 0.25 p.u.

Transmission lines

Ln(1& 2) : 200 kM
Ln (3) : 90 kM

Rated V : 230 KV
Rated current : 1 kA
Resistance R : 0 ohm/kM
Reactance X : 0.46 ohm/kM
Susceptance B :3.4 μS / kM
Transformer - TR 1

LV Vrated : 13.8 kV
HV Vrated : 230 kV
Srated : 150 MVA
Impedance : 0.03 p.u = 3%
X/R : 8
SCC positive sequence impedance :3%

Loads –

LD 1 & 2 - 80MW and 40 Mvar

Squirrel Cage Induction Generator

Active power: 8 MW
Reactive power: -6 Mvar
Rated Apparent Power: 10 MVA, Rated Voltage :11 kV
Poles : 2 pole pairs
Inertia : 1.215333s
Stator resistance: 0.01 p.u.
Stator reactance: 0.098 p.u.
Magnetising reactance: 2.48 p.u.
Rotor resistance : 0.012 p.u.
Rotor reactance : 0.12 p.u.

Doubly-fed Induction Generator

Active power: 8 MW
Reactive power: -6 Mvar
Rated slip-ring voltage : 1939 V
Rated Apparent Power : 10 MVA
Poles : 2 pole pairs
Inertia : 1.215333s
Stator resistance: 0.01 p.u.
Stator reactance: 0.098 p.u.
Magnetising reactance: 2.48 p.u.
Rotor resistance : 0.012 p.u.
Rotor reactance : 0.12 p.u.
Crowbar resistance: 0.1 p.u.
Crowbar reactance: 0.1 p.u.

DFIG Converter Initial Settings:

Rated AC voltage - 0.69kV
Rated DC voltage – 3.5kV
Rated Power - 3MVA
DC – Voltage set-point – 1.15 p.u.
Control mode - $V_{dc}$-Q
Reactive power setpoint – 0MVAr
Reactive power limits - -3MVAr
+3MVAr
Current controller:
Proportional gain - $K_{d,q}$ is 0.1
Integration time constant - $T_{d,q}$ is 0.01

Converter Driven Synchronous Generator

Active Power: 8 MW
Reactive power: 6 Mvar
Inertia : 1.215333 s
Stator resistance : 0.0001 p.u.
Stator reactance : 0.05 p.u.

- Synchronous reactance
Xd : 1.5 p.u.
Xq : 0.5 p.u.

- Transient time constants
Td' : 0.1 s

- Transient reactances
Xd': 0.25 p.u.

- Stransient time constants

Td'' : 0.02s
Tq" : 0.05s

- Subtransient reactances

Xd" : 0.17 p.u
Xq" : 0.17 p.u.

CDSG Converter settings:

Line Side Converter:
Rated AC voltage – 3.3 kV
Rated DC voltage – 6.6 kV
Rated Power - 15 MVA
DC – Voltage set-point – 1.15 p.u.
Control mode - $V_{dc}$-Q
Reactive power setpoint – 0MVAr
Reactive power limits - -15 MVAr
+15 MVAr
Current controller:
Proportional gain - $K_{d,q}$ is 0.8
Integration time constant - $T_{d,q}$ is 0.01

Generator Side Converter:
Rated AC voltage – 3.3 kV
Rated DC voltage – 6.6 kV
Rated Power - 15 MVA
Control mode - P-Q
Reactive power setpoint – 0 / -3 MVAr
Active power setpoint - -8 MW
Reactive power limits - -15 MVAr
+15 MVAr
Current controller:
Proportional gain - $K_{d,q}$ is 0.8
Integration time constant - $T_{d,q}$ is 0.01

# APPENDIX 3

*Derivations of Power Sent and Received within the Power Network*

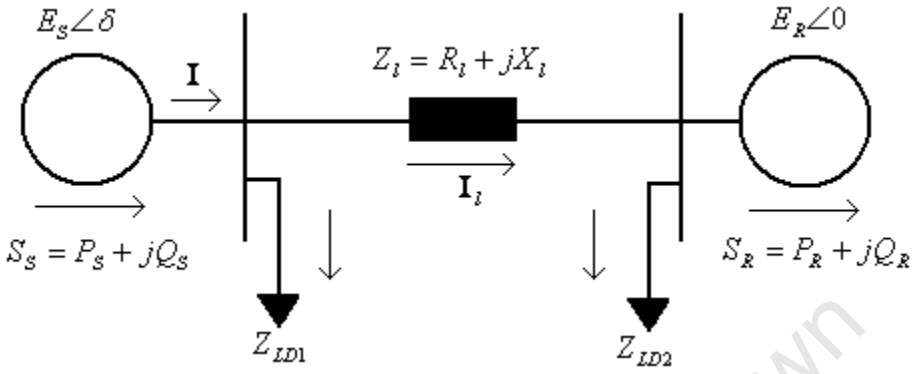


The complex power at the sending end is

$$S_S = E_S I^* = E_S\angle\delta\left(\frac{E_S\angle\delta - E_R\angle 0}{Z_l\angle\theta} + \frac{E_S\angle\delta}{Z_{LD1}\angle\beta}\right)^* = \frac{E_S^2\angle\theta}{Z_l} - \frac{E_S E_R}{Z_l}\angle(\delta+\theta) + \frac{E_S}{Z_{LD1}}\angle\beta - \delta$$

$$P_S = \frac{E_S^2}{Z_l}\cos\theta - \frac{E_S E_R}{Z_l}\cos(\delta+\theta) + \frac{E_S}{Z_{LD1}}\cos(\beta-\delta) \qquad \text{(A3-1)}$$

$$Q_S = \frac{E_S^2}{Z_l}\sin\theta - \frac{E_S E_R}{Z_l}\sin(\delta+\theta) + \frac{E_S}{Z_{LD1}}\sin(\beta-\delta) \qquad \text{(A3-2)}$$

Where $\delta$ is the power angle, $\theta = \tan^{-1}(X_l / R_l)$ and $\beta$ is load impedance angle

Likewise, the complex power at the receiving end is

$$S_R = E_R I^* = E_R\angle 0\left(\frac{E_S\angle\delta - E_R\angle 0}{Z_l\angle\theta} - \frac{E_R\angle 0}{Z_{LD2}\angle\beta}\right)^* = \frac{E_R E_S}{Z_l}\angle(\theta-\delta) - \frac{E_R^2}{Z_l}\angle\theta - \frac{E_R}{Z_{LD2}}\angle\beta$$

$$P_R = \frac{E_R E_S}{Z_l}\cos(\theta-\delta) - \frac{E_R^2}{Z_l}\cos\theta - \frac{E_R}{Z_{LD2}}\cos\beta \qquad \text{(A3-3)}$$

$$Q_R = \frac{E_R E_S}{Z_l}\sin(\theta-\delta) - \frac{E_R^2}{Z_l}\sin\theta - \frac{E_R}{Z_{LD2}}\sin\beta \qquad \text{(A3-4)}$$

# APPENDIX 4

*Equal Area Criterion (EAC) and Critical Clearing angle time*

The Equal area criterion is a graphical method that compares the amount of accelerating energy during the fault with the amount of decelerating energy after the fault is cleared. The fault corresponds to the power angle interval from the pre-fault power angle $\delta_0$ to the fault clearing angle $\delta_c$. Figure A 5.1 illustrates that during the fault the mechanical power $P_m$ is greater than the electrical power transferred $P_e$, which causes the rotor to accelerate and the angle $\delta$ increases. [30]

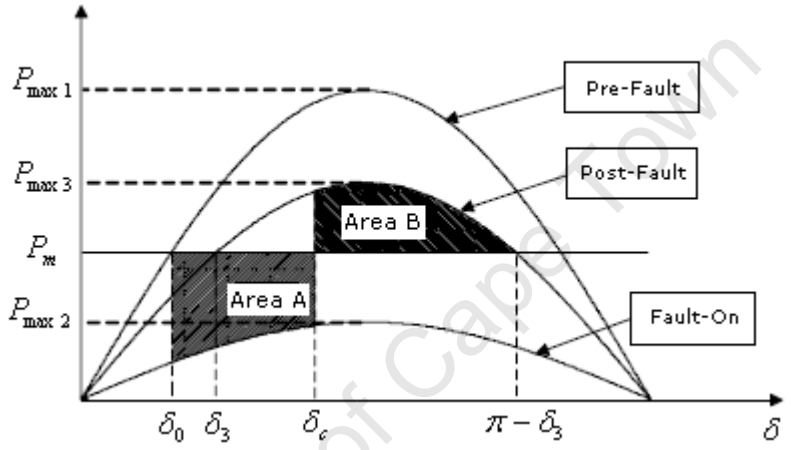


**Fig A 5.1:** Pre-fault, Fault-on and Post – fault power angle curves [30]

The *area A* in figure A 5.1 is the accelerating area, representing the kinetic energy stored in the machine because of acceleration of the rotor angle during the fault. The *area B* is the decelerating area which represents the maximum amount of energy that could be absorbed by the system after the fault is cleared. The two areas are defined as:[30]

$$Area\ A = \int_{\delta_0}^{\delta_c} (P_m - P_{\max 2} \sin\delta) d\delta\ ; \qquad Area\ B = \int_{\delta_c}^{\pi-\delta_3} (P_{\max 3} \sin\delta - P_m) d\delta \quad \text{(A5-1)}$$

According to the EAC, if the *area A* is less than the *area B*, then the system is transiently stable . In terms of energy this implies that the system will be able to absorb the excess kinetic energy stored in the rotor during the fault on. When the clearing angle is increased to a certain level such that the *area A* is equal to *area B*, the system is at a boundary condition. Under this condition, the clearing angle is called the critical angle denoted as $\delta_{cc}$. This is defined as the maximum power angle such that when the fault is cleared before this angle the system is transiently stable. An expression for critical clearing time is obtained by equating *area A* to *area B*: [30]

$$\delta_{cc} = \cos^{-1}\left[\frac{P_m(\pi - \delta_3 - \delta_0) - P_{\max 3}\cos\delta_3 - P_{\max 2}\cos\delta_0}{P_{\max 3} - P_{\max 2}}\right] \quad \text{(A5-2)}$$

Due to the non-linearity of the swing equation, an analytical solution for critical clearing time is not possible. The critical clearing time is the time when the power angle reaches the critical clearing angle during the first swing. By way of mathematical manipulation of the swing equation, the critical clearing time can be obtained by [30]

$$t_{cc} = \int_{\delta_0}^{\delta_{cc}} f(\delta, \delta_0)\, d\delta \quad \text{(A5-3)}$$

Where $$f(\delta, \delta_0) = \frac{1}{\sqrt{\frac{2}{M}(P_m(\delta - \delta_0) + P_{\max 2}(\cos\delta - \cos\delta_0))}} \quad \text{(A5-4)}$$

And $M$ is the moment of inertia of the generator.

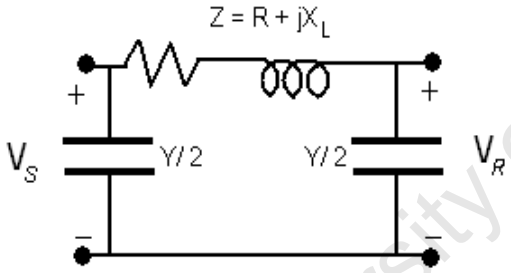


**Fig A 5.2**: Medium length transmission line model

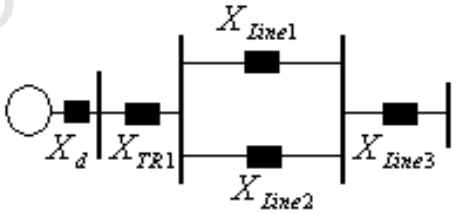


**Fig A 5.3:** Reactance representation of network model

$$X_{Line1} = \frac{jX_L \cdot (-j)X_C}{jX_L - jX_C} = X_{Line2} \quad \text{(A5-5)}$$

Where: $X_C$ and $X_L$ is capacitive reactance and inductive reactance respectively.

Thus,

$$X_T = X_d + X_{TR1} + (X_{Line1} // X_{Line2}) + X_{Line3} \quad \text{(A5-6)}$$

# APPENDIX 6

*Results of the SMIB following a 3-phase fault, without wind generators:* ***chapter 3***

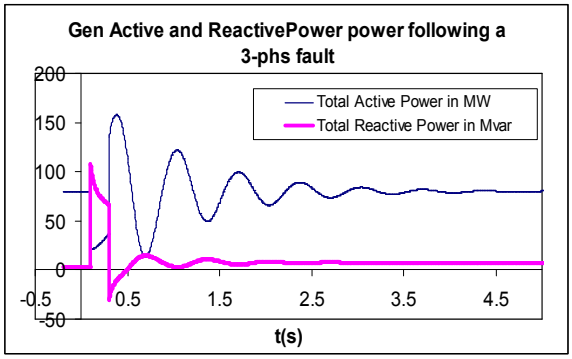


**Fig A 6.1**

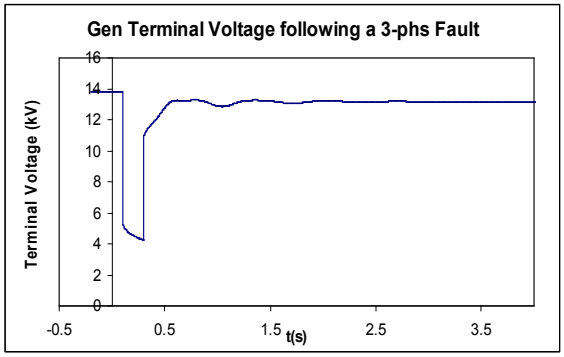


**Fig A 6.2**

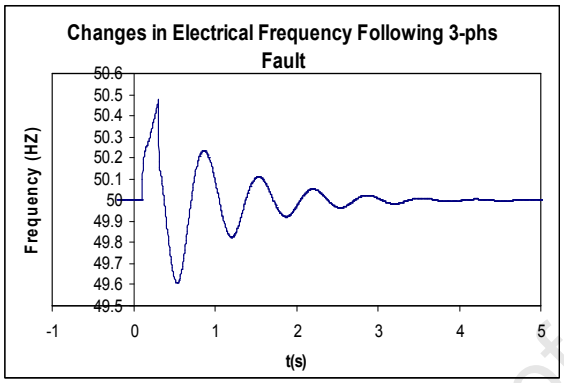


**Fig A 6.3**

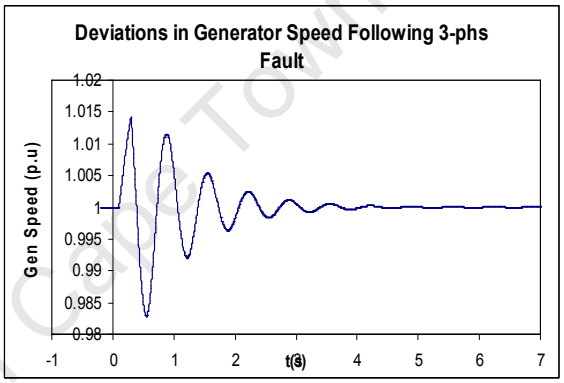


**Fig A 6.4**

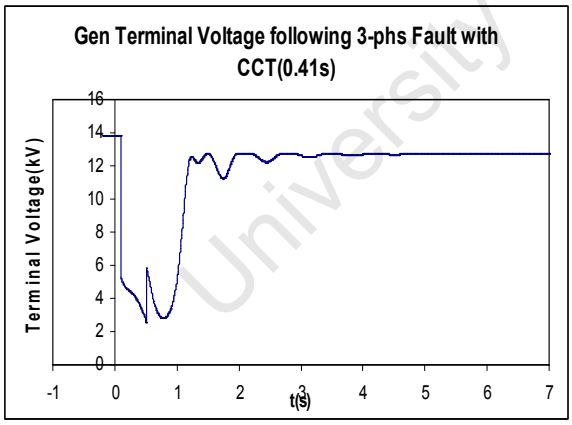


**Fig A 6.5**

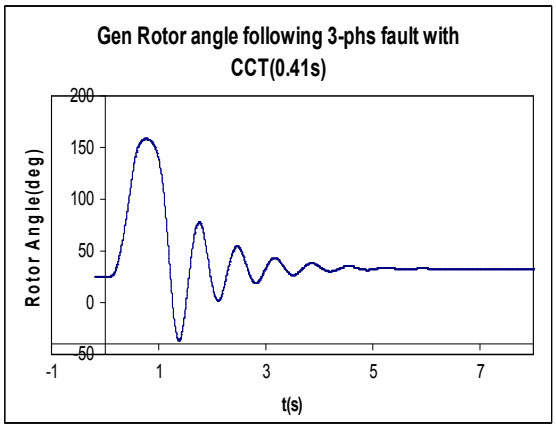


**Fig A 6.6**

**FCT –** Fault Clearing Time.

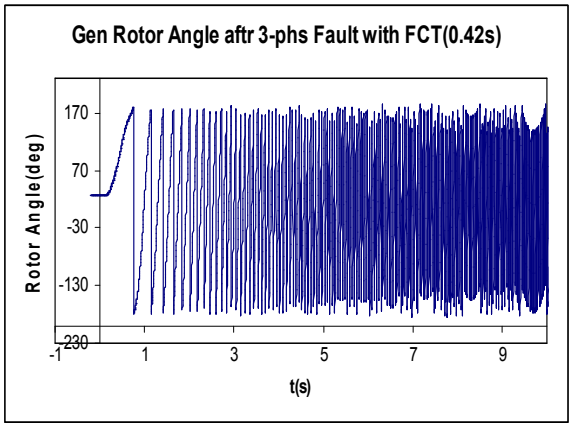


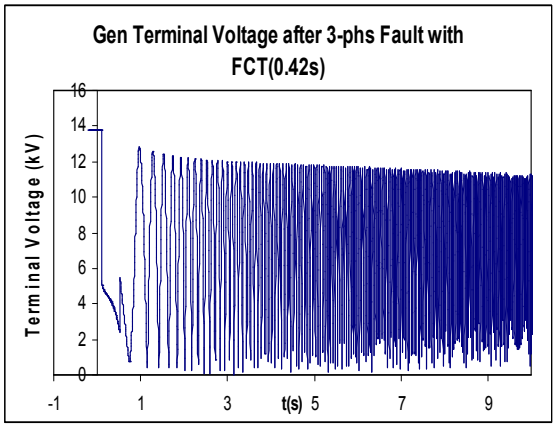


**Fig A 6.7**

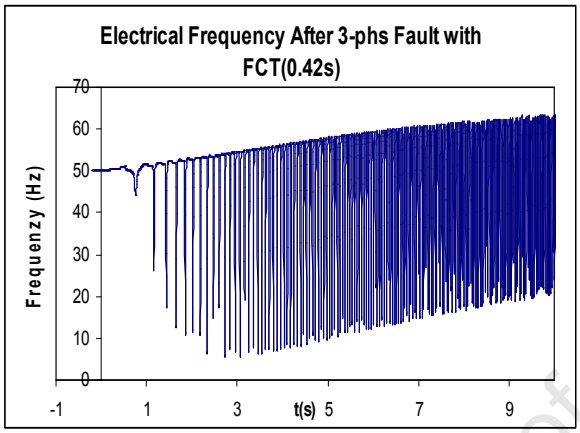


**Fig A 6.9**

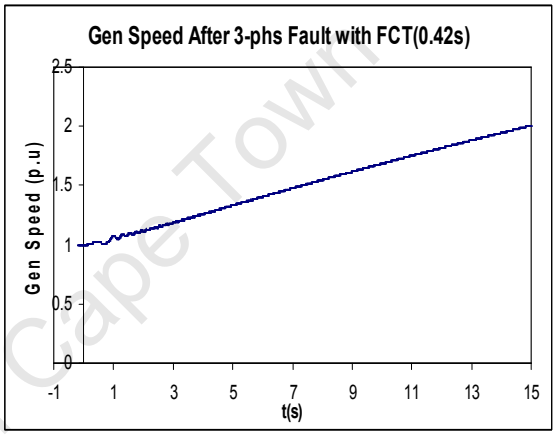


**Fig A 6.10**

# APPENDIX 7

*Results of the SMIB following a 3-phase fault, with SCIG:* ***chapter 4***

No Capacitor Bank

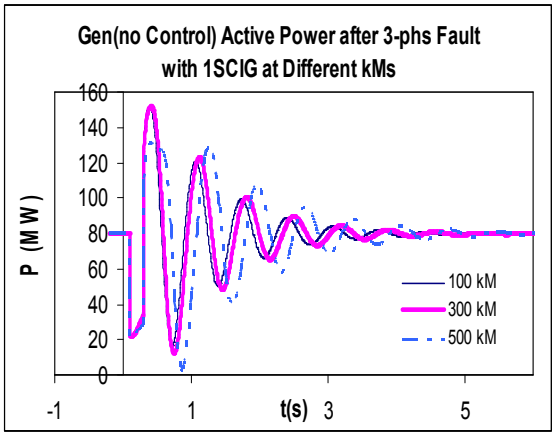


Fig A 7.1

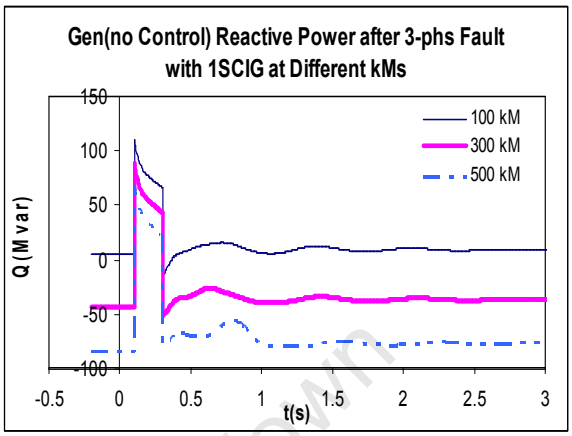


Fig A 7.2

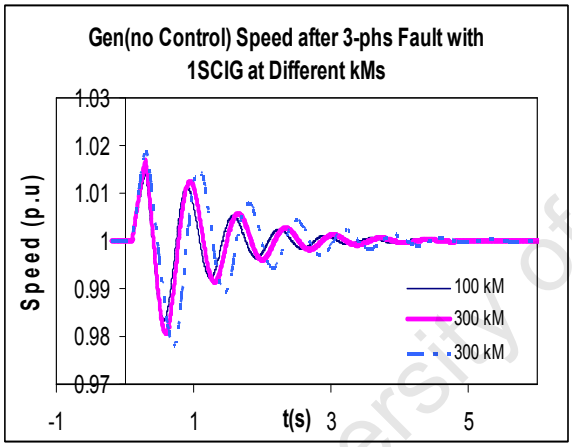


Fig A 7.3

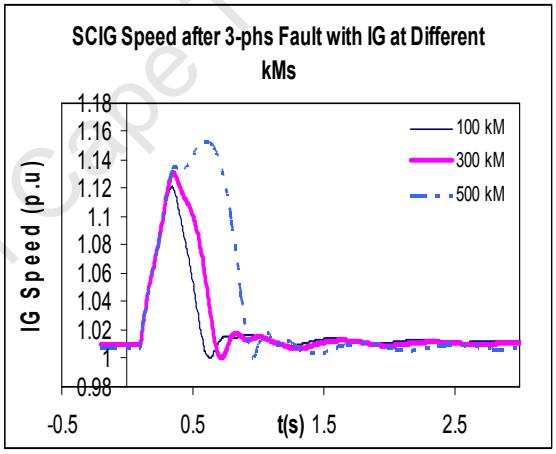


Fig A 7.4

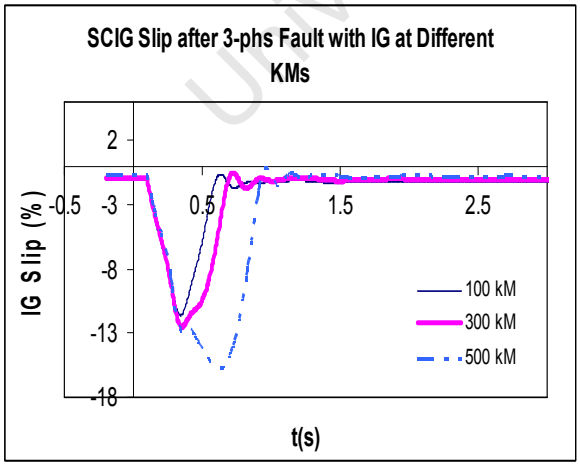


Fig A 7.5

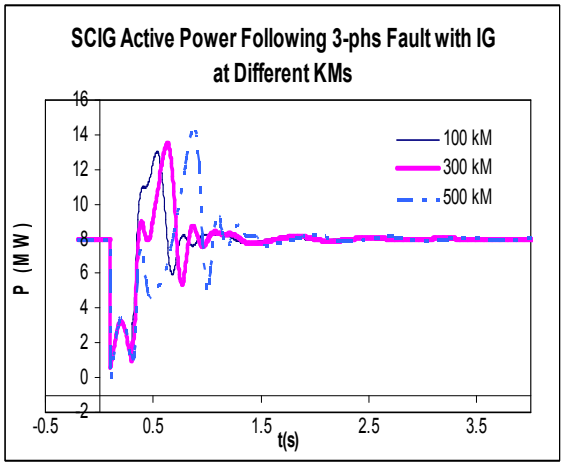


Fig A 7.6

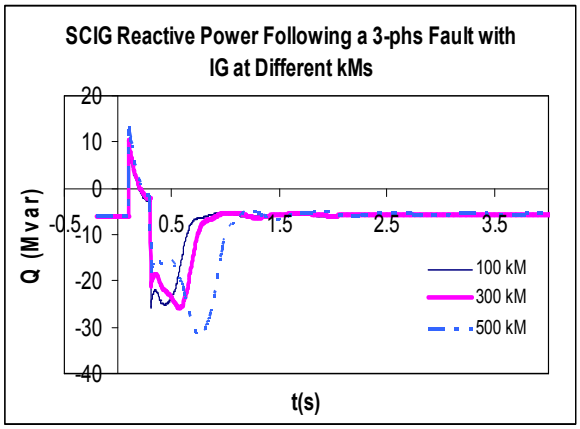


Fig A 7.7

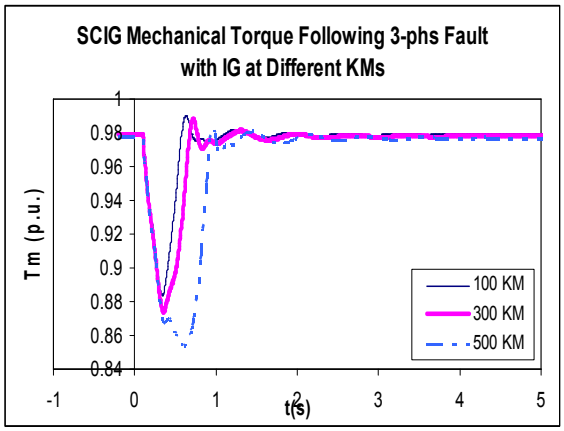


Fig A 7.8

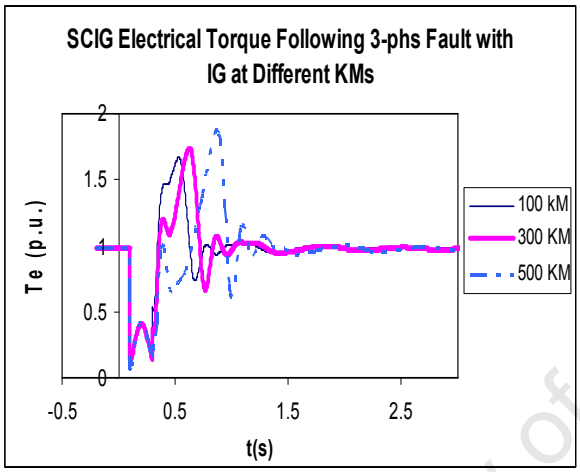


Fig A 7.9

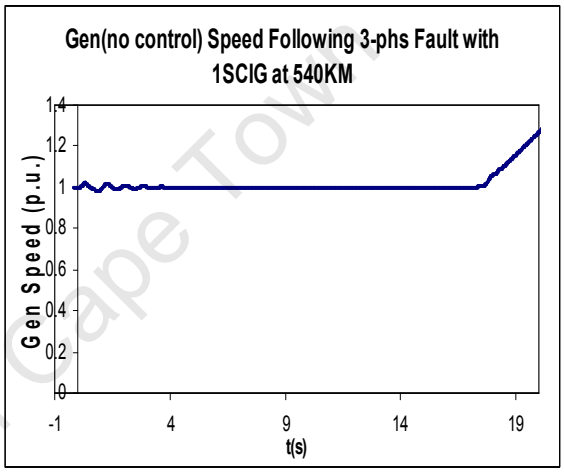


Fig A 7.10

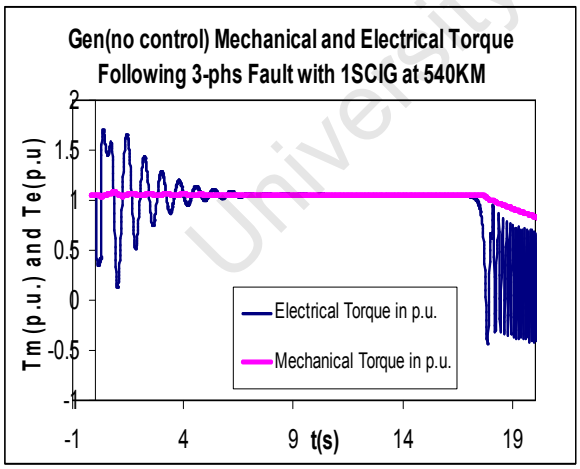


Fig A 7.11

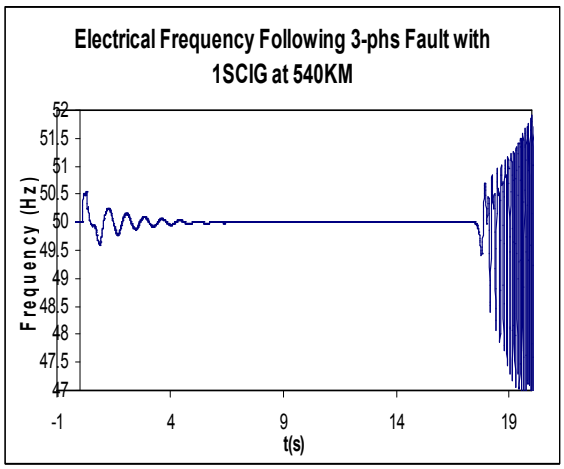


Fig A 7.12

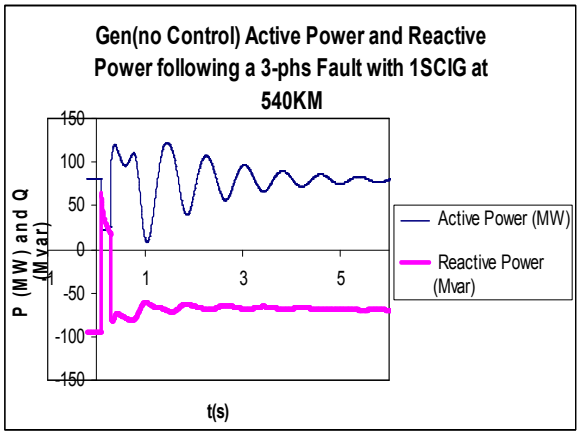


Fig A 7.13

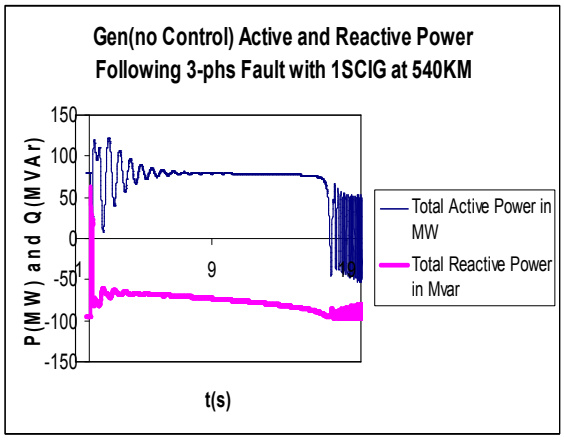


Fig A 7.14

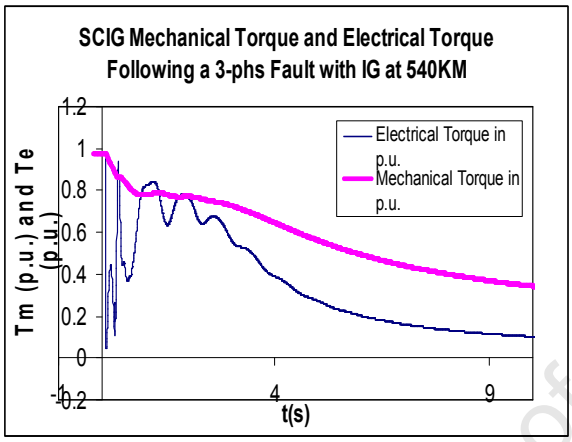


Fig A 7.15

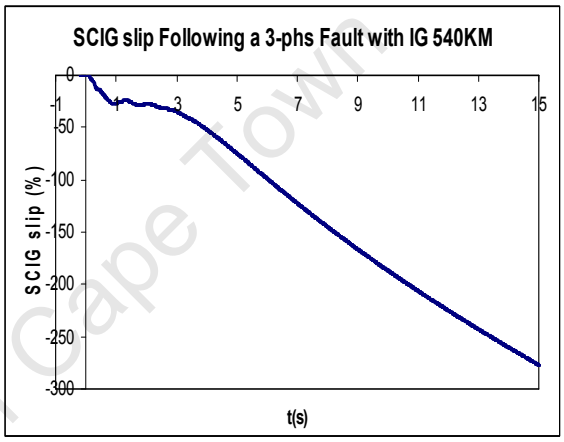


Fig A 7.16

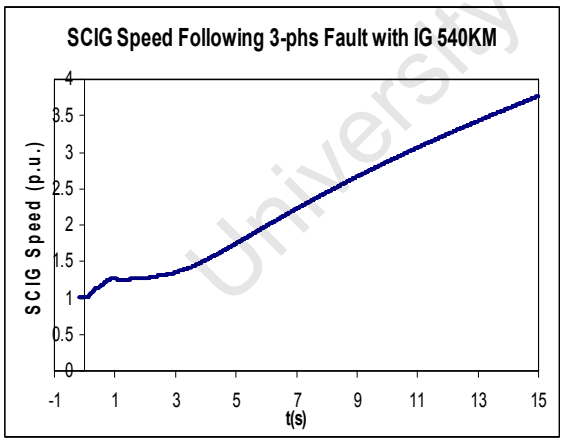


Fig A 7.17

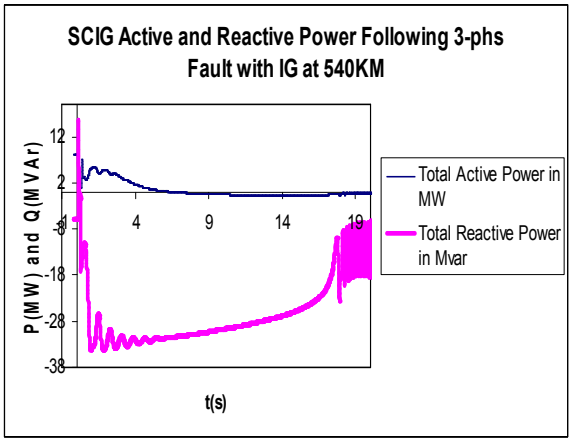


Fig A 7.18

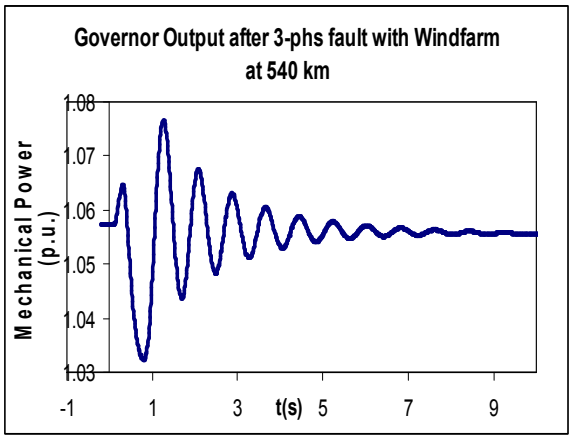


Fig A 7.19

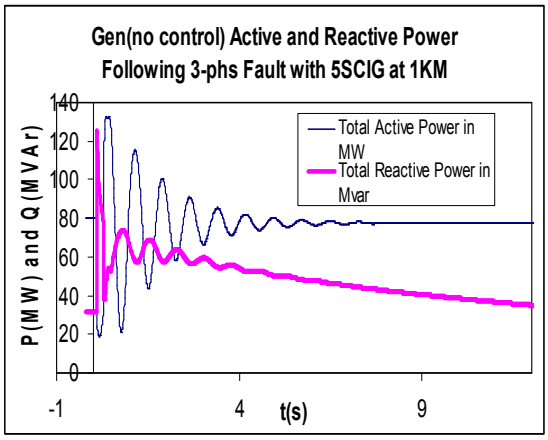


Fig A 7.20

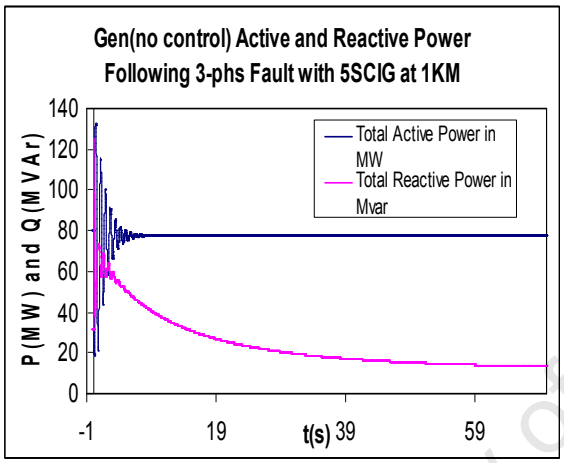


Fig A 7.21

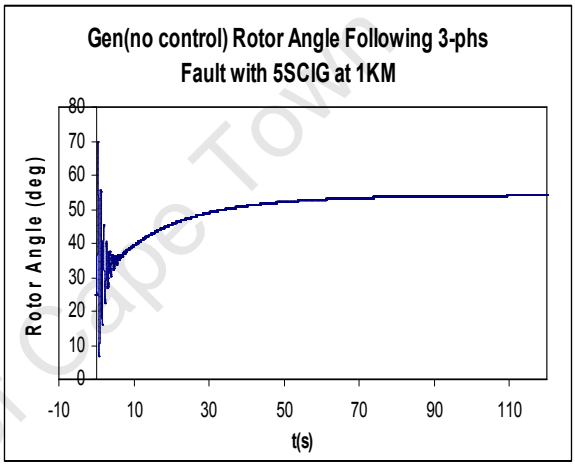


Fig A 7.22

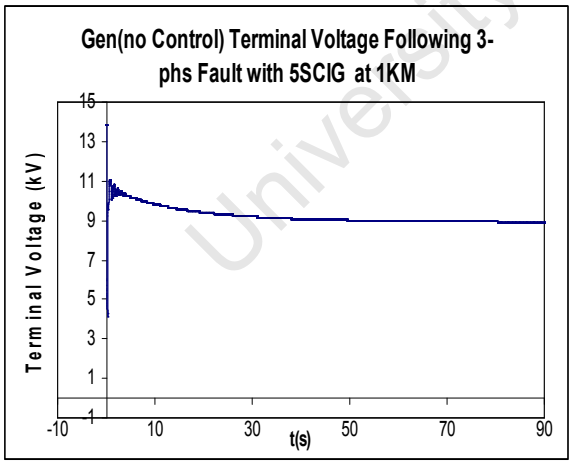


Fig A 7.23

Gen(no control)7SCIG Following 3-phs Fault at 1KM

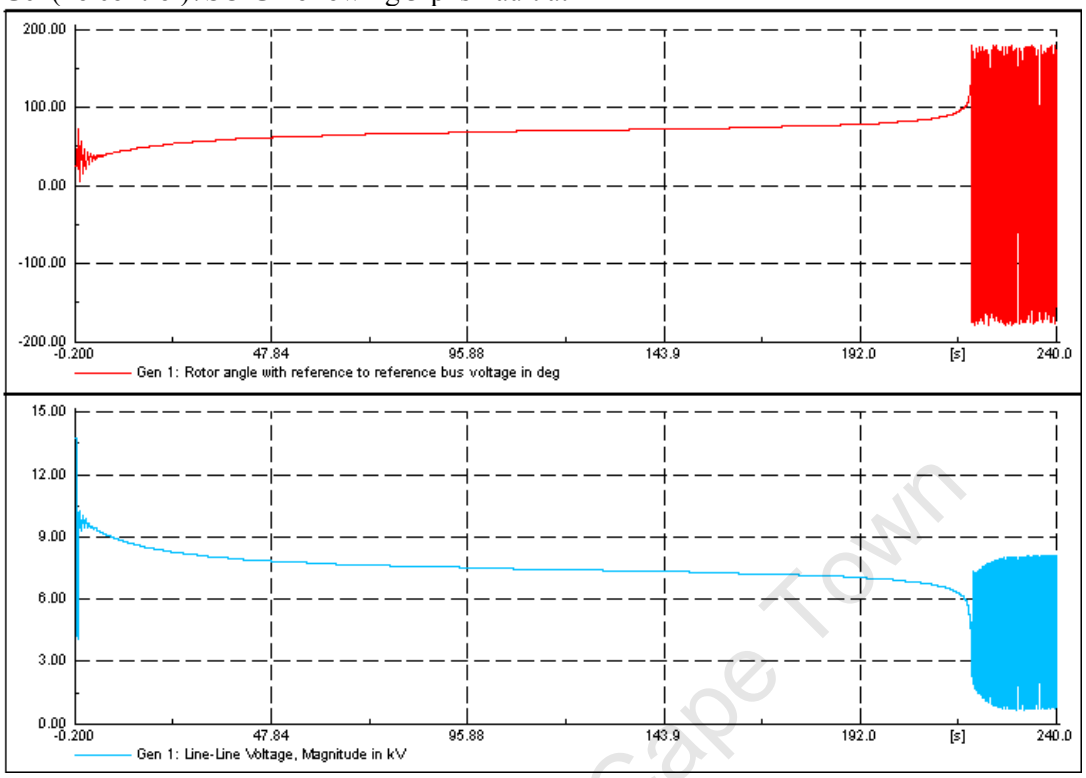


**Fig A 7.24**

Gen (Governor) 7SCIG Following 3-phs Fault at 1KM

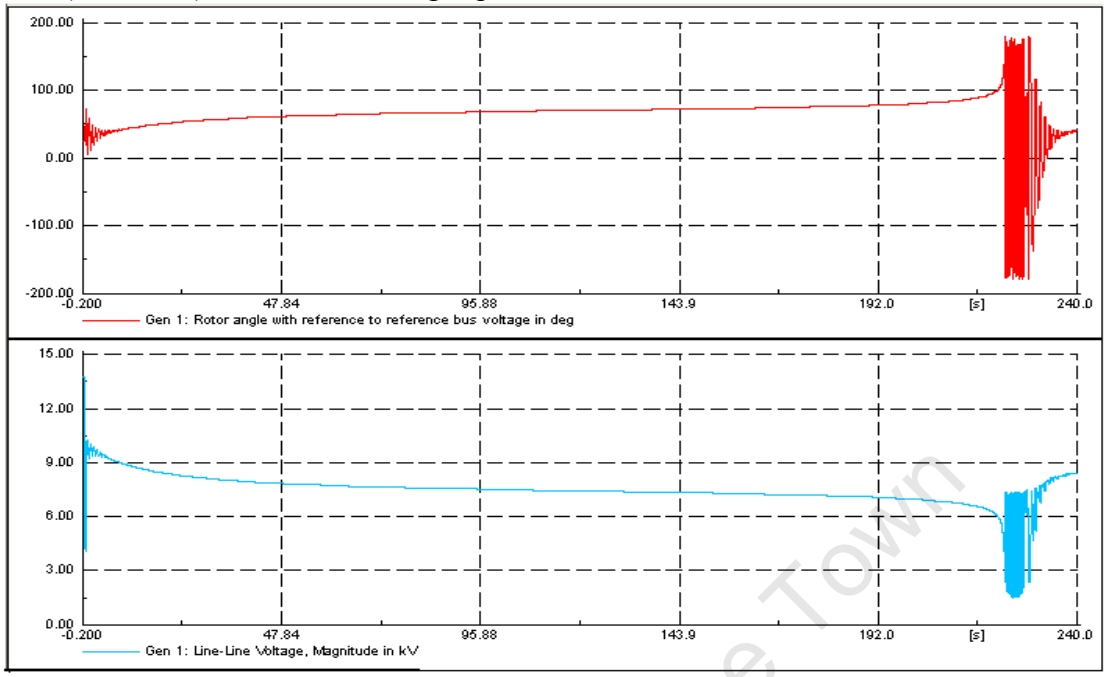


**Fig A 7.25**

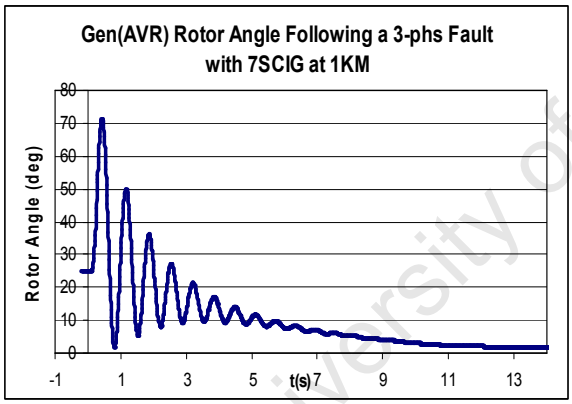


**Fig A 7.26**

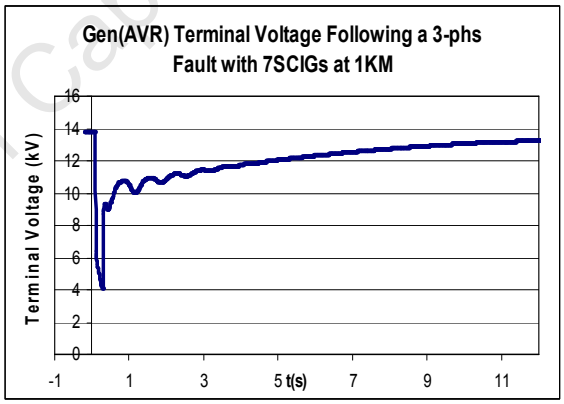


**Fig A 7.27**

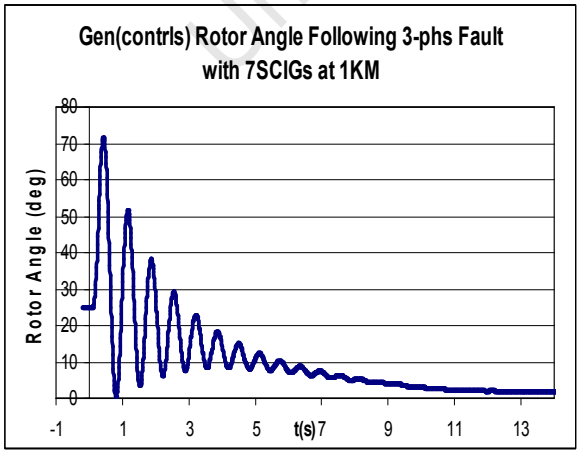


**Fig A 7.28**

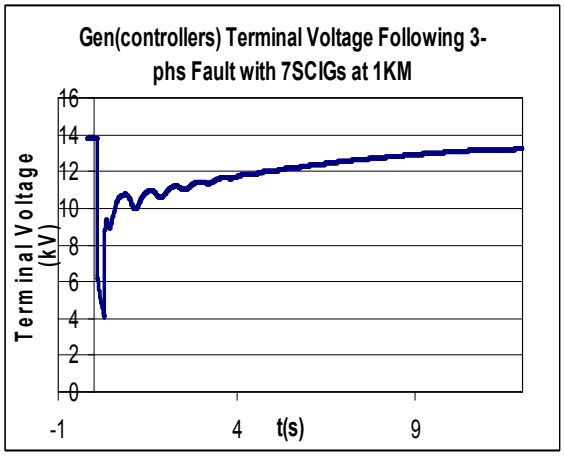


**Fig A 7.29**

# APPENDIX 8

*Pre-Fault Power Flow Results For 1SCIG at 1 km :**Chapter 4***

1. 1SCIG (no Reactive Power Compensation) 1 km

| | P(MW) | Q(MVAr) |
|---|---|---|
| **Gen 1** | 80.00 | 8.36 |
| **SCIG(PCC)** | 8.00 | -6.21 |
| **SCIG** | 8.00 | -6.00 |
| **Ld 1** | 80.00 | 40 |
| **Ld 2** | 80.00 | 40 |
| **Infinite Bus** | 72.16 | -5.01 |

| | V(kV) | δ(deg) |
|---|---|---|
| **Bus 1** | 13.80 | -1.94 |
| **Bus 2** | 229.19 | -2.85 |
| **Bus 3** | 229.81 | -3.24 |
| **Bus 4** | 230.00 | 0.00 |
| **Bus 5** | 229.18 | -2.84 |
| **Bus 6** | 10.83 | -1.90 |

| | P(MW) | Q(MVAr) | Loading (%) |
|---|---|---|---|
| **Line 2B2** | 3.92 | -19.48 | 5.00 |
| **Line 2B3** | -3.92 | -16.45 | 5.00 |
| **Line 3B3** | -72.16 | -7.10 | 18.22 |
| **Line 3B4** | 72.16 | -5.01 | 18.22 |
| **Line 4B2** | -8.00 | 6.03 | 2.55 |

*Pre-Fault Power Flow Results For 1 SCIG at 100 km, 300 km and 500 km*

2. 1SCIG (no Reactive Power Compensation) 100 km

| | P(MW) | Q(MVAr) |
|---|---|---|
| **Gen 1** | 80.00 | -7.92 |
| **SCIG(PCC)** | 8.00 | -6.05 |
| **SCIG** | 8.00 | -6.00 |
| **Ld 1** | 80.00 | 40.00 |
| **Ld 2** | 80.00 | 40.00 |
| **Infinite Bus** | 72.16 | -7.06 |

| | V(kV) | δ(deg) |
|---|---|---|
| **Bus 1** | 13.80 | -1.92 |
| **Bus 2** | 229.93 | -2.84 |
| **Bus 3** | 230.18 | -3.23 |
| **Bus 4** | 230.00 | 0.00 |
| **Bus 5** | 230.52 | -2.44 |
| **Bus 6** | 10.99 | -2.21 |

| | P(MW) | Q(MVAr) | Loading (%) |
|---|---|---|---|
| **Line 2B2** | 3.92 | -18.65 | 4.78 |
| **Line 2B3** | -3.92 | -17.46 | 4.78 |
| **Line 3B3** | -72.16 | -5.09 | 18.20 |
| **Line 3B4** | 72.16 | -7.06 | 18.20 |
| **Line 4B2** | -8.00 | -11.91 | 3.60 |

3. 1SCIG (no Reactive Power Compensation) 300 km

| | P(MW) | Q(MVAr) |
|---|---|---|
| **Gen 1** | 80.00 | -42.55 |
| **SCIG(PCC)** | 8.00 | -6.04 |
| **SCIG** | 8.00 | -6.00 |
| **Ld 1** | 80.00 | 40.00 |
| **Ld 2** | 80.00 | 40.00 |
| **Infinite Bus** | 72.20 | -11.41 |

| | V(kV) | δ(deg) |
|---|---|---|
| **Bus 1** | 13.80 | -1.88 |
| **Bus 2** | 231.52 | -2.84 |
| **Bus 3** | 230.96 | -3.22 |
| **Bus 4** | 230.00 | 1.00 |
| **Bus 5** | 245.34 | 1.07 |
| **Bus 6** | 11.70 | -1.52 |

| | P(MW) | Q(MVAr) | Loading (%) |
|---|---|---|---|
| **Line 2B2** | 3.90 | -16.86 | 5.00 |
| **Line 2B3** | -3.90 | -19.61 | 5.00 |
| **Line 3B3** | -72.20 | -0.78 | 18.35 |
| **Line 3B4** | 72.20 | -11.41 | 18.35 |
| **Line 4B2** | -8.00 | -50.45 | 12.74 |

4. 1SCIG (no Reactive Power Compensation) 500 km

| | P(MW) | Q(MVAr) |
|---|---|---|
| **Gen 1** | 80.00 | -84.19 |
| **SCIG(PCC)** | 8.00 | -6.03 |
| **SCIG** | 8.00 | -6.00 |
| **Ld 1** | 80.00 | 40.00 |
| **Ld 2** | 80.00 | 40.00 |
| **Infinite Bus** | 72.33 | -16.63 |

| | V(kV) | δ(deg) |
|---|---|---|
| **Bus 1** | 13.80 | -1.83 |
| **Bus 2** | 233.42 | -2.84 |
| **Bus 3** | 231.90 | -3.21 |
| **Bus 4** | 230.00 | 1.00 |
| **Bus 5** | 283.96 | -1.25 |
| **Bus 6** | 13.55 | -1.10 |

| | P(MW) | Q(MVAr) | Loading (%) |
|---|---|---|---|
| **Line 2B2** | 3.83 | -14.68 | 5.61 |
| **Line 2B3** | -3.83 | -22.22 | 5.61 |
| **Line 3B3** | -72.33 | 4.44 | 18.63 |
| **Line 3B4** | 72.33 | -16.63 | 18.63 |
| **Line 4B2** | -8.00 | -97.79 | 24.19 |

5. 1SCIG (no Reactive Power Compensation) 540 km

| | P(MW) | Q(MVAr) |
|---|---|---|
| **Gen 1** | 80.00 | -94.06 |
| **SCIG(PCC)** | 8.00 | -6.12 |
| **SCIG** | 8.00 | -6.00 |
| **Ld 1** | 80.00 | 40.00 |
| **Ld 2** | 80.00 | 40.00 |
| **Infinite Bus** | 72.38 | -17.86 |

| | V(kV) | δ(deg) |
|---|---|---|
| **Bus 1** | 13.80 | -1.82 |
| **Bus 2** | 233.87 | -2.85 |
| **Bus 3** | 232.12 | -3.12 |
| **Bus 4** | 230.00 | 0.00 |
| **Bus 5** | 296.18 | -1.20 |
| **Bus 6** | 14.06 | -0.64 |

| | P(MW) | Q(MVAr) | Loading (%) |
|---|---|---|---|
| **Line 2B2** | 3.81 | -14.16 | 5.46 |
| **Line 2B3** | -3.81 | -22.84 | 5.76 |
| **Line 3B3** | -72.38 | 5.68 | 18.71 |
| **Line 3B4** | 72.38 | -17.86 | 18.71 |
| **Line 4B2** | -8.00 | -108.76 | 26.92 |

6. 1SCIG (no Reactive Power Compensation) 1 km

| | P(MW) | Q(MVAr) |
|---|---|---|
| **Gen 1** | 80.00 | 8.22 |
| **SCIG(PCC)** | 8.00 | -6.05 |
| **SCIG** | 8.00 | -6.00 |
| **Ld 1** | 80.00 | 40.00 |
| **Ld 2** | 80.00 | 40.00 |
| **Infinite Bus** | 72.16 | -5.03 |

| | V(kV) | δ(deg) |
|---|---|---|
| **Bus 1** | 13.80 | -1.94 |
| **Bus 2** | 229.20 | -2.85 |
| **Bus 3** | 229.81 | -3.23 |
| **Bus 4** | 230.00 | 0.00 |
| **Bus 5** | 229.18 | -2.84 |
| **Bus 6** | 10.93 | -2.61 |

| | P(MW) | Q(MVAr) | Loading (%) |
|---|---|---|---|
| **Line 2B2** | 3.92 | -19.47 | 5.00 |
| **Line 2B3** | 3.92 | -16.46 | 5.00 |
| **Line 3B3** | -72.16 | -7.08 | 18.22 |
| **Line 3B4** | 72.16 | -5.03 | 18.22 |
| **Line 4B2** | -8.00 | 5.87 | 2.53 |

7. 2SCIG (no Reactive Power Compensation) 1 km

| | P(MW) | Q(MVAr) |
|---|---|---|
| **Gen 1** | 80.00 | 14.02 |
| **SCIG(PCC)** | 16.00 | -12.50 |
| **SCIG** | 16.00 | -12.00 |
| **Ld 1** | 80.00 | 40.00 |
| **Ld 2** | 80.00 | 40.00 |
| **Infinite Bus** | 64.17 | -4.92 |

| | V(kV) | δ(deg) |
|---|---|---|
| **Bus 1** | 13.80 | -1.20 |
| **Bus 2** | 228.93 | -2.09 |
| **Bus 3** | 229.72 | -2.88 |
| **Bus 4** | 230.00 | 0.00 |
| **Bus 5** | 228.91 | -2.08 |
| **Bus 6** | 10.79 | -0.95 |

| | P(MW) | Q(MVAr) | Loading (%) |
|---|---|---|---|
| **Line 2B2** | 7.92 | -19.81 | 5.38 |
| **Line 2B3** | -7.92 | -15.98 | 5.38 |
| **Line 3B3** | -64.17 | -8.04 | 16.25 |
| **Line 3B4** | 64.17 | -4.92 | 16.25 |
| **Line 4B2** | -16.00 | 12.32 | 5.12 |

8. 4SCIG (no Reactive Power Compensation) 1 km

| | P(MW) | Q(MVAr) |
|---|---|---|
| **Gen 1** | 80.00 | 25.14 |
| **SCIG(PCC)** | 32.00 | -24.49 |
| **SCIG** | 32.00 | -24.00 |
| **Ld 1** | 80.00 | 40.00 |
| **Ld 2** | 80.00 | 40.00 |
| **Infinite Bus** | 48.18 | -4.43 |

| | V(kV) | δ(deg) |
|---|---|---|
| **Bus 1** | 13.8 | 0.31 |
| **Bus 2** | 228.42 | -0.57 |
| **Bus 3** | 229.50 | -2.16 |
| **Bus 4** | 230.00 | 0.00 |
| **Bus 5** | 228.37 | -0.56 |
| **Bus 6** | 10.84 | 0.01 |

| | P(MW) | Q(MVAr) |
|---|---|---|
| **Line 2B2** | 15.91 | -20.29 |
| **Line 2B3** | -15.91 | -15.04 |
| **Line 3B3** | -48.18 | -9.91 |
| **Line 3B4** | 48.18 | -4.43 |
| **Line 4B2** | -32.00 | 24.33 |

9. 5SCIG (no Reactive Power Compensation) 1 km

| | P(MW) | Q(MVAr) |
|---|---|---|
| **Gen 1** | 80.00 | 31.63 |
| **SCIG(PCC)** | 39.99 | -31.31 |
| **SCIG** | 40.00 | -30.00 |
| **Ld 1** | 80.00 | 40.00 |
| **Ld 2** | 80.00 | 40.00 |
| **Infinite Bus** | 40.20 | -3.90 |

| | V(kV) | δ(deg) |
|---|---|---|
| **Bus 1** | 13.80 | 1.06 |
| **Bus 2** | 228.13 | 0.18 |
| **Bus 3** | 229.36 | -1.80 |
| **Bus 4** | 230.00 | 0.00 |
| **Bus 5** | 228.06 | 0.21 |
| **Bus 6** | 10.74 | 1.40 |

| | P(MW) | Q(MVAr) | Loading (%) |
|---|---|---|---|
| **Line 2B2** | 19.90 | -20.50 | 7.23 |
| **Line 2B3** | -19.90 | -14.51 | 7.23 |
| **Line 3B3** | -40.20 | -10.98 | 10.49 |
| **Line 3B4** | 40.20 | -3.90 | 10.49 |
| **Line 4B2** | -39.99 | 31.16 | 12.86 |

10. 7SCIG (no Reactive Power Compensation) 1 km

| | P(MW) | Q(MVAr) |
|---|---|---|
| **Gen 1** | 80.00 | 43.66 |
| **SCIG(PCC)** | 55.98 | -43.54 |
| **SCIG** | 56.00 | -42.00 |
| **Ld 1** | 80.00 | 40.00 |
| **Ld 2** | 80.00 | 40.00 |
| **Infinite Bus** | 24.22 | -2.65 |

| | V(kV) | δ(deg) |
|---|---|---|
| **Bus 1** | 13.80 | 2.57 |
| **Bus 2** | 227.58 | 1.71 |
| **Bus 3** | 229.06 | -1.09 |
| **Bus 4** | 230.00 | 0.00 |
| **Bus 5** | 227.49 | 1.74 |
| **Bus 6** | 10.74 | 2.74 |

| | P(MW) | Q(MVAr) | Loading (%) |
|---|---|---|---|
| **Line 2B2** | 27.89 | -20.70 | 8.81 |
| **Line 2B3** | -27.89 | -13.50 | 8.81 |
| **Line 3B3** | 24.22 | -13.00 | 6.93 |
| **Line 3B4** | 24.22 | -2.65 | 6.93 |
| **Line 4B2** | -55.98 | 43.41 | 18.00 |

11. 5SCIG (15 Mvar reactive power compensation) 1 km

| | P(MW) | Q(MVAr) |
|---|---|---|
| **Gen 1** | 80.00 | 17.89 |
| **SCIG(PCC)** | 39.99 | -16.34 |
| **SCIG** | 40.00 | -30.00 |
| **Ld 1** | 80.00 | 40.00 |
| **Ld 2** | 80.00 | 40.00 |
| **Capacitor Bank** | 0.00 | 14.60 |
| **Infinite Bus** | 40.18 | -5.63 |

| | V(kV) | δ(deg) |
|---|---|---|
| **Bus 1** | 13.80 | 1.07 |
| **Bus 2** | 228.75 | 0.18 |
| **Bus 3** | 229.67 | -1.80 |
| **Bus 4** | 230.00 | 0.00 |
| **Bus 5** | 228.72 | 0.20 |
| **Bus 6** | 10.85 | 1.37 |

| | P(MW) | Q(MVAr) | Loading (%) |
|---|---|---|---|
| **Line 2B2** | 19.91 | -19.81 | 7.09 |
| **Line 2B3** | -19.91 | -15.36 | 7.09 |
| **Line 3B3** | -40.16 | -9.28 | 10.37 |
| **Line 3B4** | 40.18 | -5.63 | 10.37 |
| **Line 4B2** | -39.99 | 16.18 | 10.90 |

12. 5SCIG (20 Mvar reactive power compensation) 1 km

| | P(MW) | Q(MVAr) |
|---|---|---|
| **Gen 1** | 80.00 | 13.25 |
| **SCIG(PCC)** | 39.99 | -11.26 |
| **SCIG** | 40.00 | -30.00 |
| **Ld 1** | 80.00 | 40.00 |
| **Ld 2** | 80.00 | 40.00 |
| **Capacitor Bank** | 0.00 | 19.61 |
| **Infinite Bus** | 40.17 | -6.21 |

| | V(kV) | δ(deg) |
|---|---|---|
| **Bus 1** | 13.80 | 1.07 |
| **Bus 2** | 228.97 | 0.18 |
| **Bus 3** | 229.77 | -1.80 |
| **Bus 4** | 230.00 | 0.00 |
| **Bus 5** | 228.94 | 0.20 |
| **Bus 6** | 10.89 | 1.37 |

| | P(MW) | Q(MVAr) | Loading (%) |
|---|---|---|---|
| **Line 2B2** | 19.91 | -19.58 | 7.04 |
| **Line 2B3** | -19.91 | -15.65 | 7.04 |
| **Line 3B3** | -40.17 | -8.71 | 10.33 |
| **Line 3B4** | 40.17 | -6.21 | 10.33 |
| **Line 4B2** | -39.99 | 11.10 | 10.48 |

13. 5SCIG (30 Mvar reactive power compensation) 1 km

| | P(MW) | Q(MVAr) |
|---|---|---|
| **Gen 1** | 80.00 | 3.87 |
| **SCIG(PCC)** | 39.99 | -0.97 |
| **SCIG** | 40.00 | -30.00 |
| **Ld 1** | 80.00 | 40.00 |
| **Ld 2** | 80.00 | 40.00 |
| **Capacitor Bank** | 0.00 | 29.84 |
| **Infinite Bus** | 40.00 | -7.39 |

| | V(kV) | δ(deg) |
|---|---|---|
| **Bus 1** | 13.80 | 1.08 |
| **Bus 2** | 229.40 | 0.18 |
| **Bus 3** | 229.99 | -1.80 |
| **Bus 4** | 230.00 | 0.00 |
| **Bus 5** | 229.39 | 0.20 |
| **Bus 6** | 10.97 | 1.35 |

| | P(MW) | Q(MVAr) | Loading (%) |
|---|---|---|---|
| **Line 2B2** | 19.92 | -19.10 | 6.95 |
| **Line 2B3** | -19.92 | -16.23 | 6.95 |
| **Line 3B3** | -40.17 | -7.55 | 10.26 |
| **Line 3B4** | 40.17 | -7.39 | 10.26 |
| **Line 4B2** | -39.99 | 0.80 | 10.07 |

# APPENDIX 9

*IEEET1 AVR Parameter settings*

| | | |
|---|---|---|
| $T_r$ | Measurement delay[s] | 0.028 |
| $K_a$ | Controller gain[p.u] | 175 |
| $T_a$ | Controller time constant[s] | 0.03 |
| $K_e$ | Exciter constant[p.u] | 1 |
| $K_f$ | Stabilization path[p.u] | 0.0025 |
| $T_e$ | Exciter time constant[s] | 0.266 |
| $T_f$ | Stabilization path time[s] | 1.5 |
| $E_1$ | Saturation factor1 [p.u] | 4.5 |
| $Se_1$ | Saturation factor2 [p.u] | 1.5 |
| $E_2$ | Saturation factor3[p.u] | 6 |
| $Se_2$ | Saturation factor4 [p.u] | 2.46 |
| $V_{r\min}$ | Controller output Minimum [p.u.] | -12 |
| $V_{r\max}$ | Controller output Maximumu [p.u.] | 12 |

*IEEEG2 Speed Governor Settings*

| | | |
|---|---|---|
| $K$ | Controller gain[p.u] | 20.83 |
| $T_1$ | Governor time constant[s] | 0.5 |
| $T_2$ | Governor derivative time constant[s] | 1 |
| $T_3$ | Servo time constant[s] | 7.76 |
| $T_4$ | Water starting time[s] | 0.2 |
| $P_{\min}$ | Minimum gate limit[p.u.] | 0 |
| $P_{\max}$ | Maximum gate limit[p.u.] | 1.5 |

# APPENDIX 10

*Transient Simulation Results with 5DFIGs at 1 km:* ***Chapter 5***

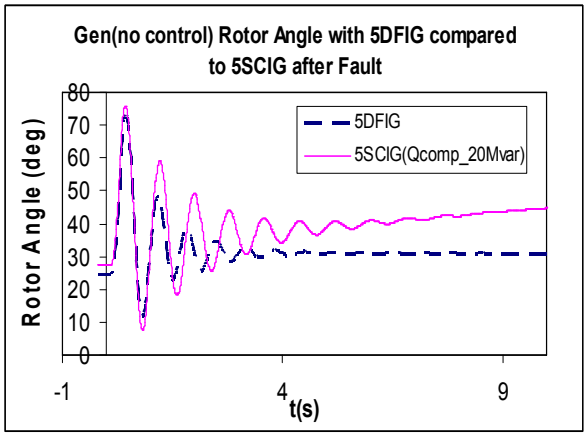


Fig A 10.1

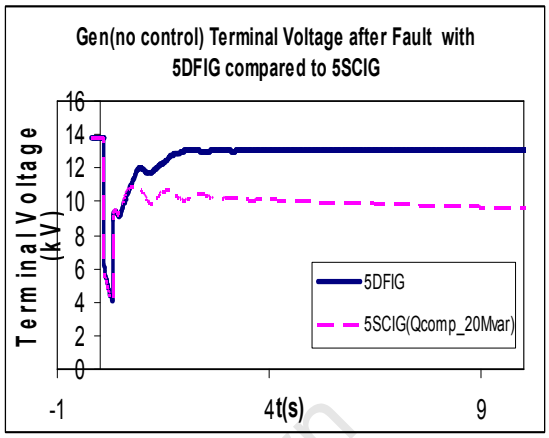


Fig A 10.2

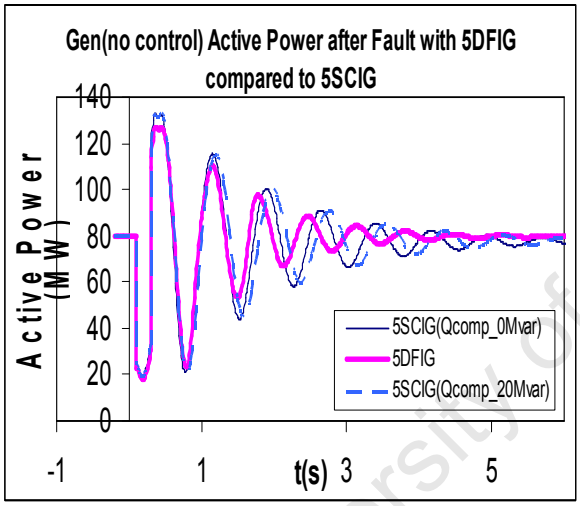


Fig A 10.3

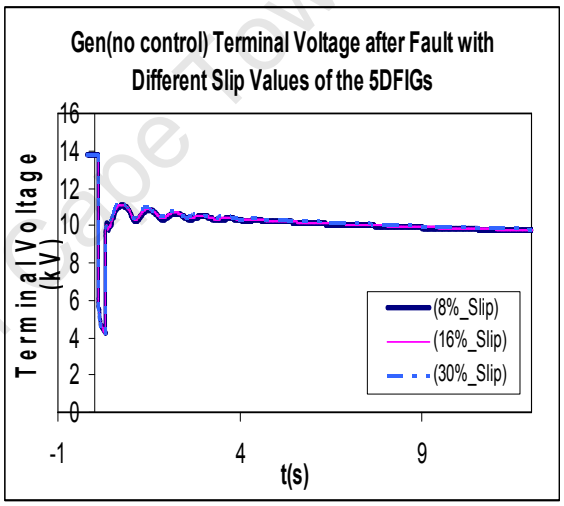


Fig A 10.4

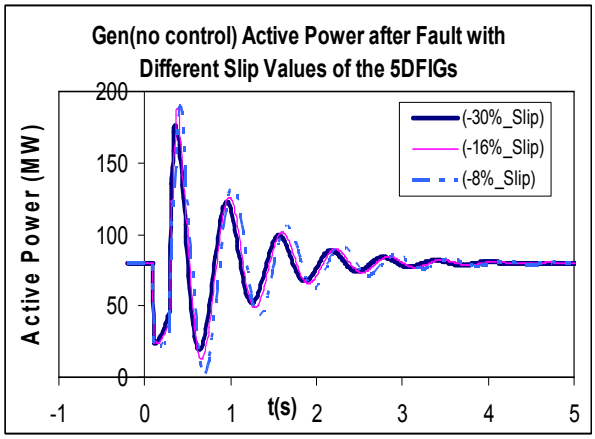


Fig A 10.5

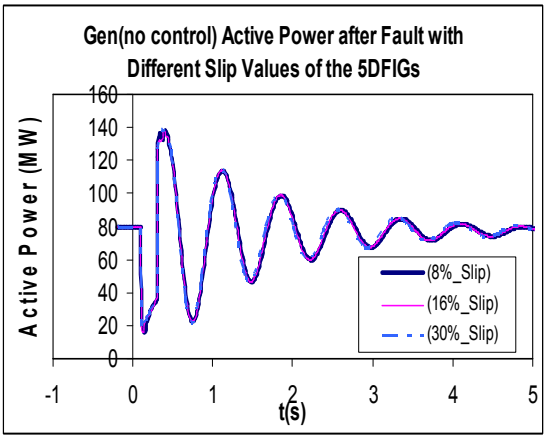


Fig A 10.6

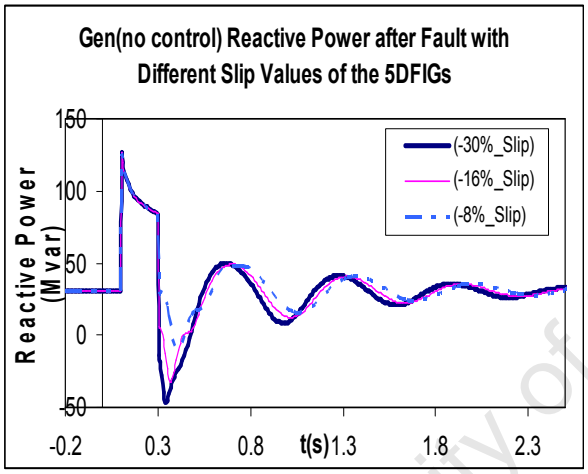


Fig A 10.7

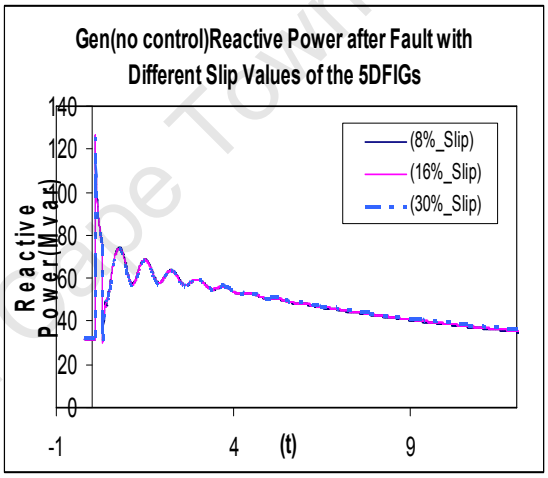


Fig A 10.8

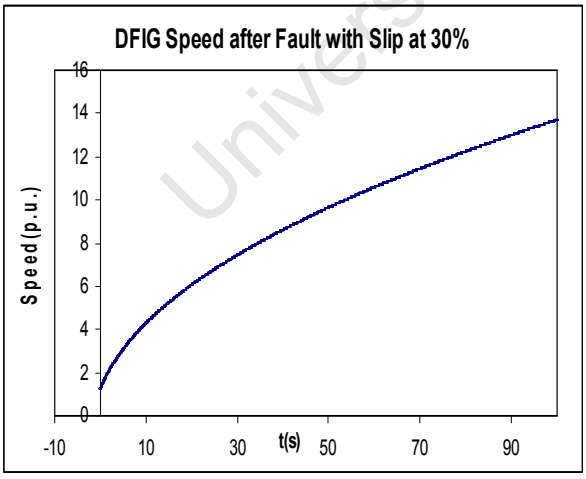


Fig A 10.9

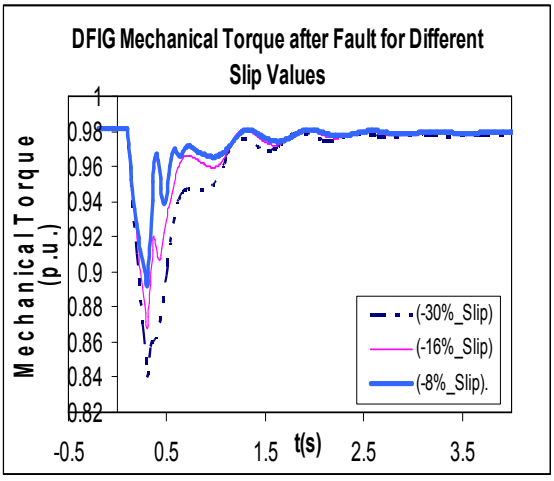


Fig A 10.10

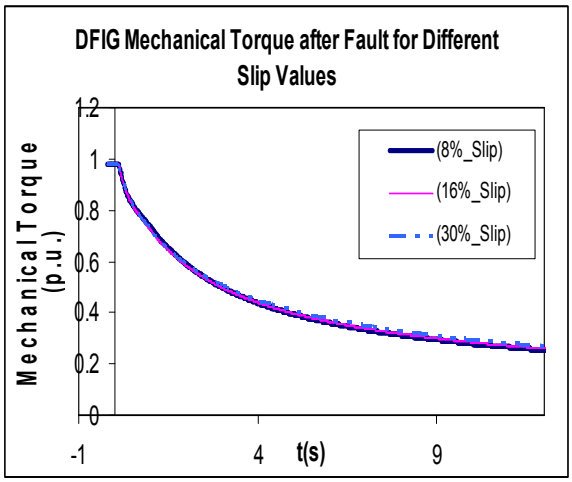


Fig A 10.11

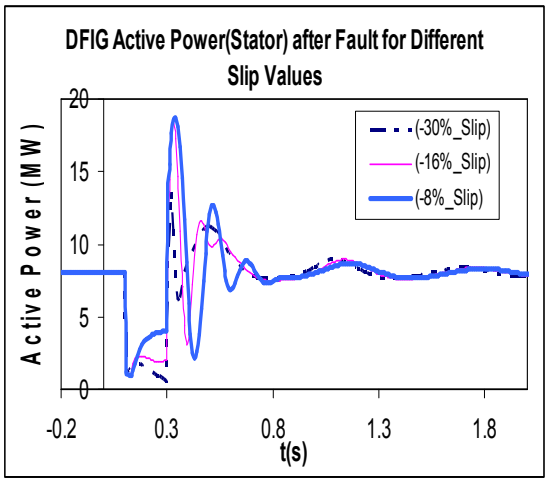


Fig A 10.12

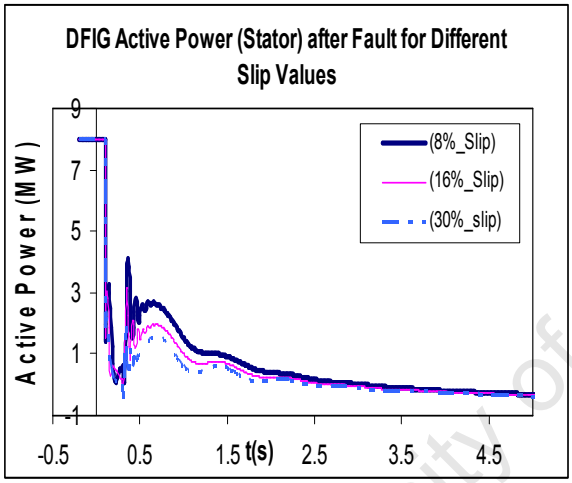


Fig A 10.13

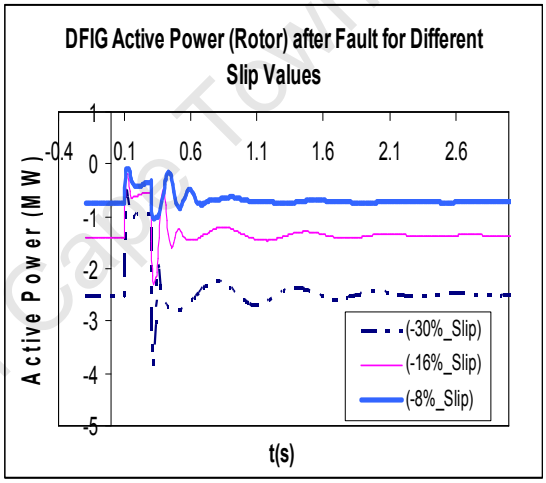


Fig A 10.14

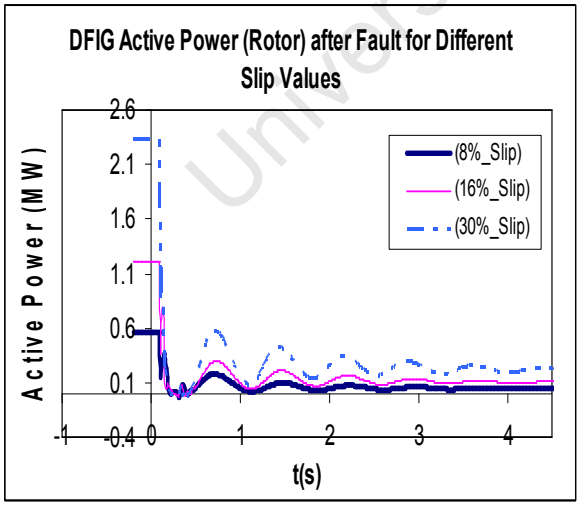


Fig A 10.15

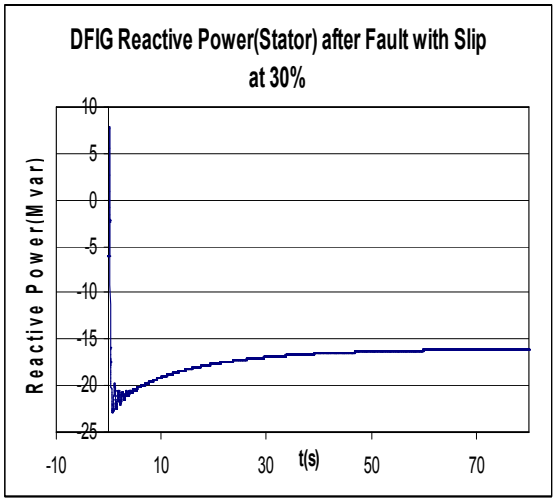


Fig A 10.16

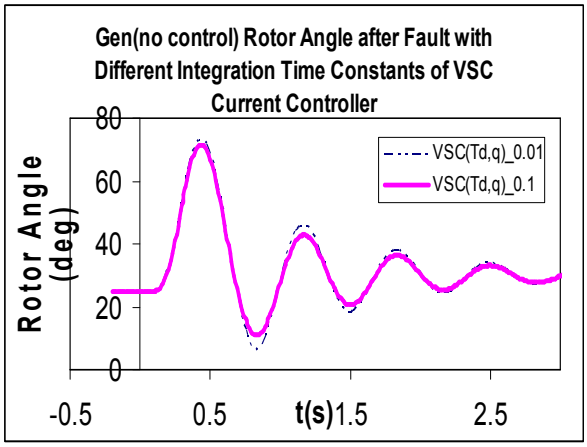


Fig A 10.17

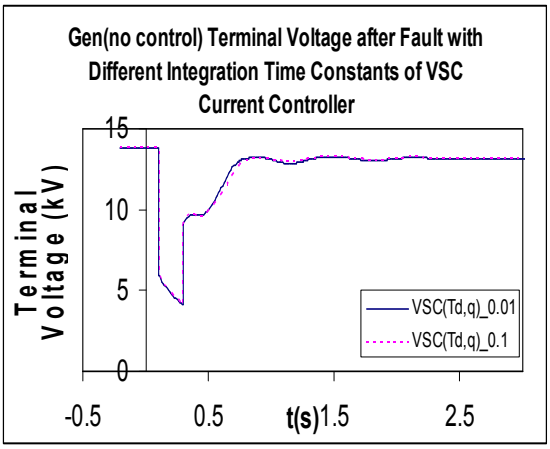


Fig A 10.18

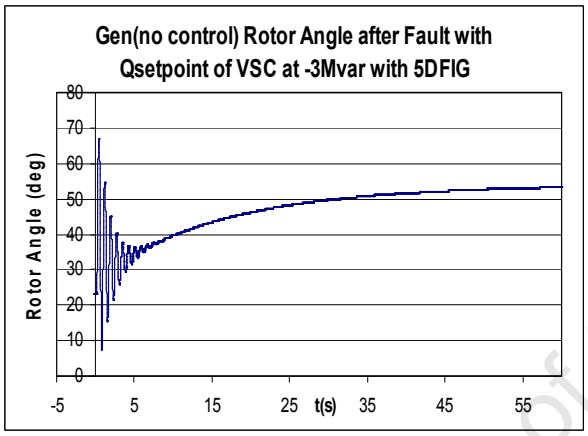


Fig A 10.19

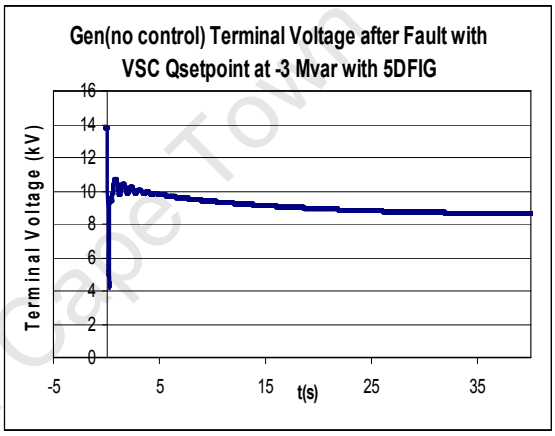


Fig A 10.20

# APPENDIX 11

*Pre-Fault Powerflow Results with 5DFIG at 1 km:* ***Chapter 5***

14. 5DFIG(VSC(Q-setpoint_3 MVAr))_1 km

| | P(MW) | Q(MVAr) |
|---|---|---|
| **Gen 1** | 80.00 | 17.53 |
| **DFIG(PCC)** | 39.39 | -15.97 |
| **DFIG(stator)** | 8.00 | -6.00 |
| **LSC(CONVERTER)** | -0.12 | 3.00 |
| **Ld 1** | 80.00 | 40.00 |
| **Ld 2** | 80.00 | 40.00 |
| **Infinite Bus** | 40.77 | -5.66 |

| | V(kV) | δ(deg) |
|---|---|---|
| **Bus 1** | 13.80 | 1.01 |
| **Bus 2** | 228.77 | 0.12 |
| **Bus 3** | 229.68 | -1.83 |
| **Bus 4** | 230.00 | 0.00 |
| **Bus 5** | 0.69 | 0.59 |
| **Bus 6** | 10.84 | 1.07 |
| **Bus 7** | 4.02 | 0.00 |
| **Bus 8** | 228.74 | 0.14 |

| | P(MW) | Q(MVAr) | Loading (%) |
|---|---|---|---|
| **Line 2B2** | 19.61 | -19.80 | 7.03 |
| **Line 2B3** | -19.61 | -15.39 | 7.03 |
| **Line 3B3** | -40.77 | -9.22 | 10.51 |
| **Line 3B4** | 40.77 | -5.66 | 10.51 |
| **Line 4B2** | -39.39 | 15.81 | 10.73 |

15. 5DFIG(VSC(Q-setpoint_2 MVAr))_1 km

| | P(MW) | Q(MVAr) |
|---|---|---|
| **Gen 1** | 80.00 | 22.10 |
| **DFIG(PCC)** | 39.40 | -20.96 |
| **DFIG(stator)** | 8.00 | -6.00 |
| **LSC(CONVERTER)** | -0.12 | 2.00 |
| **Ld 1** | 80.00 | 40.00 |
| **Ld 2** | 80.00 | 40.00 |
| **Infinite Bus** | 40.77 | -5.08 |

| | V(kV) | δ(deg) |
|---|---|---|
| **Bus 1** | 13.80 | 1.01 |
| **Bus 2** | 228.56 | 0.13 |
| **Bus 3** | 229.57 | -1.83 |
| **Bus 4** | 230.00 | 0.00 |
| **Bus 5** | 0.69 | 0.59 |
| **Bus 6** | 10.82 | 1.08 |
| **Bus 7** | 4.02 | 0.00 |
| **Bus 8** | 228.52 | 0.15 |

| | P(MW) | Q(MVAr) | Loading (%) |
|---|---|---|---|
| **Line 2B2** | 19.61 | -20.03 | 7.08 |
| **Line 2B3** | -19.61 | -15.11 | 7.08 |
| **Line 3B3** | -40.77 | -9.78 | 10.54 |
| **Line 3B4** | 40.77 | -5.08 | 10.54 |
| **Line 4B2** | -39.40 | 20.80 | 11.28 |

16. 5DFIG(VSC(Q-setpoint_-2 MVAr))_1 km

| | P(MW) | Q(MVAr) |
|---|---|---|
| **Gen 1** | 80.00 | 40.75 |
| **DFIG(PCC)** | 39.39 | -41.23 |
| **DFIG(stator)** | 8.00 | -6.00 |
| **LSC(CONVERTER)** | -0.12 | -2.00 |
| **Ld 1** | 80.00 | 40.00 |
| **Ld 2** | 80.00 | 40.00 |
| **Infinite Bus** | 40.81 | -2.74 |

| | V(kV) | δ(deg) |
|---|---|---|
| **Bus 1** | 13.80 | 0.99 |
| **Bus 2** | 227.71 | 0.13 |
| **Bus 3** | 229.15 | -1.83 |
| **Bus 4** | 230.00 | 0.00 |
| **Bus 5** | 0.67 | 0.60 |
| **Bus 6** | 10.73 | 1.09 |
| **Bus 7** | 4.02 | 0.00 |
| **Bus 8** | 227.63 | 0.15 |

| | P(MW) | Q(MVAr) | Loading (%) |
|---|---|---|---|
| **Line 2B2** | 19.59 | -20.97 | 7.28 |
| **Line 2B3** | -19.59 | -13.96 | 7.28 |
| **Line 3B3** | -40.81 | -12.08 | 10.72 |
| **Line 3B4** | 40.81 | -2.74 | 10.72 |
| **Line 4B2** | -39.39 | 41.08 | 14.46 |

17. 5DFIG(VSC(Q-setpoint -3 MVAr)) 1 km

| | P(MW) | Q(MVAr) |
|---|---|---|
| **Gen 1** | 80.00 | 45.51 |
| **DFIG(PCC)** | 39.37 | -46.38 |
| **DFIG(stator)** | 8.00 | -6.00 |
| **LSC(CONVERTER)** | -0.13 | -3.00 |
| **Ld 1** | 80.00 | 40.00 |
| **Ld 2** | 80.00 | 40.00 |
| **Infinite Bus** | 40.84 | -2.14 |

| | V(kV) | δ(deg) |
|---|---|---|
| **Bus 1** | 13.80 | 0.98 |
| **Bus 2** | 227.49 | 0.13 |
| **Bus 3** | 229.05 | -1.84 |
| **Bus 4** | 230.00 | 0.00 |
| **Bus 5** | 0.67 | 0.60 |
| **Bus 6** | 10.70 | 1.10 |
| **Bus 7** | 4.02 | 0.00 |
| **Bus 8** | 227.40 | 0.15 |

| | P(MW) | Q(MVAr) | Loading (%) |
|---|---|---|---|
| **Line 2B2** | 19.58 | -21.20 | 7.33 |
| **Line 2B3** | -19.58 | -13.67 | 7.33 |
| **Line 3B3** | -40.84 | -12.66 | 10.78 |
| **Line 3B4** | 40.84 | -2.14 | 10.74 |
| **Line 4B2** | -39.37 | 46.24 | 15.45 |

# APPENDIX 12

*Pre-fault Powerflow Results with 5CDSGs at 1 km:* ***Chapter 6***

18. 5CDSG(LSC(Q-setpoint_-9 MVAr))_1 km

| | P(MW) | Q(MVAr) |
|---|---|---|
| **Gen 1** | 80.00 | 49.82 |
| **CDSG(PCC)** | 38.79 | -51.06 |
| **CDSG(stator)** | 8.00 | 0.00 |
| **LSC(CONVERTER)** | 8.00 | -9.00 |
| **Ld 1** | 80.00 | 40.00 |
| **Ld 2** | 80.00 | 40.00 |
| **Infinite Bus** | 41.43 | -1.53 |

| | V(kV) | δ(deg) |
|---|---|---|
| **Bus 1** | 13.80 | 0.92 |
| **Bus 2** | 227.29 | 0.07 |
| **Bus 3** | 228.95 | -1.86 |
| **Bus 4** | 230.00 | 0.00 |
| **Bus 5** | 227.19 | 0.09 |
| **Bus 6** | 3.06 | 4.51 |
| **Bus 7** | 7.26 | 0.00 |
| **Bus 8** | 3.30 | 0.00 |

| | P(MW) | Q(MVAr) | Loading (%) |
|---|---|---|---|
| **Line 2B2** | 19.28 | -21.43 | 7.32 |
| **Line 2B3** | 19.28 | -13.41 | 7.32 |
| **Line 3B3** | -41.43 | -13.17 | 10.96 |
| **Line 3B4** | 41.43 | -1.53 | 10.96 |
| **Line 4B2** | -38.79 | 50.92 | 16.30 |

19. 5CDSG(LSC(Q-setpoint_-5 MVAr)) 1 km

| | P(MW) | Q(MVAr) |
|---|---|---|
| **Gen 1** | 80.00 | 28.96 |
| **CDSG(PCC)** | 39.31 | -28.44 |
| **CDSG(stator)** | 8.00 | 0.00 |
| **LSC(CONVERTER)** | 8.00 | -5.00 |
| **Ld 1** | 80.00 | 40.00 |
| **Ld 2** | 80.00 | 40.00 |
| **Infinite Bus** | 40.87 | -4.22 |

| | V(kV) | δ(deg) |
|---|---|---|
| **Bus 1** | 13.80 | 1.00 |
| **Bus 2** | 228.25 | 0.12 |
| **Bus 3** | 229.42 | -1.83 |
| **Bus 4** | 230.00 | 0.00 |
| **Bus 5** | 228.19 | 0.14 |
| **Bus 6** | 3.18 | 4.02 |
| **Bus 7** | 7.26 | 0.00 |
| **Bus 8** | 3.30 | 0.00 |

| | P(MW) | Q(MVAr) | Loading (%) |
|---|---|---|---|
| **Line 2B2** | 19.57 | -20.38 | 7.15 |
| **Line 2B3** | -19.57 | -14.69 | 7.15 |
| **Line 3B3** | -40.87 | -10.63 | 10.63 |
| **Line 3B4** | 40.87 | -4.22 | 10.63 |
| **Line 4B2** | -39.31 | 28.28 | 12.28 |

20. 5CDSG(LSC(Q-setpoint_0 MVAr))_1 km

| | P(MW) | Q(MVAr) |
|---|---|---|
| **Gen 1** | 80.00 | 5.04 |
| **CDSG(PCC)** | 39.55 | -2.27 |
| **CDSG(stator)** | 8.00 | 0.00 |
| **LSC(CONVERTER)** | 8.00 | 0.00 |
| **Ld 1** | 80.00 | 40.00 |
| **Ld 2** | 80.00 | 40.00 |
| **Infinite Bus** | 40.61 | -7.23 |

| | V(kV) | δ(deg) |
|---|---|---|
| **Bus 1** | 13.80 | 1.04 |
| **Bus 2** | 229.34 | 0.13 |
| **Bus 3** | 229.96 | -1.82 |
| **Bus 4** | 230.00 | 0.00 |
| **Bus 5** | 229.34 | 0.15 |
| **Bus 6** | 3.32 | 3.44 |
| **Bus 7** | 7.26 | 0.00 |
| **Bus 8** | 3.30 | 0.00 |

| | P(MW) | Q(MVAr) | Loading (%) |
|---|---|---|---|
| **Line 2B2** | 19.69 | -19.17 | 6.92 |
| **Line 2B3** | -19.69 | -16.16 | 6.92 |
| **Line 3B3** | -40.61 | -7.68 | 10.36 |
| **Line 3B4** | 40.61 | -7.23 | 10.38 |
| **Line 4B2** | -39.55 | 2.10 | 9.97 |

21. 5CDSG(LSC(Q-setpoint_5 MVAr))_1 km

| | P(MW) | Q(MVAr) |
|---|---|---|
| **Gen 1** | 80.00 | -17.01 |
| **CDSG(PCC)** | 39.41 | 22.07 |
| **CDSG(stator)** | 8.00 | 0.00 |
| **LSC(CONVERTER)** | 8.00 | 5.00 |
| **Ld 1** | 80.00 | 40.00 |
| **Ld 2** | 80.00 | 40.00 |
| **Infinite Bus** | 40.75 | -9.99 |

| | V(kV) | δ(deg) |
|---|---|---|
| **Bus 1** | 13.80 | 1.05 |
| **Bus 2** | 230.35 | 0.11 |
| **Bus 3** | 230.45 | -1.82 |
| **Bus 4** | 230.00 | 0.00 |
| **Bus 5** | 230.39 | 0.13 |
| **Bus 6** | 3.45 | 2.89 |
| **Bus 7** | 7.26 | 0.00 |
| **Bus 8** | 3.30 | 0.00 |

| | P(MW) | Q(MVAr) | Loading (%) |
|---|---|---|---|
| **Line 2B2** | 19.62 | -18.05 | 6.68 |
| **Line 2B3** | -19.62 | -17.53 | 6.68 |
| **Line 3B3** | -40.75 | -4.94 | 10.53 |
| **Line 3B4** | 40.75 | -9.99 | 10.53 |
| **Line 4B2** | -39.41 | -22.24 | 11.34 |

22. 5CDSG(LSC(Q-setpoint_9 MVAr))_1 km

| | P(MW) | Q(MVAr) |
|---|---|---|
| **Gen 1** | 80.00 | -30.26 |
| **CDSG(PCC)** | 39.16 | 36.81 |
| **CDSG(stator)** | 8.00 | 0.00 |
| **LSC(CONVERTER)** | 8.00 | 9.00 |
| **Ld 1** | 80.00 | 40.00 |
| **Ld 2** | 80.00 | 40.00 |
| **Infinite Bus** | 41.02 | -11.65 |

| | V(kV) | δ(deg) |
|---|---|---|
| **Bus 1** | 13.80 | 1.03 |
| **Bus 2** | 230.96 | 0.08 |
| **Bus 3** | 230.76 | -1.83 |
| **Bus 4** | 230.00 | 0.00 |
| **Bus 5** | 231.03 | 0.10 |
| **Bus 6** | 3.46 | 2.84 |
| **Bus 7** | 7.26 | 0.00 |
| **Bus 8** | 3.30 | 0.00 |

| | P(MW) | Q(MVAr) | Loading (%) |
|---|---|---|---|
| **Line 2B2** | 19.49 | -17.37 | 6.70 |
| **Line 2B3** | -19.49 | -18.36 | 6.70 |
| **Line 3B3** | -41.02 | -3.28 | 10.70 |
| **Line 3B4** | 41.02 | -11.65 | 10.70 |
| **Line 4B2** | -39.16 | -36.96 | 13.46 |

# APPENDIX 13

*Background Theory to Three-Phase Converters*

In the three phase converter in figure A13.1, the instantaneous waveform $V_d$ consists of six segments per cycle. Hence the rectifier is often termed a six-pulse rectifier. Figure A13.2 shows one of the six voltage segments ($V_d$) within one cycle. Each segment belongs to one of the six line-to-line voltage combinations. To obtain the average value of the dc voltage, we consider one voltage segment over a $\pi/3$ rad interval as shown in figure A13.2

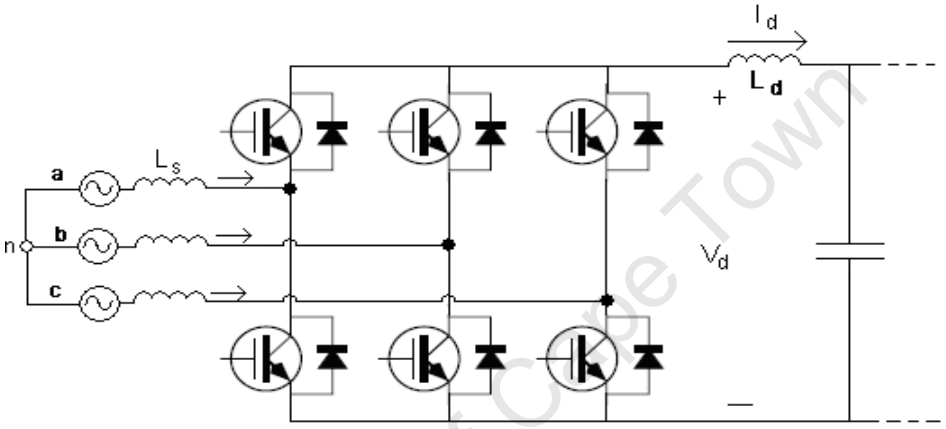


**Fig A 13.1:** Three – phase IGBT converter

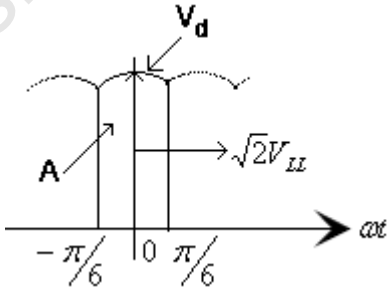


**Fig A 13.2:** One voltage segment of the six-pulse rectifier

Therefore:

$$V_d = V_{ab} = \sqrt{2}V_{LL}\cos\ \omega t \qquad -\pi/6 < \omega t < \pi/6 \quad \text{(A 13-1)}$$

By integrating $V_d$ within the segment duration and dividing by the $\pi/3$ interval yields

$$V_{d0} = \frac{1}{\pi/3}\int_{-\pi/6}^{\pi/6}\sqrt{2}\,V_{LL}\cos\ \omega t = \frac{3}{\pi}\sqrt{2}\,V_{LL} \qquad \text{(A13-2)}$$

The effect of the firing angle $\alpha$ of the IGBTs results with a reduction of the average dc voltage. So, equation A14-2 becomes

$$V_{d\alpha} = \frac{3}{\pi}\sqrt{2}\,V_{LL}\cos\ \alpha \qquad \text{(A13-3)}$$

In practical IGBT converters, the ac-side inductance $L_s$ cannot be ignored. In fact the German VDE standards require that this inductance must be a minimum of 5 %, that is:

$$\omega L_s \geq 0.05\frac{V_{LL}/\sqrt{3}}{I_{S1}} \qquad \text{(A13-4)}$$

Where $I_{S1}$ is the rms value of the fundamental –frequency component given as:

$$I_{S1} = 0.78I_d \qquad \text{(A13-5)}$$

With $L_s$ current commutation takes a finite commutation interval $u$, during which the IGBT turning off and the one turning on conduct simultaneously. This results with a further reduction on the average output dc voltage, where equation A13-3 becomes

$$V_{d\alpha} = \frac{3}{\pi}\sqrt{2}\,V_{LL}\cos\ \alpha - \frac{3\omega L_s}{\pi}I_d \qquad \text{(A13-6)}$$

An assumption of a very large value of $L_d$ allows for the postulation that $I_d$ is a constant dc. Therefore, the average power through the converter is deduced as

$$P = I_d\left(\frac{1}{T}\int_0^T v_d\ dt\right) = I_d V_d = I_d \cdot \left[\frac{3\sqrt{2}}{\pi} V_{LL}\cos\alpha - \frac{3\omega L_s}{\pi} I_d\right] \qquad \text{(A13-7)}$$

The fundamental reactive volt-amperes are defined as

$$Q = I_d \cdot \left[\frac{3\sqrt{2}}{\pi} V_{LL}\sin\alpha - \frac{3\omega L_s}{\pi} I_d\right] \qquad \text{(A13-8)}$$

The converter operates as an inverter when the IGBT firing angle ($\alpha$) is $90° < \alpha < 180°$. In this mode of operation, the average power is negative since $V_d$ is negative. Power flows from the dc side to the ac side. It is worth noting that, this mode of operation is possible due to the presence of an energy source on the dc side. This dc source could be a battery, photovoltaic source or a dc voltage produced by a wind electric system.